1974

# A quadrupole mass spectrometer for the identification and characterization of neutral fragments formed by the interaction of gaseous molecules with electrons

John Readshaw Reeher
*Iowa State University*

# A quadrupole mass spectrometer for the identification and characterization of neutral fragments formed by the interaction of gaseous molecules with electrons

by

John Readshaw Reeher

A Dissertation Submitted to the

Graduate Faculty in Partial Fulfillment of

The Requirements for the Degree of

DOCTOR OF PHILOSOPHY

Department: Chemistry
Major: Physical Chemistry

Approved:

Signature was redacted for privacy.

In Charge of Major Work

Signature was redacted for privacy.

For the Major Department

Signature was redacted for privacy.

For the Graduate College

Iowa State University
Ames, Iowa

1974

TABLE OF CONTENTS

# LIST OF FIGURES

# LIST OF TABLES

# I. INTRODUCTION

## A. Description of the Problem

In a conventional mass spectrometer ion source, gaseous molecules interact with energetic electrons by means of various processes (Figure 1) to produce many species, including positive ions, negative ions, and neutral radicals and molecules, all of which may be formed in ground or excited states. In order to characterize completely the behavior of gaseous molecules under electron impact, all of these species must be detected and the energetics of their formation and ionization determined. The application of mass spectrometric methods to the detection of positive and negative ions and the determination of the energetics of their formation are well documented. In fact, a mass spectrometer capable of simultaneous detection of positive and negative ions has been developed (1) and is currently being utilized for studies in our laboratory. However, the neutral fragments formed during decomposition processes and the energetics of their formation and ionization are not so well known. Indirect methods, including isotopic labelling, studies of metastable ion transitions, and deconvolution of ionization efficiency curves, are available for deducing the makeup and the energies of formation (appearance potentials) of neutral

Figure 1. Unimolecular processes resulting from the interaction of a molecule, ABC, with an energetic electron

## ION SOURCE REACTIONS

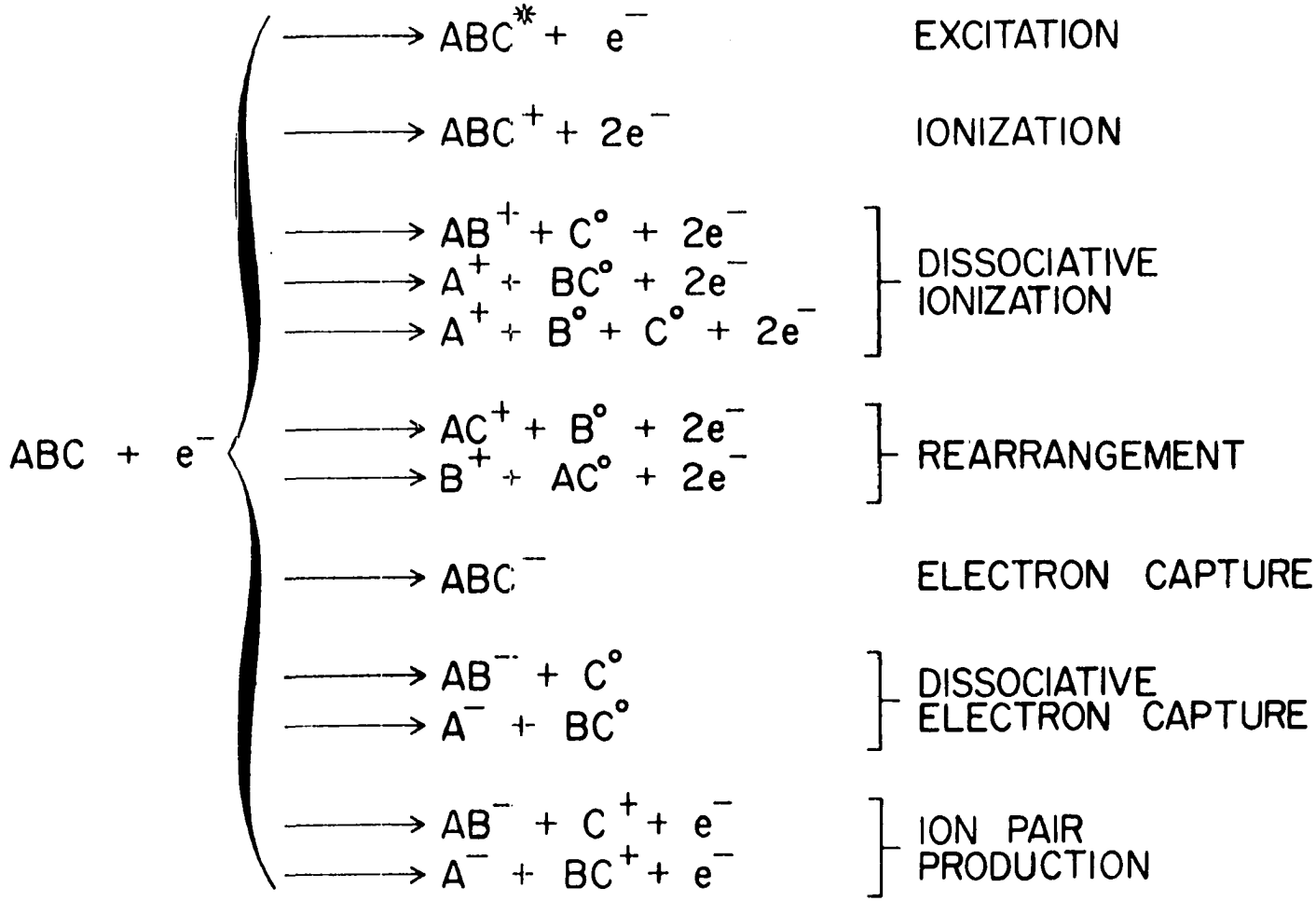

fragments, but these methods do not provide direct information about the properties, such as ionization potentials, of the neutral fragments themselves.

Isotope labelling studies can be difficult to interpret or even misleading because of scrambling of the atoms within a molecule after interaction with an energetic electron and before dissociation. Such scrambling almost certainly occurs to some extent in all complex molecules, and recent studies with aromatic (2-9) and heteroaromatic (10,11) compounds indicate that scrambling in these molecules is particularly pronounced, with complete hydrogen randomization and major scrambling of the carbon skeleton.

Studies of metastable ion transitions, on the other hand, are generally less ambiguous. The apparent mass of the metastable peak defines the masses of the parent and daughter ions and thus the mass of the resultant neutral fragment (or fragments). The reactions studied by this method are, therefore, well defined. However, metastable transitions result from processes with precursor ion lifetimes on the order of $10^{-5}$ to $10^{-6}$ second (12) and constitute typically less than 0.1% of the total ions collected. The bulk of the ions which constitute the normal mass spectrum are formed in $10^{-8}$ second or less. Since fewer electronic states will be involved in the dissociation mechanism for processes with long half-lives (13), the validity of extrapolating the

information gained from studies of metastable transitions to the much faster and more abundant processes which produce normal ions and neutral fragments is subject to some question.

The deconvolution of ionization efficiency curves (14-16) is probably the best method available for indirect measurement of the abundance and appearance potential of ions and neutral fragments produced by various processes in an electron impact ion source, as it yields useful measurements of the abundances and energies of both the processes occurring at initial onset potential and those occurring at higher energies. As presently utilized, the method is limited by an energy resolution of about $\pm$ 0.5 volt and by the fact that some compounds give meaningful results for only a few volts above initial onset potential.

Several investigators in the past have attempted to develop a mass spectrometer ion source for direct detection of the neutral fragments formed by the interaction of electrons with gaseous molecules. While all of them claim some degree of success, the problem of direct detection of neutral fragments has not been solved satisfactorily, as evidenced by the paucity of neutral fragment mass spectra, appearance potentials, and ionization potentials which have been reported. Before discussing the work of previous investigators of this problem, a brief discussion of the technique used for detecting and characterizing the neutral

fragments produced by the interaction of electrons with gaseous molecules is appropriate.

All of the mass spectrometers developed to date for direct detection of neutral fragments rely on the concept of an ion source with two ionization chambers; a primary reaction chamber, in which the neutral fragments are generated by the interaction of electrons with sample gas molecules, and a secondary ionization chamber, to which the neutral fragments diffuse and in which they interact with electrons to produce positive ions which are subsequently mass analyzed and detected. In both chambers, processes producing negative ions are ignored, since processes producing positive ions are generally more abundant (17) by a factor of about $10^3$.

The processes which occur in the primary reaction chamber to produce positive ions and neutral fragments from a molecule, AB, are given in Equation 1. The neutral fragments

$$AB \xrightarrow{e^-} \begin{cases} AB^* \\ AB^+ + e^- \\ A^+ + B^\circ + e^- \\ A^\circ + B^+ + e^- \end{cases} \qquad (1)$$

produced in the primary reaction chamber are free to diffuse to the secondary ionization chamber, but the charged particles are prevented from doing so by the electric fields in the ion source.

The processes which occur in the secondary ionization chamber result in the production of two components of positive ion current (Equations 2,3). The first component of ion

Component 1

$$AB \xrightarrow{e^-} \begin{cases} AB^+ + e^- \\ A^+ + B^\circ + e^- \\ A^\circ + B^+ + e^- \end{cases} \qquad (2)$$

Component 2

$$AB^* \xrightarrow{e^-} \begin{cases} AB^+ + e^- \\ A^+ + B^\circ + e^- \\ A^\circ + B^+ + e^- \end{cases} \qquad (3)$$

$$A^\circ \xrightarrow{e^-} A^+ + e^-$$

$$B^\circ \xrightarrow{e^-} B^+ + e^-$$

current (Equation 2) is that produced by gas molecules which enter the secondary ionization chamber <u>without</u> having interacted with an electron in the primary reaction chamber. Upon mass analysis, this component of ion current yields the normal positive ion mass spectrum of the sample gas.

The second component of ion current (Equation 3) is that produced by those particles which enter the secondary ionization chamber <u>after</u> having interacted with an electron in the primary reaction chamber. Upon mass analysis, this component of ion current yields the neutral fragment mass spectrum of

the sample gas.

In general, the first component of ion current is greater than the second component by a factor of about $10^3$ to $10^5$. Therefore, the relative success of a mass spectrometer developed for direct detection of neutral fragments depends upon its capability to enhance the ion current from ionized neutral fragments with respect to the ion current from other processes and upon its capability to separate the two components from each other. In addition, the successful instrument should provide the capability for convenient measurement of the relative abundances, appearance potentials, and vertical ionization potentials of the neutral fragments detected.

The appearance potential (A.P.) of a neutral fragment is defined as the energy required to produce that neutral fragment from its parent molecule, which, for the following process (Equation 4) is equal to the appearance potential of

$$AB \xrightarrow{e^-} A^+ + B^\circ + e^- \qquad (4)$$

its complementary ion (Equation 5). Thus, the appearance

$$\Delta H_{react} = A.P.(B^\circ) = A.P.(A^+) \qquad (5)$$

potential of a neutral fragment can be determined directly by measuring its abundance as a function of the energy of the electrons in the primary reaction chamber.

The vertical ionization potential (I.P.) of a neutral fragment is defined as the energy required to remove an electron from that neutral fragment to produce a positive ion (Equations 6,7). The vertical ionization potential of a

$$B^\circ \xrightarrow{e^-} B^+ + e^- \tag{6}$$

$$\Delta H_{react} = I.P.(B^\circ) \tag{7}$$

neutral fragment can be determined by measuring the ion current produced by that neutral fragment as a function of the energy of the electrons in the secondary ionization chamber.

## B. History of the Problem

Beck and Osberghaus (18) pioneered the development of a dual ionization chamber ion source for direct detection of neutral fragments, and their basic design has been adopted by subsequent investigators. In the primary reaction chamber, neutral fragments were produced by the interaction of sample gas molecules with the primary electron beam, which had a fixed energy of 200 eV and an average intensity of 20 mA and was pulsed at a frequency of 32 Hz. The neutral fragments were ionized by interaction with the secondary electron beam, which was a DC electron beam with variable energy and an intensity of 100 μA. The ion current produced

in the secondary ionization chamber was analyzed by means of a 60° magnetic sector mass spectrometer, and the component of ion current due to ionization of neutral fragments was detected with a phase-sensitive detector at a frequency of 32 Hz.

With this ion source, the neutral fragment mass spectra of propane (18,19), n-hexane (18), butane (19,20), benzene (19,21), fluorobenzene (21), and toluene (21) were observed and reported. The vertical ionization potentials for many of the neutral fragments from these compounds were also measured. However, the ion source used in this work had several limitations:

1. Sensitivity (i.e., signal/noise ratio) for detecting neutral fragments was poor. Errors in the measurement of neutral fragment abundances from $\pm$ 20 to $\pm$ 50 percent could not be excluded.

2. Since the energy of the primary electron beam was fixed at 200 eV, the appearance potentials of neutral fragments could not be measured directly. Also, a choice of 50 eV or 70 eV for the energy of the primary electron beam would have been more appropriate, since these are the energies at which mass spectra are generally tabulated in the literature.

3. Neutral fragment mass spectra and ionization efficiency curves could not be scanned automatically. Thus, the measurement of relative abundances and ionization potentials of neutral fragments was very tedious and time-consuming.

4. The electric field created by the intense primary electron beam may have complicated the observed results because of ion trapping.

Niehaus (22), with a modified version of Beck's original ion source, succeeded in improving the signal/noise ratio for detecting neutral fragments and in extending the capabilities of the instrument. This modification consisted chiefly of pulsing both the primary and secondary electron beams, the primary electron beam at a frequency, $\nu_1$, of 1010 Hz, and the secondary electron beam at a frequency, $\nu_2$, of 750 Hz. The component of ion current due to ionization of neutral fragments was detected at the difference frequency, $\nu_1-\nu_2$, of 260 Hz. Also included in the modification was provision for varying the energies of both the electron beams, making possible the measurement of neutral fragment appearance potentials and vertical ionization potentials. With this instrument, Niehaus (22) obtained values for the vertical ionization potentials and appearance potentials for neutral fragments from butane, cis-2-butene, 1,3-butadiene and hexane. Later, Lampe and Niehaus (23) utilized this instrument to measure the vertical ionization potentials of methylstannyl radicals.

Melton (24,25), in an attempt to completely characterize radiolysis processes, developed a dual ionization chamber ion source for detecting neutral fragments. The two electron beams in this ion source were only 0.1 in. apart and were

separated by an electrode with a 0.005 in. x 0.250 in. slit which prevented the transmission of positive ions, yet allowed the neutral fragments produced in the primary chamber to diffuse to the secondary chamber. Since neither electron beam was pulsed, ionized neutral fragments were observed manually by focussing the mass spectrometer to detect ions at a given mass/charge ratio and looking for an increase in the detected ion current when the primary electron beam was activated. However, this method of detection entails the measurement of small changes in large ion currents and therefore yields extremely poor signal/noise ratios (10 or less). Also, the measurement of neutral fragment abundances, appearance potentials, and vertical ionization potentials by this method, although not impossible, is very tedious and time-consuming. Despite these limitations, Melton was able to measure and report the abundances and vertical ionization potentials of the neutral fragments produced by the interaction of 100 eV electrons with simple molecules, including ammonia (25,26), methane (26,27), and water (28,29).

Saunders, Larkins, and Saalfeld (30) modified an Atlas CH4 dual ionization chamber mass spectrometer in order to detect neutral fragments directly, but their instrument, too, had several limitations. As with Melton's instrument, the neutral fragments were detected manually, resulting in poor signal/noise ratios and tedious, time-consuming measurements.

In addition, the energy of the primary electron beam was fixed at 70 eV, and that of the secondary electron beam was variable only over the narrow range of 10 eV to 21 eV. Thus, the appearance potentials of neutral fragments could not be measured, and vertical ionization potentials of these species were measurable only over a very limited range. The relative abundances of neutral fragments produced from two compounds, carbon tetrachloride and 2-pentanone, were reported by these investigators.

Preston, Tsuchiya, and Svec (31) utilized a 60° magnetic sector mass spectrometer with a dual ionization chamber ion source and modified ion detection system for direct detection of neutral fragments. The conditions utilized by these investigators for generating and ionizing the neutral fragments were more nearly those used in conventional mass spectrometry. The neutral fragments were generated in the primary reaction chamber of the ion source by the interaction of sample gas molecules with a variable energy electron beam pulsed at a frequency of 1 KHz. The neutral fragments diffused to the secondary ionization chamber where they were ionized by a variable energy, dc electron beam and subsequently mass analyzed. The component of ion current due to ionization of neutral fragments was detected at a frequency of 1 KHz by means of a lock-in amplifier.

However, problems in pulsing the primary electron beam and pickup of the pulse signal by various other ion source components were encountered, resulting in poor signal/noise ratios. Also, pickup of the pulse signal by other ion source components resulted in the production of extraneous phase-sensitive output signals, making the interpretation of results difficult in some cases. These problems proved to be difficult, if not impossible, to eliminate because of the high ion source potentials (2 KV) necessary for operation of the magnetic sector mass spectrometer. Despite these problems, the abundances, vertical ionization potentials, and appearance potentials of neutral fragments from propane were measured. In addition, rare gas atoms excited by interaction with electrons in the primary reaction chamber were observed and characterized.

## C. Importance of the Problem

In addition to providing information essential to complete characterization of the processes which occur in a conventional mass spectrometer ion source, a mass spectrometer successfully developed for detecting and characterizing neutral fragments provides information which is important to many other areas of study, including radiation chemistry, thermochemistry, combustion chemistry, and ion physics. Such an instrument can be utilized for the following kinds of

studies.

1. Identification of ion source processes

The identification of all of the species present, including the neutral fragments, is essential to the complete characterization of ion source processes. By comparing the relative abundances and appearance potentials of the neutral fragments produced from a sample gas with those of the positive ions which make up its normal mass spectrum (Equations 4,5), individual processes and their associated energetics can be characterized with greater certainty.

2. Studies of excited species

A mass spectrometer designed for detecting neutral fragments may also be utilized to detect and characterize gaseous atoms and molecules excited, but not ionized, by interaction with energetic electrons. Such excited species are generated by the interaction of sample gas molecules with electrons in the primary reaction chamber (Equation 8), ionized by interactions with electrons in the secondary ionization chamber (Equation 9), and subsequently mass analyzed

$$A \xrightarrow{e^-} A^* \qquad (8)$$

$$A^* \xrightarrow{e^-} A^+ + e^- \qquad (9)$$

and detected. By varying the energy of the primary electron beam, the appearance potential of the excited atom or molecule, A.P.(A*), can be measured. The vertical ionization potentials of these species, I.P.(A*), can be measured by varying the energy of the secondary electron beam. The excitation energy, $E_{ex}$, of the excited atom or molecule is equal to its appearance potential (Equation 10) and is also equal

$$E_{ex} = A.P.(A^*) = I.P.(A) - I.P.(A^*) \qquad (10)$$

to the difference between the vertical ionization potential of the unexcited atom or molecule, I.P.(A), and that of the excited specie, I.P.(A*). Thus, the dual ionization chamber technique provides two independent measurements of the excitation energies of such species. Excited rare gas atoms, including helium (24), argon (31), and neon (31), have been detected and characterized utilizing the dual ionization chamber technique.

3. Calculation of bond dissociation energies

One of the most important characteristics of a molecule is the energy of its chemical bonds, since most chemical reactions involve the breaking of some chemical bonds and the making of new ones. Mass spectrometric methods have been largely used in the determination of bond dissociation energies since they are more widely applicable than kinetic

methods, even though the latter may generally provide more reliable results (17, p. 14).

In order to calculate bond dissociation energies from mass spectrometric data, the following types of processes are considered (Equation 11):

$$AB + e^- \rightarrow \begin{cases} A^+ + B^\circ + 2e^- \\ A^\circ + B^+ + 2e^- \end{cases} \qquad (11)$$

For these processes, the dissociation energy, D(A-B), is given by the following relationships (Equations 12,13) where $E_{ex}$

$$D(A\text{-}B) = A.P.(A^+) - I.P.(A) - E_{ex} \qquad (12)$$

$$D(A\text{-}B) = A.P.(B^+) - I.P.(B) - E_{ex} \qquad (13)$$

is the total excitation energy of the products. If a direct measurement of the excitation energies of the products is not available, they are assumed to be zero. In such cases, one must write

$$D(A\text{-}B) \leq A.P.(A^+) - I.P.(A) \qquad (14)$$

$$D(A\text{-}B) \leq A.P.(B^+) - I.P.(B) \qquad (15)$$

to show that what is really calculated is an upper limit of the bond dissociation energy.

The quasi-equilibrium theory of mass spectra (32,33) states that rates of dissociation reactions are dependent on the activation energies of the reactions, which may be equal to the endothermicity of the processes plus an additional energy barrier as in Figure 2 (17, p. 15,16). A principle known as Stevenson's rule (34) has been established which refers to the possible fragmentation processes of a molecular ion. According to this rule, when dissociative ionization occurs, the charge usually stays with the fragment having the lowest ionization potential. Thus, if I.P.(A) is less than I.P.(B), the decomposition (Equation 11) to $A^+ + B$ is more favorable than decomposition to $B^+ + A$. If the reaction yielding $B^+ + A$ occurs, the products will possess excess energy. Therefore, only the reaction producing the ion which, as a neutral particle, has the lower ionization potential should be used in calculating bond dissociation energies. Stevenson (34) has shown that for the products of dissociation processes in a large number of compounds

$$E_{ex} \approx 0 \qquad (16)$$

if the ion corresponds to the neutral fragment which, as a neutral particle, has the lower ionization potential.

While appearance potentials for a large number of dissociation processes have been measured and tabulated, relatively few neutral fragment ionization potentials are

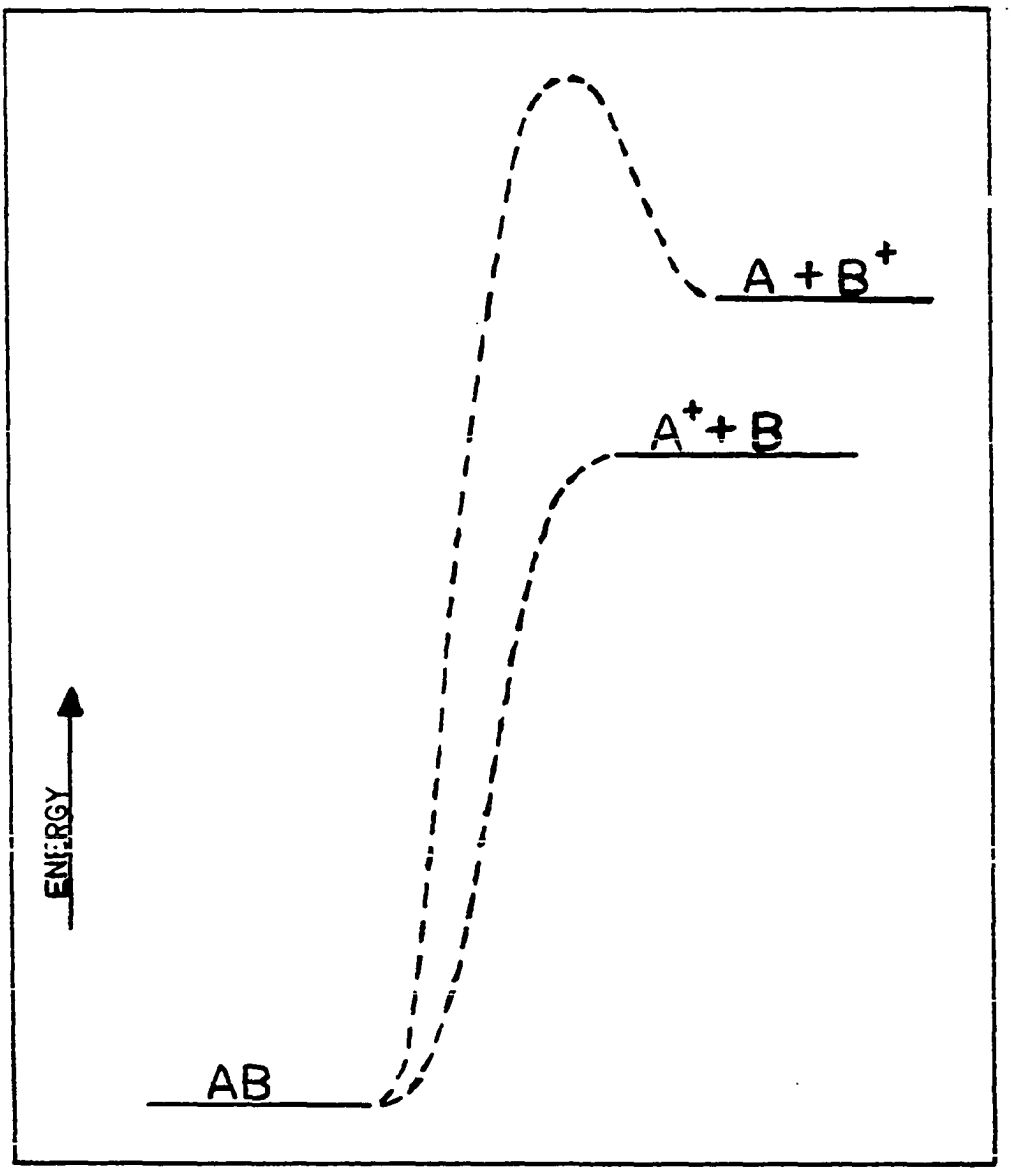


Figure 2. Simple illustration of Stevenson's Rule for the case I.P.(A) $\leq$ I.P.(B)

available for calculating bond dissociation energies. With the successful development of a mass spectrometer for detecting and characterizing neutral fragments, the measurements of the ionization potentials of a wide variety of neutral fragments is facilitated. These ionization potentials find immediate use in bond dissociation energy calculations and are, perhaps, the most important information to be gained from the development of such an instrument.

4. Applications to combustion chemistry

Information gained from studies of neutral fragments produced in a mass spectrometer ion source is also applicable in characterizing combustion processes. While the total pressure in a mass spectrometer ion source ($10^{-5}$ to $10^{-7}$ Torr) is very much smaller than that in a flame (> 1 Torr), the relative concentration of the radical species is very similar. A typical distribution of species in a flame (35) might consist of molecules, atoms and radicals, and ions in the proportions $1:10^{-2}:10^{-7}$, while that in a mass spectrometer ion source might consist of the same species in the proportions $1:10^{-3}:10^{-3}$. The low pressure in the mass spectrometer ion source facilitates detection of the radical species before they undergo collision, a condition not easily attained with direct sampling of radicals in flames. Any information about the properties of free radicals is

especially important to an understanding of combustion chemistry because free radicals play a very important role in the chemistry of flames, as they enter into virtually every important flame reaction (35, p. 206).

# II. THE INSTRUMENT

## A. General Description

The instrument described herein was designed to accommodate the technique for detecting and characterizing neutral fragments first described by Beck and Osberghaus (18) and later refined by Preston, Tsuchiya, and Svec (31). With this technique, neutral and ionic species are produced by the interaction of sample gas molecules with a pulsed (Π) electron beam (Figure 3) in the primary (1Y) chamber of a dual ionization chamber ion source. The neutral species produced are allowed to diffuse to the secondary (2Y) chamber, but the charged species are prevented from doing so by the electric fields in the ion source. In the secondary ionization chamber, two components of ion current are produced (Figure 4). A dc component is produced by the ionization of gas molecules which have not previously interacted with the pulsed primary electron beam, and an ac component is produced by ionization of neutral species produced by the interaction of sample gas molecules with the pulsed primary electron beam. The total ion current produced in the secondary ionization chamber is mass analyzed, amplified, and separated into its two components, each of which is recorded. The dc component yields the normal mass spectrum of the sample gas, while the ac component comprises its neutral fragment mass spectrum.

Figure 3. Unimolecular processes resulting from the interaction of a molecule, AB, with the pulsed (Π) primary electron beam to produce positive ions and/or neutral species

# PRIMARY CHAMBER PROCESSES

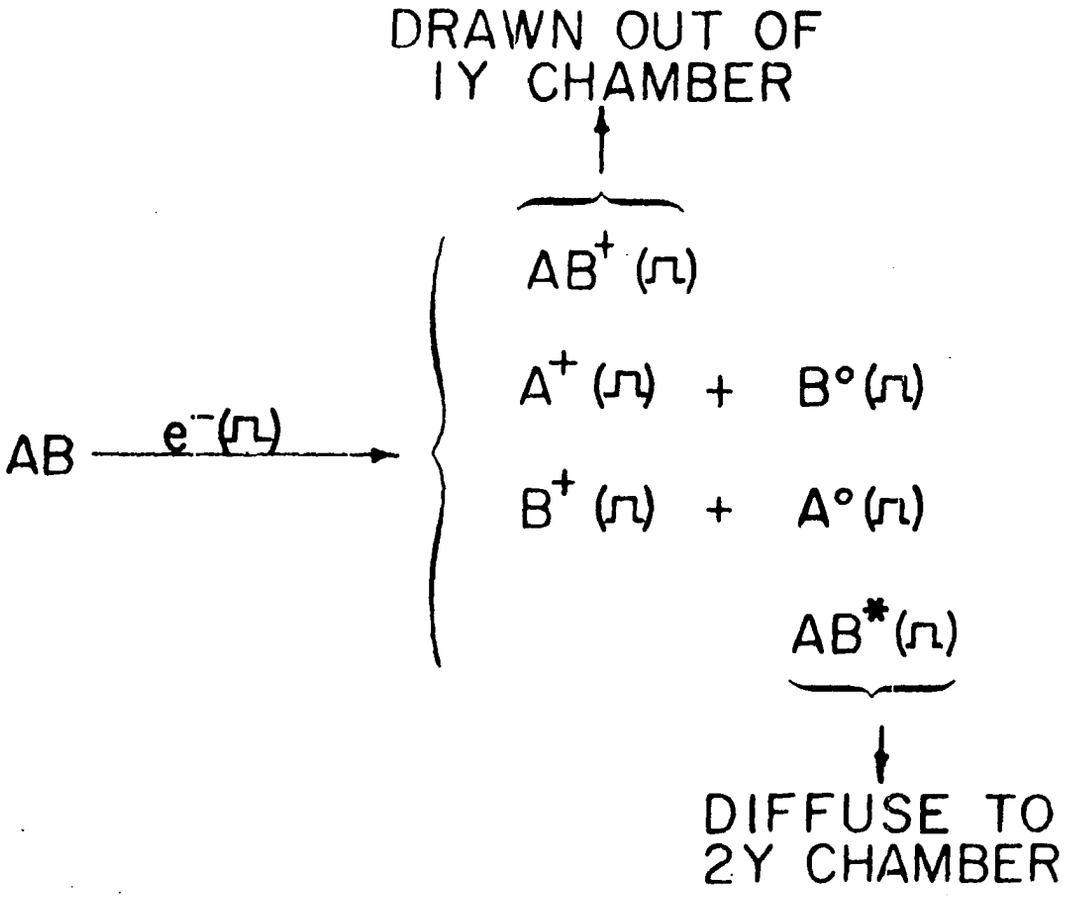

Figure 4. Unimolecular processes resulting from the interaction of neutral species with the secondary electron beam to produce the two components of positive ion current

# SECONDARY CHAMBER PROCESSES

$$AB \xrightarrow{e^-} \begin{cases} AB^+ \\ A^\circ + B^+ \\ B^\circ + A^+ \end{cases}$$

DC COMPONENT OF 2Y OUTPUT

$$AB^*(\sqcap) \xrightarrow{e^-} \begin{cases} AB^+(\sqcap) \\ A^\circ + B^+(\sqcap) \\ B^\circ + A^+(\sqcap) \end{cases}$$

$$A^\circ(\sqcap) \xrightarrow{e^-} A^+(\sqcap)$$

$$B^\circ(\sqcap) \xrightarrow{e^-} B^+(\sqcap)$$

AC COMPONENT OF 2Y OUTPUT

Because of the high ion source potentials ($\sim$ 2KV) required for operation of a magnetic sector mass spectrometer, Preston, Tsuchiya, and Svec (31) failed to satisfactorily solve problems they encountered in pulsing the primary electron beam and in eliminating extraneous phase-sensitive output signals which presumably resulted from pickup of the pulse signal by other ion source components. Thus, the decision was made to utilize a quadrupole mass filter in this work, since solution of those problems would be facilitated because of the low ion source potentials (< 50V) required for its operation. In addition, the quadrupole mass spectrometer offered advantages in sensitivity over a magnetic sector instrument.

The configuration of the mass spectrometer developed for detecting and characterizing neutral fragments is shown schematically in Figure 5. Both components of positive ion current produced in the secondary ionization chamber of the dual ionization chamber ion source are focussed into the quadrupole mass filter, where they are mass analyzed. Those ions having the proper mass/charge ratio are focussed by the mass filter and exit to the deflector, which deflects them to the first dynode of a 17-stage Cu-Be electron multiplier. The purpose of the deflector is to eliminate any direct optical path between the ion source and the first dynode of the electron multiplier.

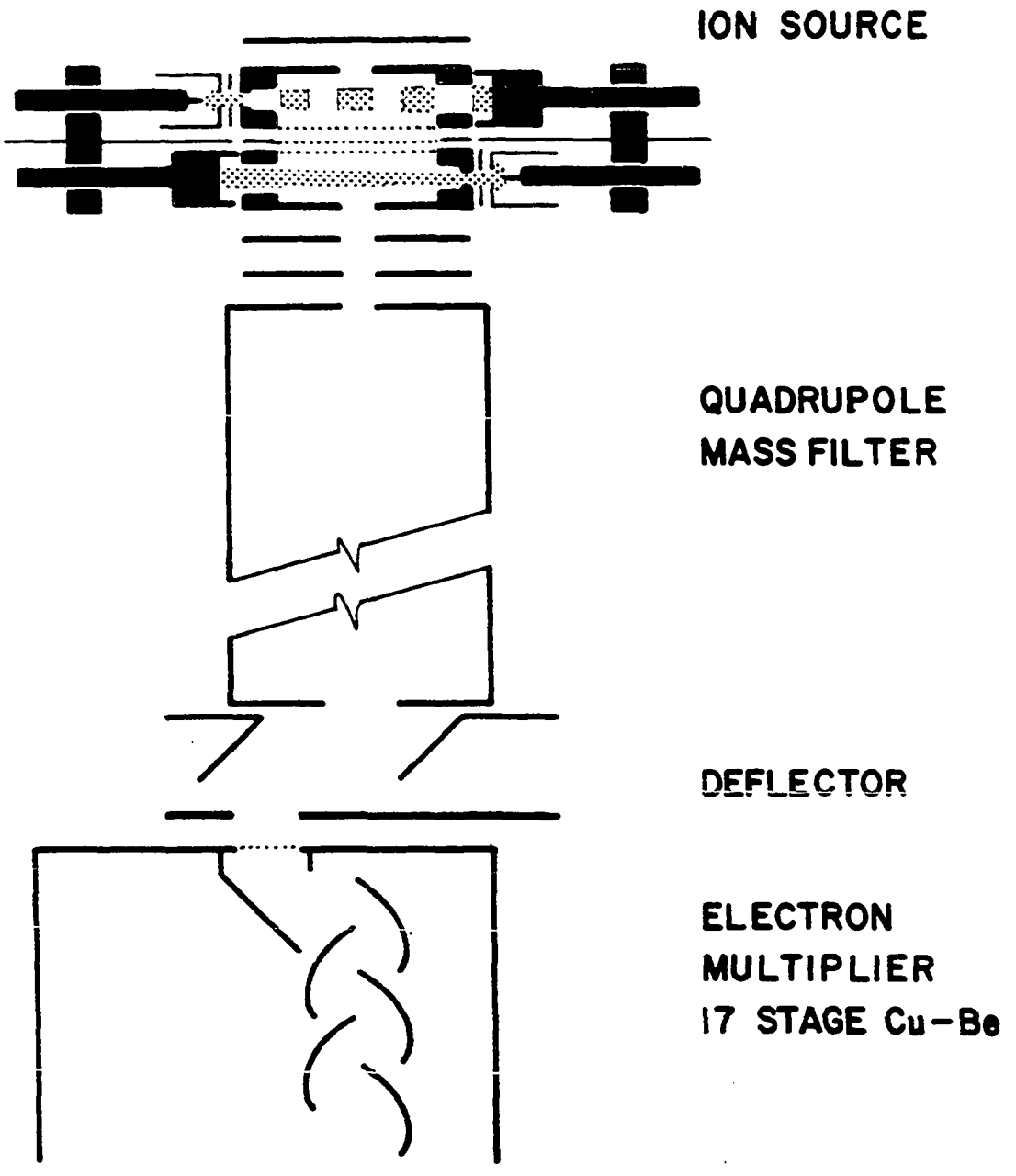


Figure 5. Configuration of the physical components of the quadrupole mass spectrometer for detecting neutral species

The electron multiplier amplifies the positive ion current which strikes its first dynode by a factor of $10^5$ to $10^6$, and the resulting anode current is processed by the signal output circuitry shown as a block diagram in Figure 6. The anode current from the electron multiplier is processed by a preamplifier which converts the current to a voltage, amplifies it, and separates the resulting electrical signal into its ac and dc components. The dc component is recorded directly as the normal mass spectrum of the sample gas, while the ac component is processed by a lock-in amplifier whose output is recorded as the neutral fragment mass spectrum of the sample gas.

A more detailed description of the physical and electrical components of the instrument and their individual roles follows below.

## B. Physical Components

### 1. Vacuum system

The main vacuum chamber (Figure 7), which houses all of the physical components of the quadrupole mass spectrometer, was designed to provide easy access to the various components and consists of two main parts, the vacuum chamber base and the vacuum chamber cover. The vacuum chamber base consists of a 10 1/2 in. i.d., 16 gauge stainless steel cylinder fitted with four 1 1/2 in. o.d. ports and a 1/4 in. o.d.

Figure 6. Block diagram of the modified output signal circuitry

# SCHEMATIC DIAGRAM OF OUTPUT SIGNAL CIRCUITRY

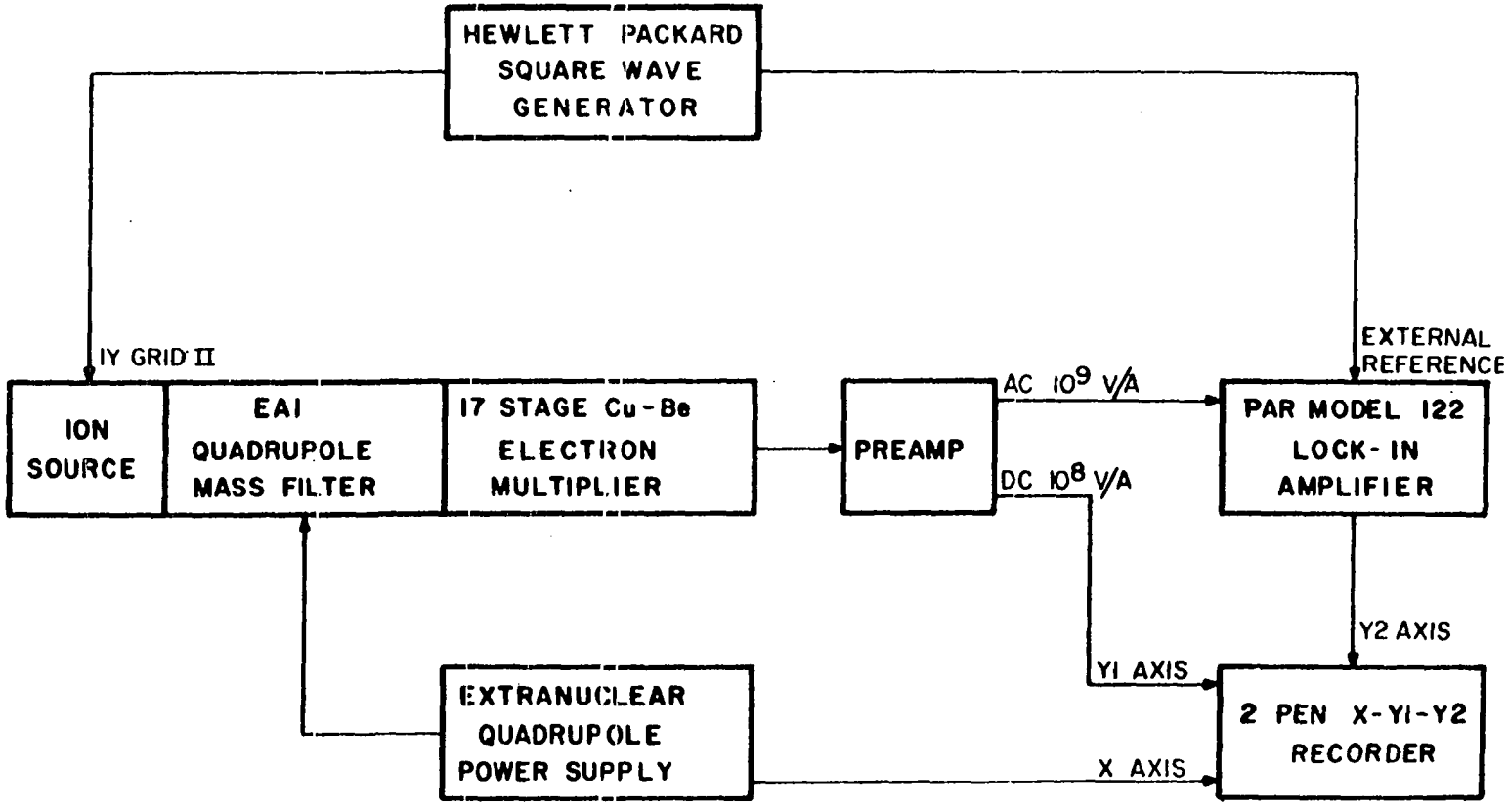

stainless steel nipple. The four 1 1/2 in. o.d. ports are fitted with 1 1/2 in. Curvac rotatable flanges (Perkin-Elmer, Ultek Division) for attaching various vacuum system components (Figure 7). The main vacuum chamber is evacuated by means of a 150 liter/sec air-cooled oil (Dow-Corning Silicon 704) diffusion pump (Vacuum Instrument Corporation Model DA-100) supplemented at pressures less than $10^{-5}$ Torr by an 8 liter/sec ion pump (Varian Model 911-1402) attached to a separate port. Contamination of the main vacuum chamber by the diffusion pump oil is prevented by a 3 in. o.d. x 1 1/2 in. i.d. glass cold trap (liquid $N_2$ cooled) between the main vacuum chamber and the diffusion pump. A 1 1/2 in. i.d., bellows sealed valve (Veeco R150S) between the main vacuum chamber and the glass cold trap is utilized to isolate the main vacuum chamber from the diffusion pump and cold trap to facilitate maintenance. Rough pumping of the main vacuum chamber is accomplished by means of a mechanical pump (Welch 1400) connected through a third port. During normal operation, the mechanical pump is isolated from the main vacuum chamber by a 3/4 in. i.d. bellows-sealed valve (Veeco R62S). The fourth 1 1/2 in. o.d. port accommodates the cold finger whose function is to condense sample gases immediately after they traverse the primary ionization chamber of the ion source. The cold finger consists of a 1 1/4 in. o.d. x 3 in. stainless steel reservoir mounted on a 3/8 in. o.d. dual liquid nitrogen feedthrough (Perkin-Elmer, Ultek Division).

A 1/8 in. o.d. stainless steel tube fed through the 1/4 in. o.d. nipple on the bottom of the vacuum chamber base transmits gas samples from the inlet system to the ion source. O-ring quick-connect fittings (Central Scientific Company) provide a vacuum seal between the 1/8 in. o.d. tube and the 1/4 in. o.d. nipple.

The main vacuum chamber cover (Figures 7-9) on which all of the physical components of the quadrupole mass spectrometer are mounted, is sealed to the vacuum chamber base by a 11 1/2 x 11 7/8 x 3/16 in. dia. Viton O-ring. Just as all of the vacuum components of the instrument are connected to the vacuum chamber base, all of the electronic components are interfaced to the mass spectrometer through the vacuum chamber cover. Three 1 1/2 in. o.d. ports through the cover are fitted with 1 1/2 in. Curvac flanges (Figure 8) to accommodate two 8-pin and one 6-pin electrical feedthroughs which transmit electrical potentials to the various components of the ion source and the deflector. Two 1/2 in. o.d. graded seal feedthroughs (Figures 7,8) welded directly to the vacuum chamber cover transmit the RF-DC electrical signals from the quadrupole power supply to the mass filter. The electrical connections to the electron multiplier are supplied by five 1/4 in. o.d. glass graded seal feedthroughs welded to the 4 in. Curvac flange insert to which the electron multiplier is mounted.

The mass filter and ion source are easily exposed for maintenance by removing the vacuum chamber cover from the vacuum chamber base (Figure 9), while access to the electron

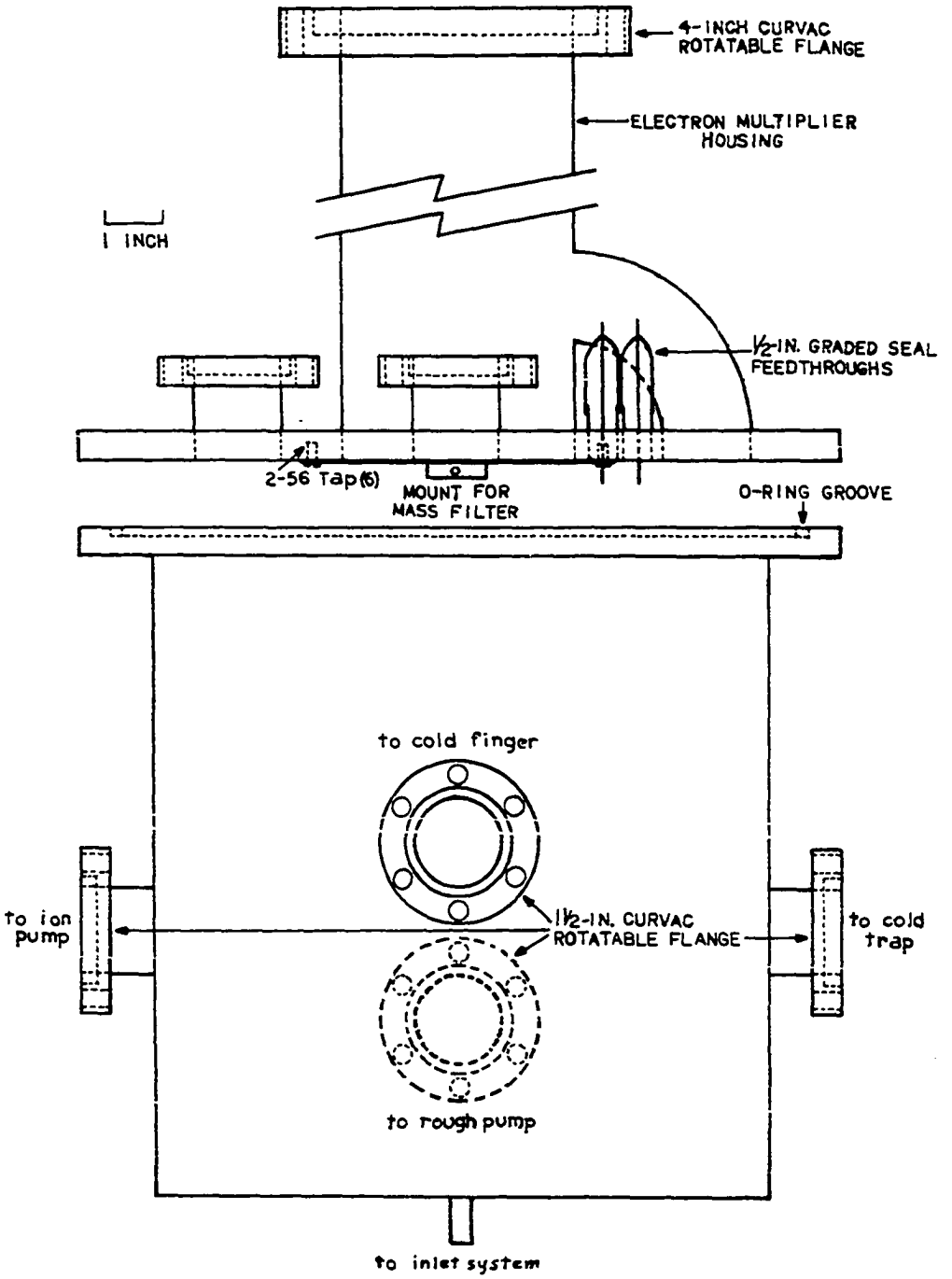


Figure 7. Side view of the main vacuum chamber

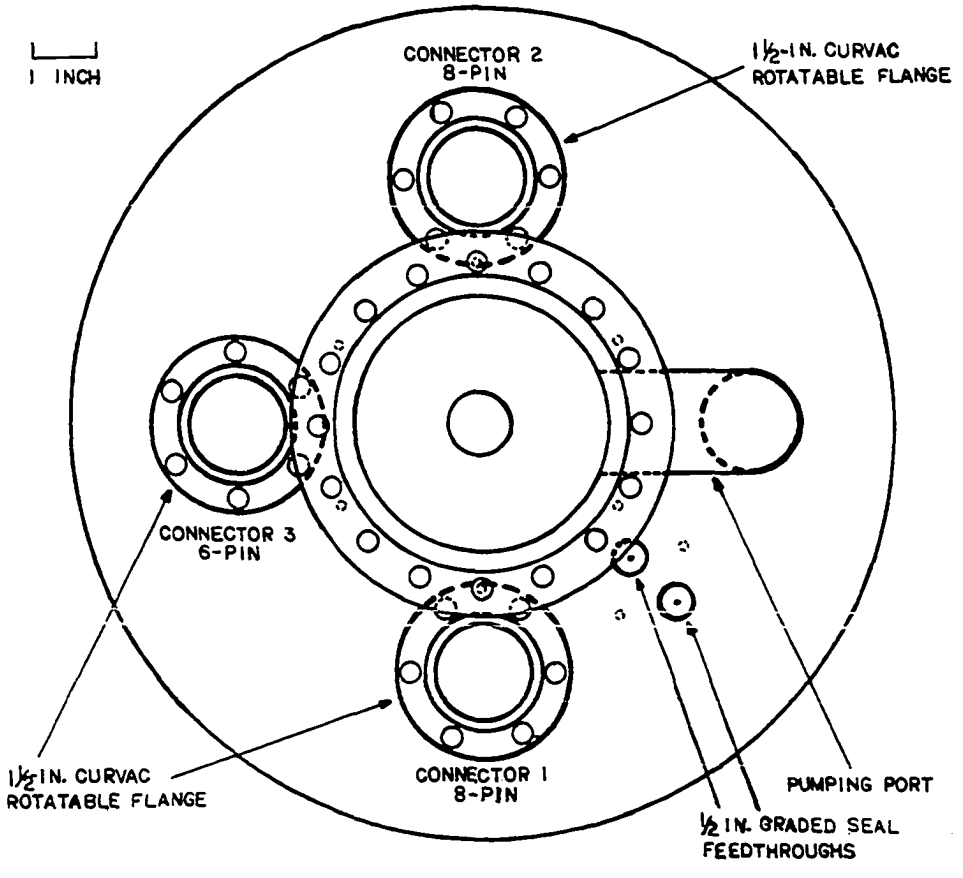


Figure 8. Top view of the vacuum chamber cover

Figure 9. Bottom view of the vacuum chamber cover showing the orientation and mounting details of the various physical components of the mass spectrometer

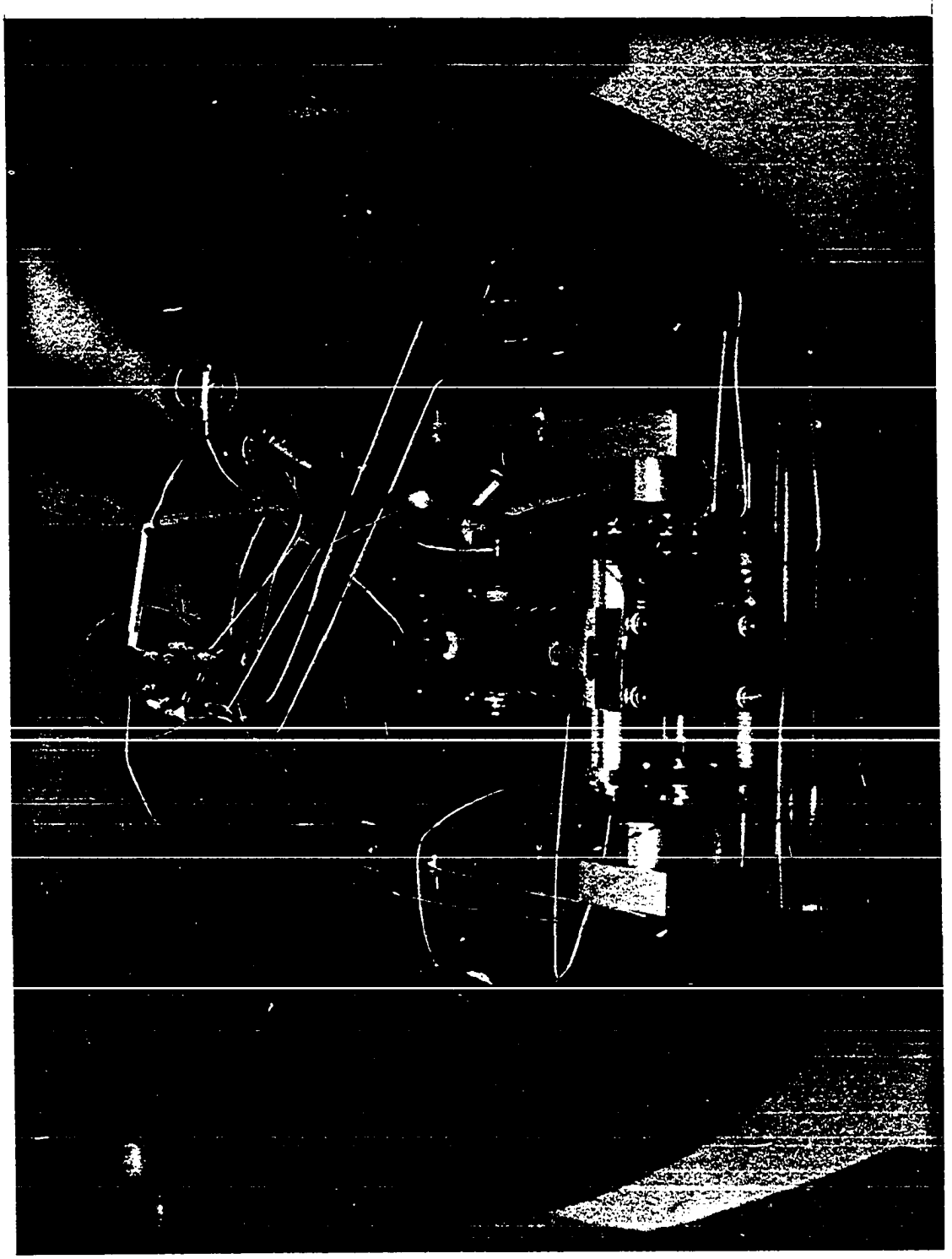

multiplier and deflector is gained by removing the 4 in. Curvac flange on which the electron multiplier is mounted. Thus, the main vacuum chamber design provides for convenient access to all of the physical components of the mass spectrometer, an important, time-saving feature while the instrument was in the developmental stage.

2. Inlet system

The inlet system (Figure 10) provides for introducing solid, liquid, and gas samples with a wide range of vapor pressures into the vacuum system and transferring the resulting vapors to the primary reaction chamber of the ion source at a constant rate. The inlet system is pumped by a water-cooled oil diffusion pump (Consolidated Vacuum Corp.) and the pressure at the diffusion pump throat is monitored by means of a thermocouple vacuum gauge (Hastings-Raydist, Inc. Model GV-3RS).

Gas samples are transferred from sample bulbs to the initial expansion volume ($\sim$ 50 $cm^3$) through stopcocks $S_1$ and $S_2$, while volatile liquid samples are inserted directly through the mercury reservoir (Figures 10,11) using a 5 µl capillary pipet. Aliquots ($\sim$ 1 $cm^3$) of the sample in the initial expansion volume are transferred to the final expansion volume ($\sim$ 700 $cm^3$) by means of stopcock $S_3$ to achieve the desired sample flow rate through the gold foil leak to the mass spectrometer.

In performing experiments during which the sample pressure is varied, the number of aliquots of sample transferred

Figure 10. Block diagram of the inlet system

$V_1$: Veeco 3/4 in. bellows-sealed valve (R62S)

$V_2$-$V_5$: Hoke 1/8 in. bellows-sealed valve (4171M2B)

$V_6$: Nupro Series M fine metering valve (SS4MA)

$S_1$, $S_2$: 2 mm bore vacuum stopcock

$S_3$: 3 mm bore Tee stopcock

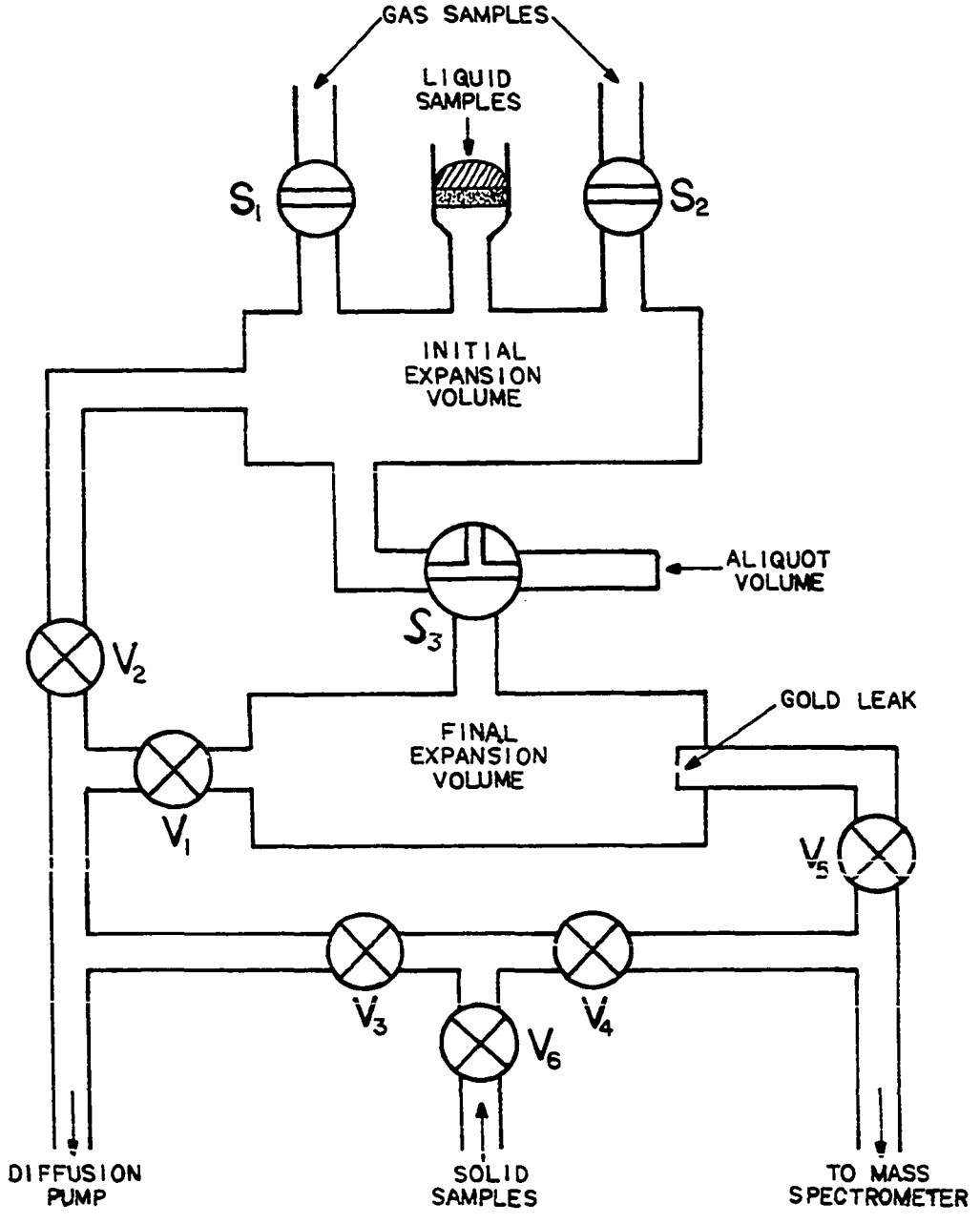
GAS SAMPLES
LIQUID SAMPLES
S1
S2
INITIAL EXPANSION VOLUME
ALIQUOT VOLUME
S3
V2
GOLD LEAK
FINAL EXPANSION VOLUME
V1
V5
V3
V4
V6
DIFFUSION PUMP
SOLID SAMPLES
TO MASS SPECTROMETER

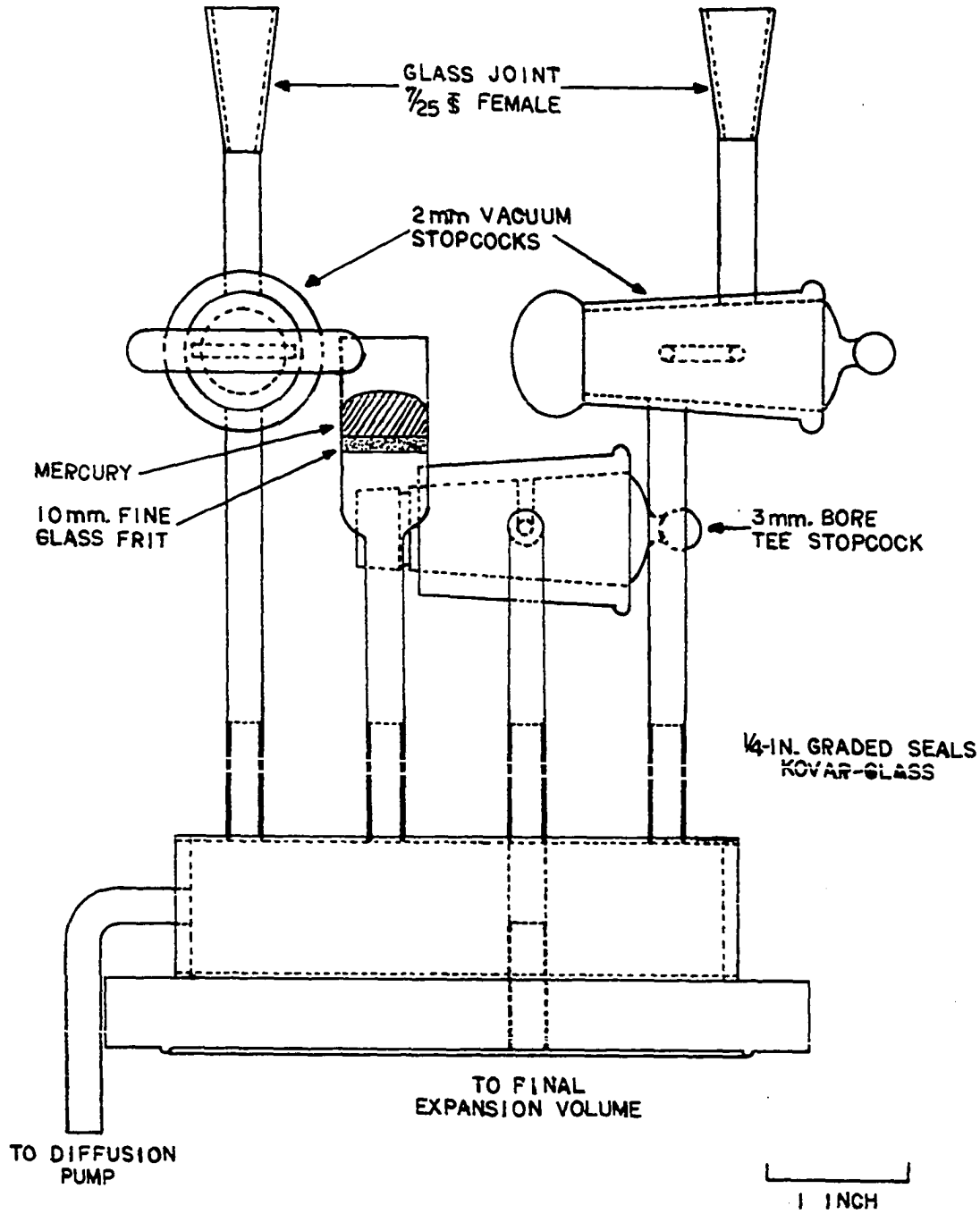


Figure 11. Side view of the inlet system cover

to the final expansion volume provides a convenient measure of the relative sample pressure in the final expansion volume (and the ion source). However, it is desirable to eliminate or at least minimize errors resulting from the reduced amount of sample transferred in each subsequent aliquot. With gas samples, these errors are minimized by attaching a large evacuated sample bulb to stopcock $S_1$ or $S_2$ before introducing the sample to increase the effective volume of the initial expansion volume. With volatile liquid and solid samples, an alternate method of transferring a constant amount of sample in each aliquot is employed. In these cases, a sample bulb containing an excess of the liquid or solid sample is attached to stopcock $S_1$ or $S_2$, and the pressure of the sample in the initial expansion volume is maintained at its equilibrium vapor pressure for the duration of the experiment.

Those solid and liquid samples with too low volatility to be admitted through the gold foil leak can be introduced by allowing their vapors to flow directly to the mass spectrometer through metering valve $V_6$. Although this method of introducing samples extends the range of volatility which can be accommodated, sample flow rates are difficult to reproduce and are not conveniently measured. Thus, the metering valve ($V_6$) is used only with those samples with too low volatility to be introduced through the gold foil leak.

Because the gain of the Cu-Be electron multiplier deteriorates with extended exposure to air, the inlet system was designed to be utilized as a convenient vacuum storage container for the electron multiplier when the instrument was being repaired or modified. The inlet system, like the main vacuum chamber, consists of two main components, the inlet system base and the inlet system cover. The inlet system base constitutes the final expansion volume of the inlet system and consists of a 4 in. o.d. x 9 in. stainless steel cylinder fitted with two ports; a 3/4 in. o.d. port to which valve $V_1$ is soldered and a 1 1/2 in. o.d. port to which the gold foil leak is attached by means of a 1 1/2 in. Curvac rotatable flange. A 5 in. o.d. x 4 in. i.d. x 1/2 in. thick stainless steel plate welded to the top of the inlet system base has a polished surface to which the inlet system cover is sealed by means of a flat Viton gasket.

The inlet system cover (Figures 11,12) consists of a 5 in. o.d. x 1/2 in. thick stainless steel plate with a raised lip on its underside which has the same dimensions as that of the 4 in. Curvac flange insert to which the electron multiplier is attached. Various components of the inlet system are welded to the top of the inlet system cover (Figures 11,12), including stopcocks $S_1$, $S_2$, and $S_3$, the mercury seal through which liquid samples may be inserted, and the initial expansion volume, to which valve $V_2$ is connected by means of

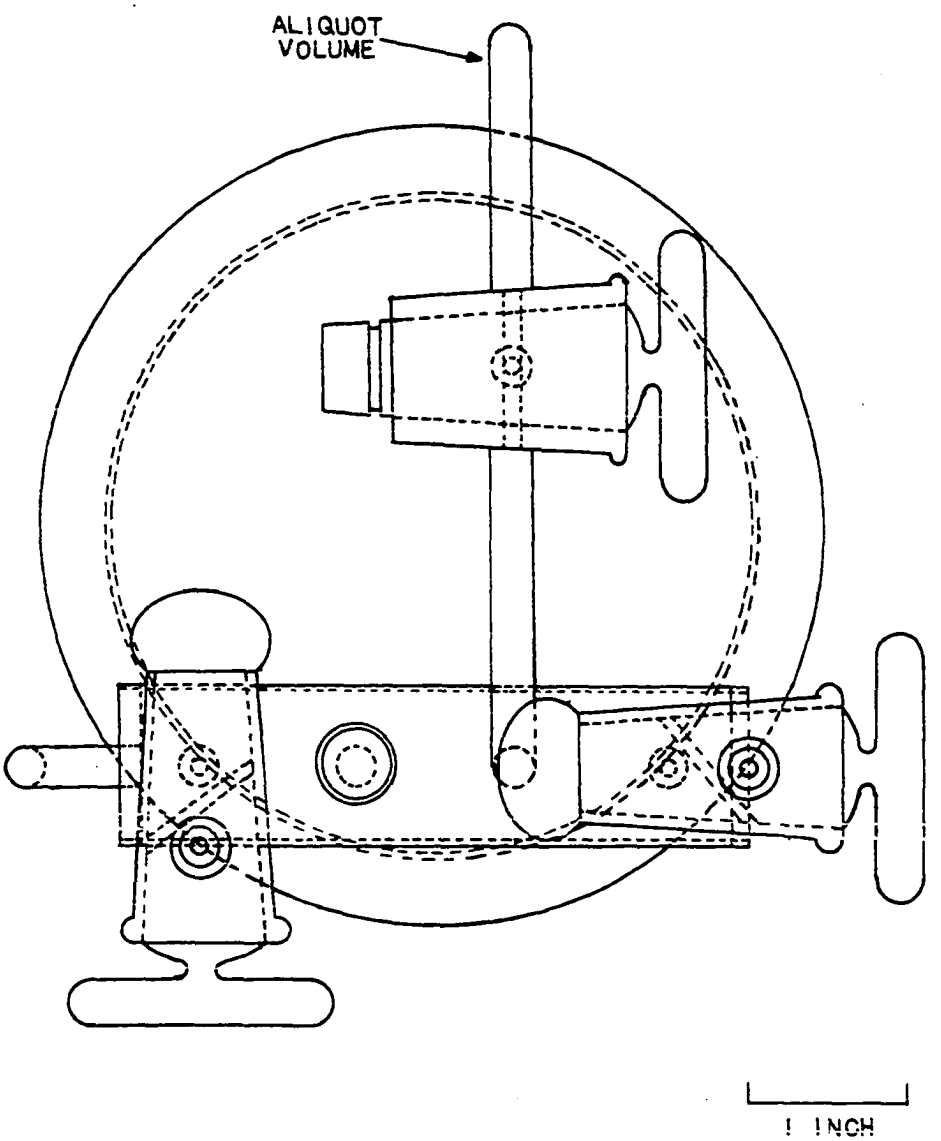


Figure 12. Top view of the inlet system cover

a 1/4 in. O-ring quick-connect fitting. By simply disconnecting this O-ring fitting, replacing the inlet system cover with the electron multiplier, and evacuating the final expansion volume through valve $V_1$, the electron multiplier can be conveniently stored under vacuum.

3. Electron multiplier

The detector for the positive ions which are focussed through the mass filter is a 17-stage Cu-Be electron multiplier (Balzers High Vacuum Corp., Model SEV 317) which amplifies the positive ion current striking its first dynode by a factor (gain) which depends on the potential applied across the dynode resistor string. As supplied, the electron multiplier has a minimum gain of $10^8$ at 3.5 KV, but the gain deteriorates rapidly with use and exposure to moisture to a stable but significantly lower value (Figure 13) of approximately $5 \times 10^6$ at 3.5 KV.

Since the electron multiplier has a large entrance slit which is mounted close to the exit aperture of the deflector, a tungsten wire (0.001 in.) grid (92% transparent) was spot-welded over the multiplier entrance slit (Figure 5) to prevent distortion of the electric fields in the vicinity of the first dynode.

The electron multiplier is mounted on a Mycroy block (Figure 14) by means of tubular stainless steel studs (3-48) which, after being screwed through the Mycroy block, are

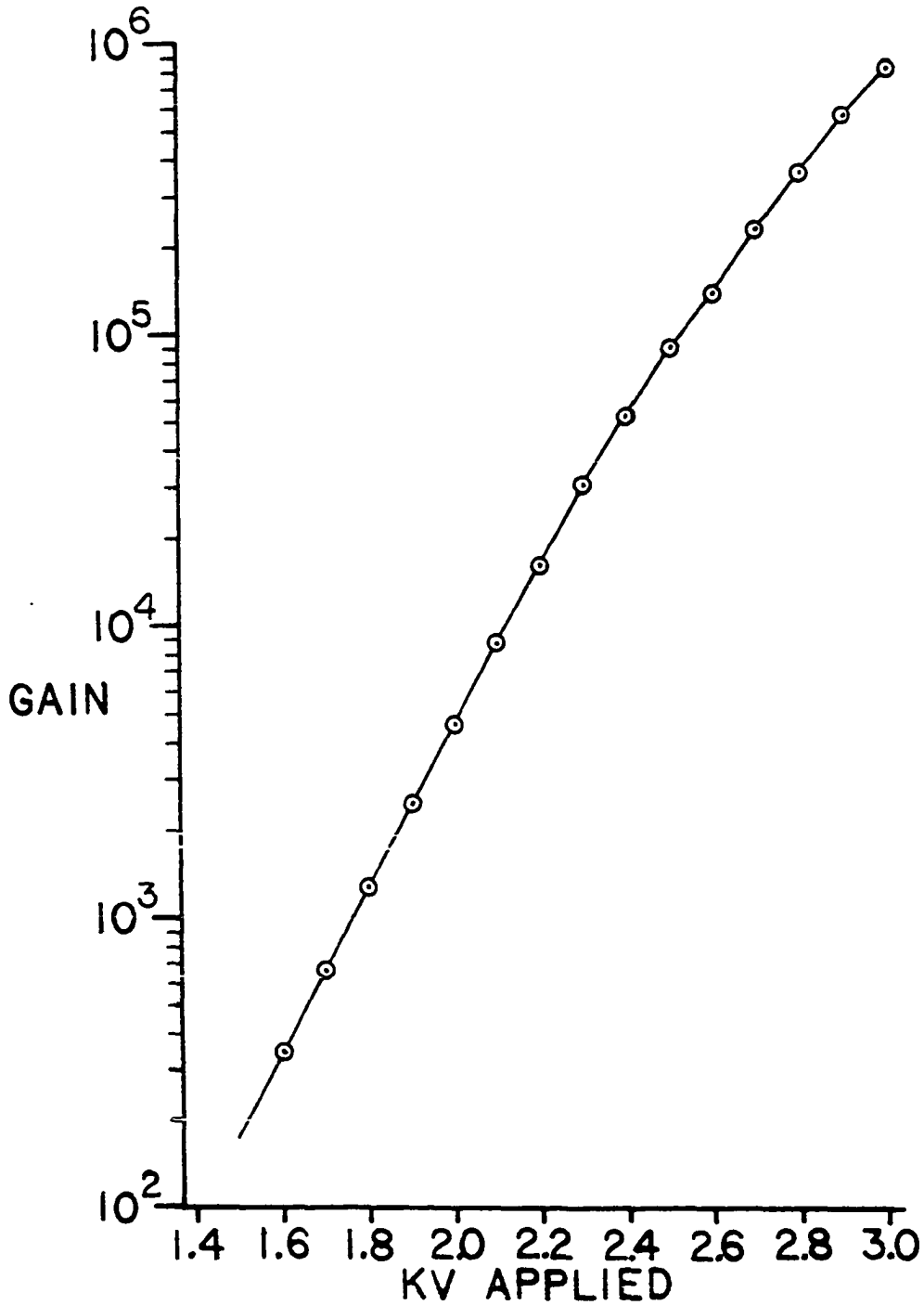


Figure 13. Plot of multiplier gain versus applied voltage. Data were taken after the multiplier had been in use for several months

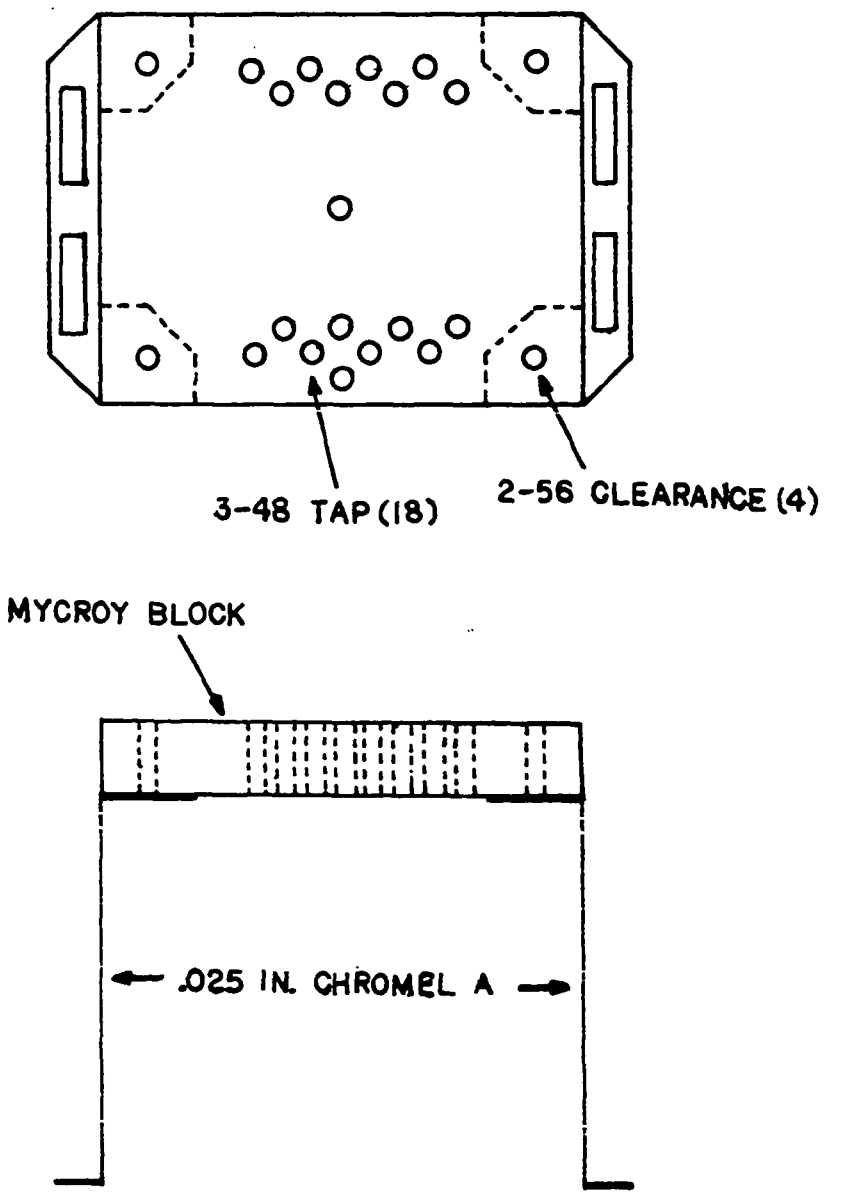


Figure 14. Mount for electron multiplier. Slotted brackets allow the electron multiplier to be offset up to 0.5 in.

crimped to the multiplier leads. The free ends of the tubular studs are used for connecting the bleeder chain resistors and electrical leads to the electron multiplier. A pair of mounting brackets (Figure 14) for attaching the Mycroy block to the 4 in. Curvac flange insert are designed so that the electron multiplier may be offset by up to 1/2 in. from the center of the flange insert. The combination of rotation of the flange insert and offsetting of the electron multiplier provide a convenient means of aligning the entrance slit of the electron multiplier with the exit aperture of the deflector.

4. Deflector

In order to eliminate any direct optical path between the ion source and the first dynode of the electron multiplier, the electron multiplier is mounted off-axis. An ion deflector inserted between the exit aperture of the mass filter and the entrance slit of the electron multiplier (Figure 5) serves to deflect the positive ions off-axis so that they may be accelerated to the first dynode of the electron multiplier.

The deflector consists of three electrodes fabricated from 0.010 in. Chromel A sheet and is attached by means of 0-80 stainless steel studs to the back side of the 5.5 in. dia. Chromel disc which serves as the mount for the mass filter. Borosilicate glass stud sleeves and machined lava

spacers serve to isolate electrically the electrodes from each other and from ground. Electrodes A and B (Figure 15), which are parallel and form a 45° angle with respect to the path of the entering ions, direct the ions to the offset exit aperture on electrode C. A platinum black surface on electrode C opposite the exit aperture of the mass filter (Figure 15) serves to absorb any photons originating in the ion source and traversing the mass filter.

During normal operation, electrodes B and C are grounded externally, and a positive potential is applied to electrode A. The deflector is tuned by focussing $N_2^+$ ions (m/e = 28) through the mass filter and adjusting the potential applied to electrode A to maximize the output current from the electron multiplier.

The deflector may also be used as a collector for the positive ions exiting the mass filter. This is done by grounding electrodes A and B, applying a negative potential to electrode C, and monitoring the positive ion current striking electrode C with an electrometer. By comparing the current collected in this manner with the output current of the electron multiplier under normal deflector operation, the gain of the electron multiplier-deflector combination can be established. If the gain of the electron multiplier is known, the transmission efficiency of the deflector can be determined.

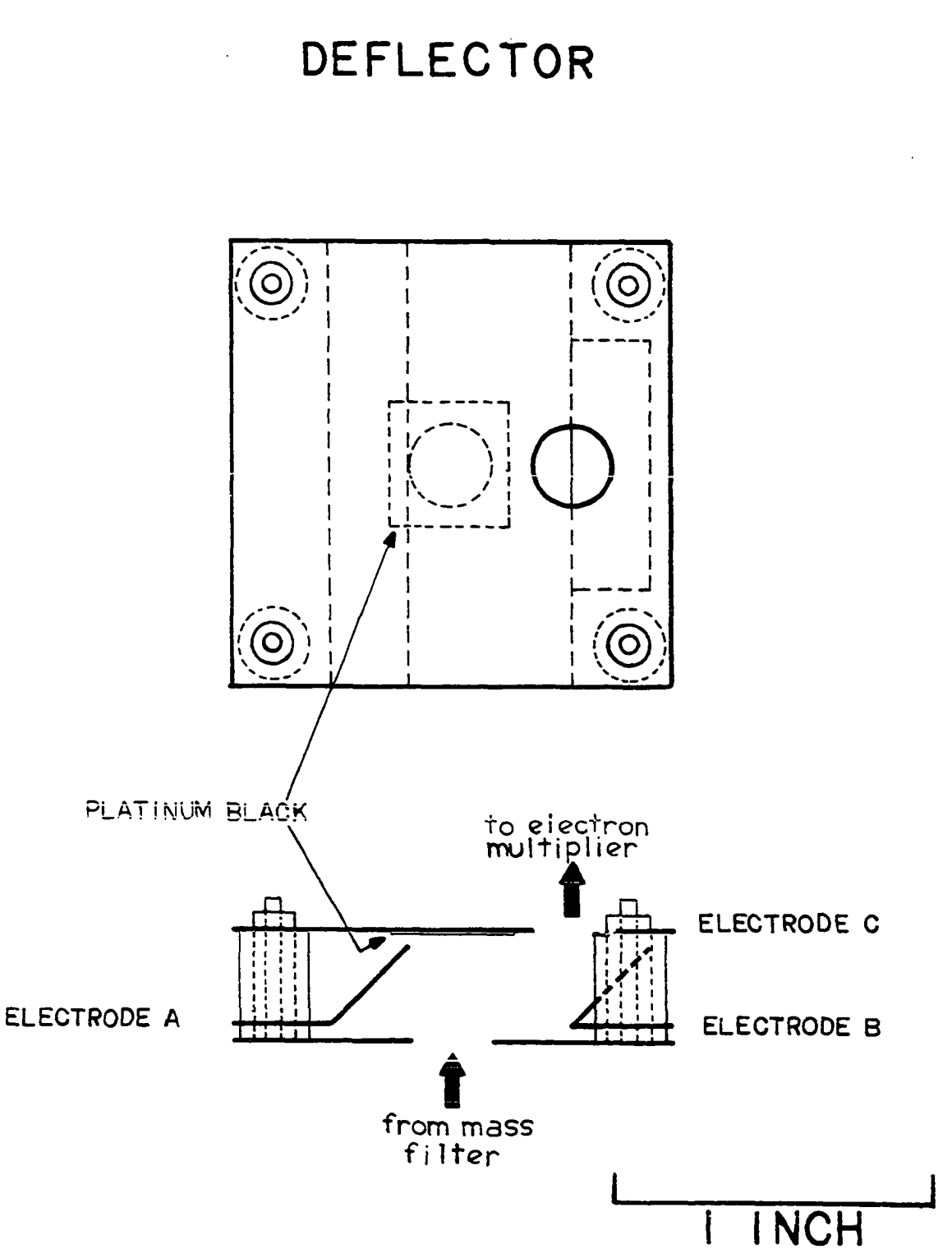


Figure 15. Configuration of the deflector. Normally, electrodes B and C are grounded, and a positive potential is applied to electrode A

5. Mass filter

The quadrupole mass filter (Electronics Associates Inc., Model S1P-224A Quad 150A) utilized in this instrument consists of four precision-machined 5 in. x 1/4 in. dia. stainless steel rods mounted on ceramic insulators. The quadrupole rods are parallel and their centers are equally-spaced on a 1/2 in. circle. Opposite quadrupole rods are connected electrically, creating two electrical pairs. The four quadrupole rods and their ceramic insulators are encased in a stainless steel housing which provides electrical shielding. As supplied, this mass filter is limited to a resolution of $\sim$ 150 amu.

6. Ion sources

Three basic ion sources were designed, constructed, and tested during the development of this instrument. The three ion sources are described in the order in which they were developed and, in order to simplify discussion, are labelled as ion source I, ion source II, and ion source III.

Ion source I (Figures 16-19), the first dual ionization chamber ion source designed for use with a quadrupole mass filter, is similar in design to that utilized by Preston, Tsuchiya, and Svec (31) in their magnetic sector instrument. The primary and secondary chambers of the ion source are separated by three tungsten (0.001 in.) mesh grids (Figure 16), each of which is 92% transparent. The grids preserve the

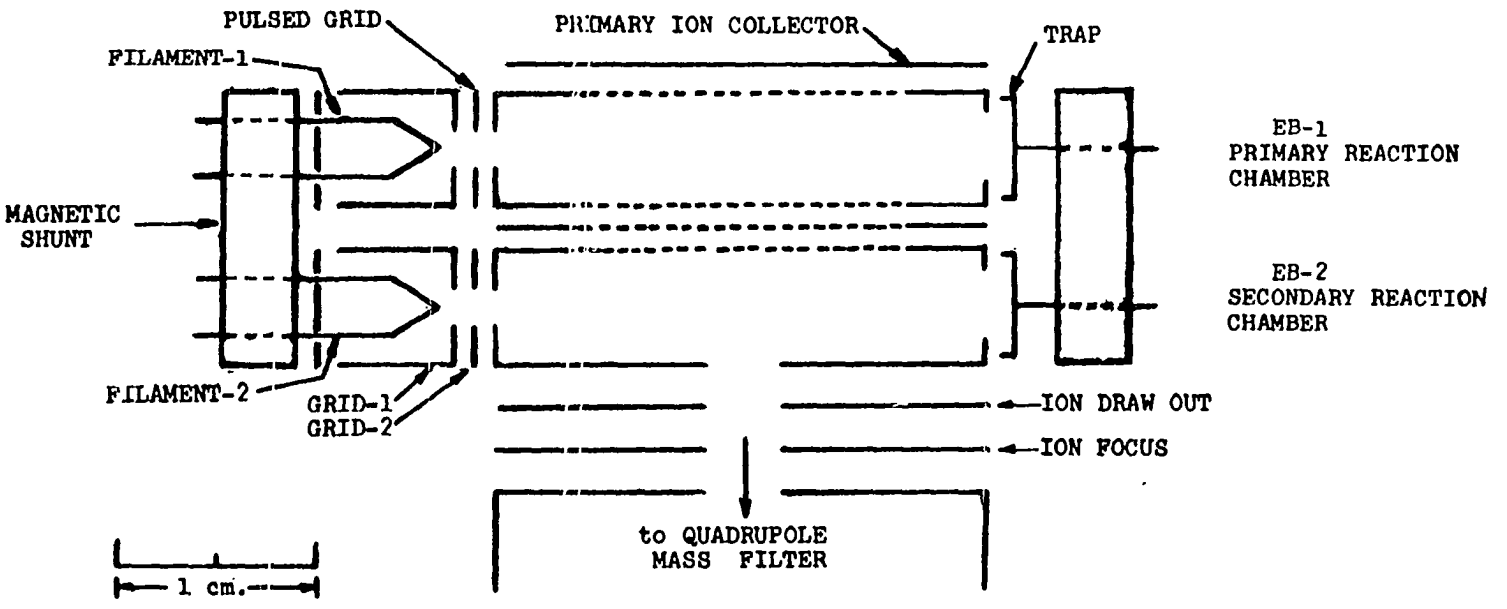


Figure 16. Configuration of ion source I. The distance between the centers of the two electron beams is 0.3 in.

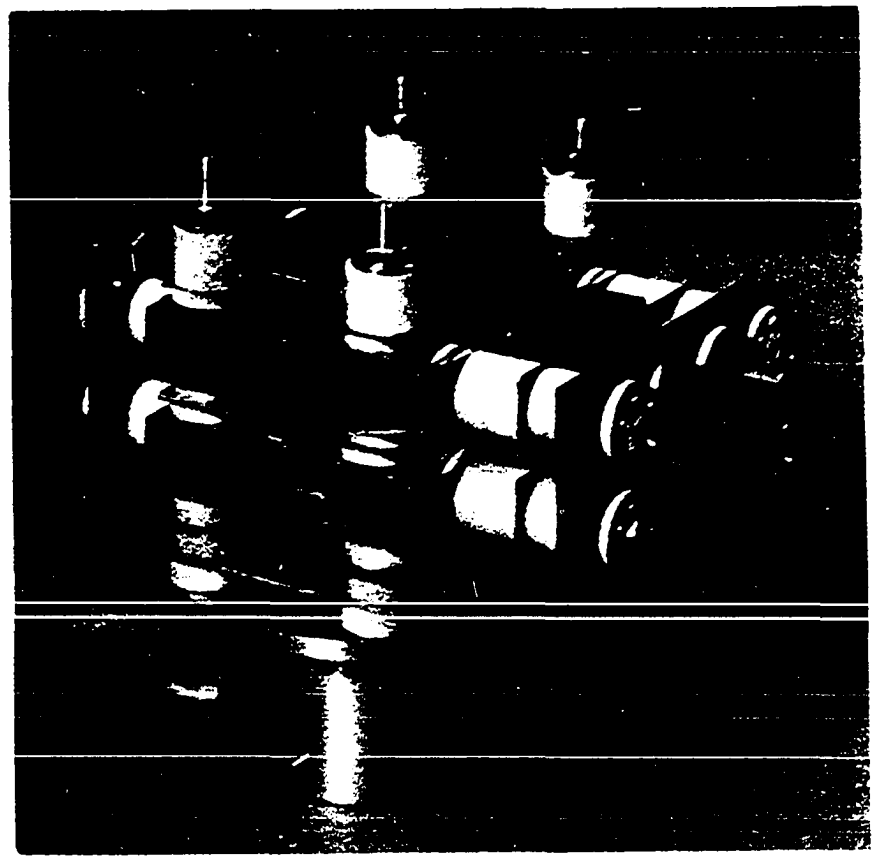

Figure 17. Photograph of ion source I fully assembled

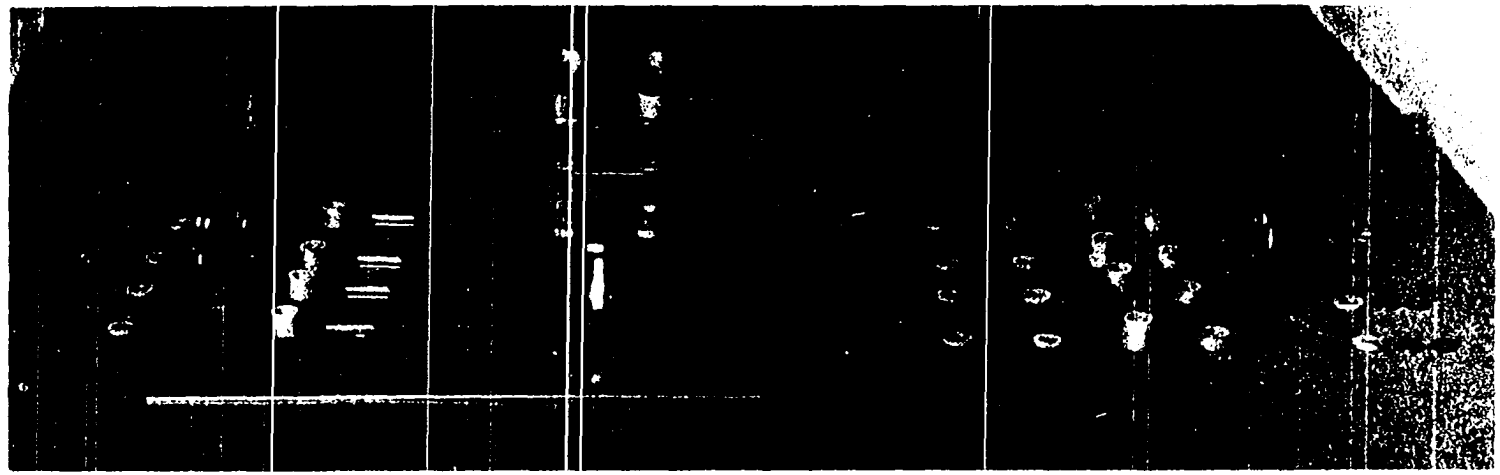

Figure 18. Photograph of ion source I with electron guns disassembled

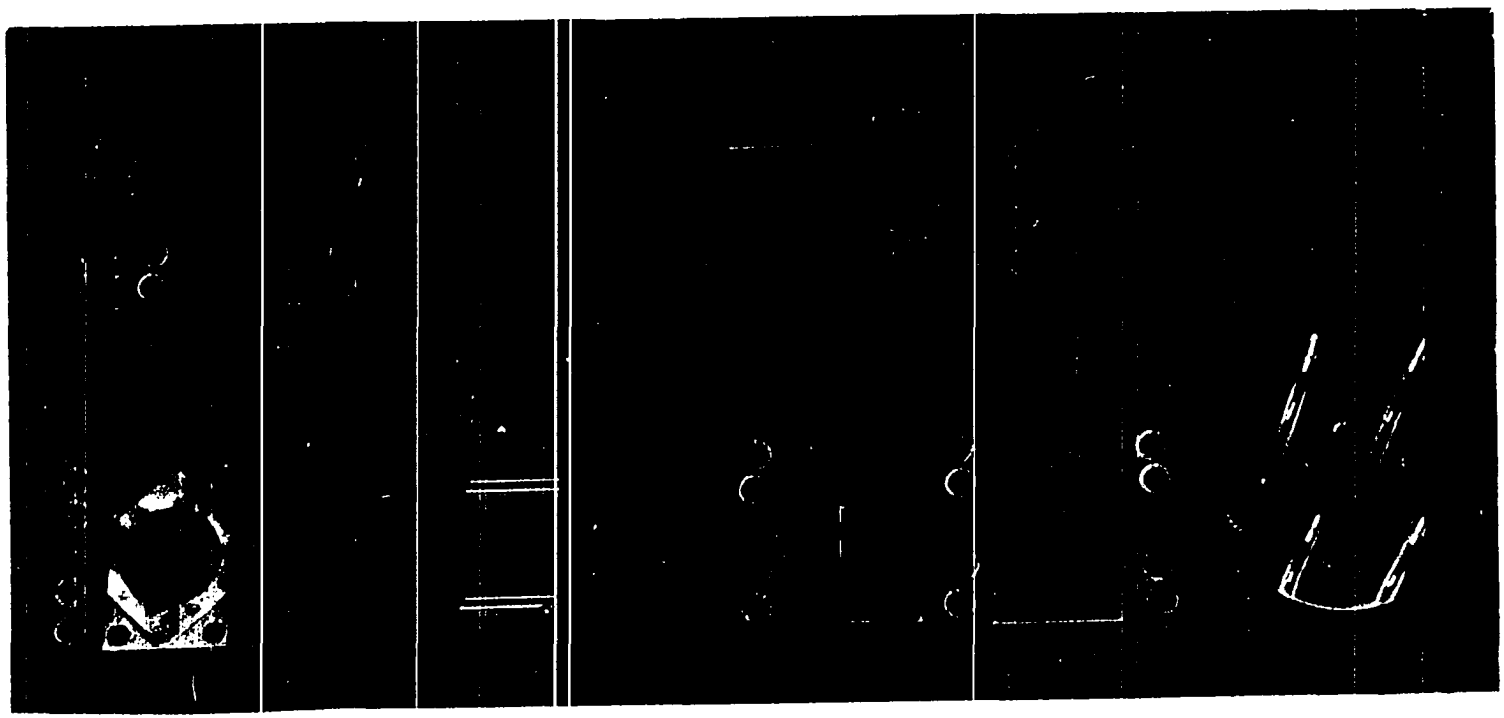

Figure 19. Photograph of ion source I fully disassembled. (For electron gun components, see Figure 18)

integrity of the electric fields in the ion source and prevent transmission of charged particles, while offering minimum resistance to transmission of neutral particles. All of the components of the ion source, with the exception of the magnetic shunts (Figure 16), are fabricated from nonmagnetic stainless steel and are assembled by means of 0-80 stainless steel screws. Glass sleeves and machined lava spacers provide electrical insulation between the various components.

Sample gas molecules are introduced into the primary (1Y) chamber through a 1 mm i.d. glass nozzle perpendicular to the primary electron beam. Multiple passage of the gas molecules through the ion source is prevented by condensing the sample gas molecules on a liquid nitrogen-cooled surface immediately ($\sim$ 4 mm) after they traverse the primary ionization region.

The positive ions produced by the interaction of sample gas molecules with the pulsed primary electron beam are accelerated through a tungsten mesh grid (92% transparent) and collected on the primary ion collector (Figure 16), but the neutral fragments are free to diffuse in any direction. A fraction of the neutral fragments produced diffuses through the three tungsten mesh grids to the secondary ionization chamber, where they interact with the secondary electron beam. The positive ions which result from the interaction of sample gas molecules and neutral fragments

with the secondary electron beam are accelerated out of the ionization region by the secondary drawout electrode and focussed into the mass filter by the secondary KE electrode (focus).

The electron guns are pentodes (Figures 16,18) with two grids between the filament (0.007 in. dia. tungsten wire) and the shield or ionization chamber. In the primary electron gun, a pulsed electron beam is generated by applying a square wave potential to the second grid. The first grid is positive with respect to the filament and prevents space charge build-up in the vicinity of the filament by collecting the electrons emitted during the off-cycle of the pulse. In the secondary electron gun, the two grids act to focus the electron beam efficiently. The filament and trap assemblies of both electron guns are mounted on Armco iron blocks (Figures 16,18) which act as magnetic shunts for the 190 G electron collimating magnet (Figure 9).

With ion source I, the neutral fragment mass spectra of several compounds were successfully scanned and tabulated, including those of neopentane, benzene, and ethanol. Ion source I was also the ion source used for debugging the instrument and from which seven types of phase-correlated output signals were isolated and identified, six of which were extraneous (i.e., not attributed to neutral fragments). As the isolation and identification of these signals will be

described in more detail later, it will suffice at this point to state that one of the phase-correlated signals resulted from pickup of the primary grid II pulse signal by components associated with the secondary ionization chamber. It was in an attempt to eliminate this problem that ion source II was designed and constructed.

Ion source II (Figures 20-22) is very similar in construction to ion source I, but several improvements were incorporated into its design. In an effort to reduce the possibility of pickup of the primary grid II pulse signal by the components of the secondary chamber, the electron guns are opposed, and grounded electrodes have been installed between the components of the two electron guns (Figure 20). The electron guns were also designed for more convenient filament replacement. In ion source I, the electron gun grids are mounted on the same studs as the filament block. Thus, when the filament block was removed and replaced, the grids had to be realigned. However, in ion source II the grids are mounted on separate studs so that their alignment is not altered by filament removal and replacement.

An additional feature of ion source II is the enlarged aperture (Figure 22) through which the sample gas molecules exit the ionization region. The larger aperture reduces the number of molecules reflected from the ion source surfaces and makes condensation on the liquid $N_2$ cooled surface more efficient.

Figure 20. Configuration of ion source II

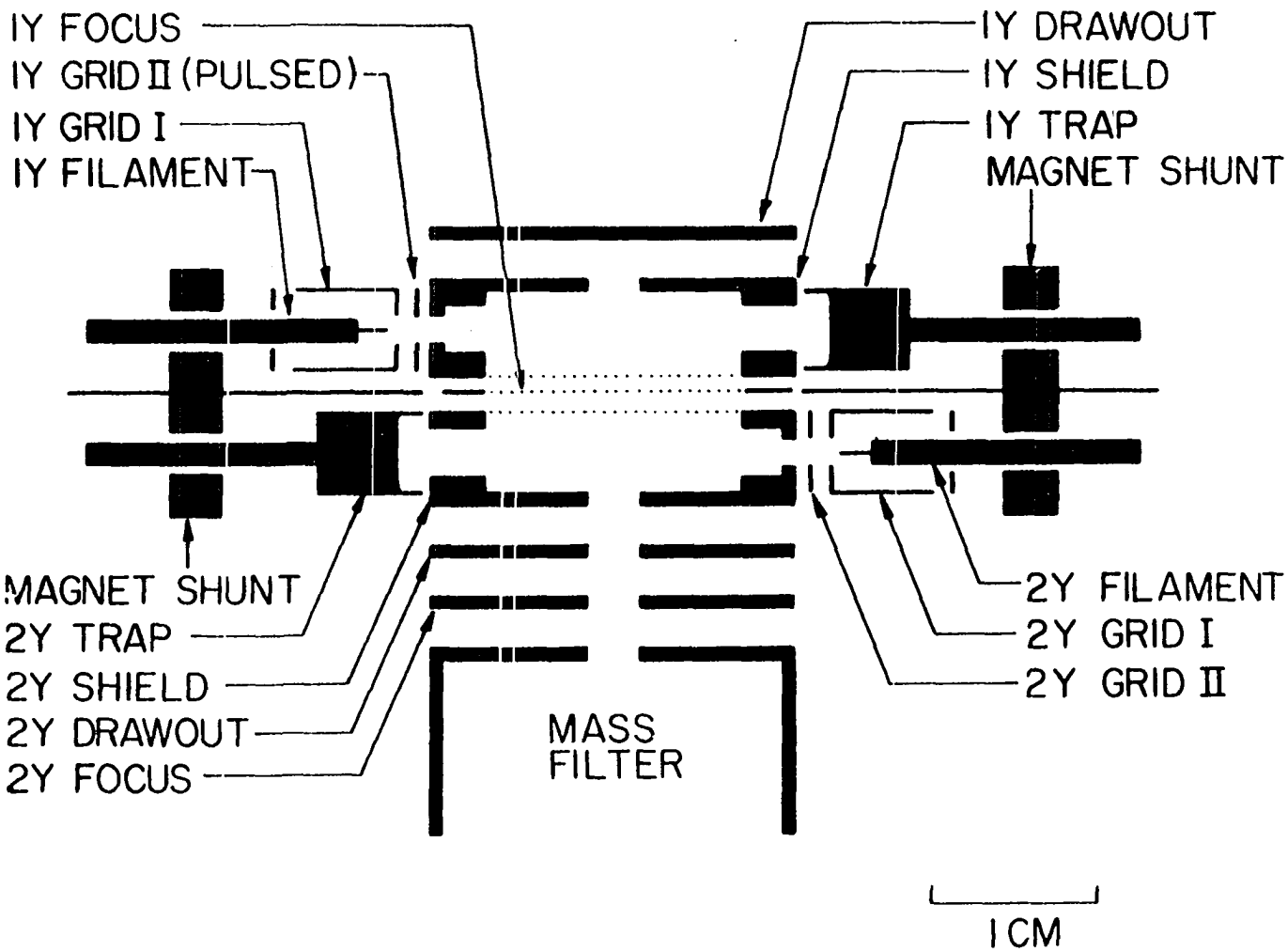
1Y FOCUS
1Y GRID II (PULSED)
1Y GRID I
1Y FILAMENT
1Y DRAWOUT
1Y SHIELD
1Y TRAP
MAGNET SHUNT
MAGNET SHUNT
2Y TRAP
2Y SHIELD
2Y DRAWOUT
2Y FOCUS
MASS FILTER
2Y FILAMENT
2Y GRID I
2Y GRID II
1 CM

Figure 21. Top view of ion source II showing the components of the primary electron gun

Figure 22. Side view of ion source II showing the enlarged exit holes for sample gas molecules to exit the ionizing region and the grounded electrodes between the components of the two electron guns

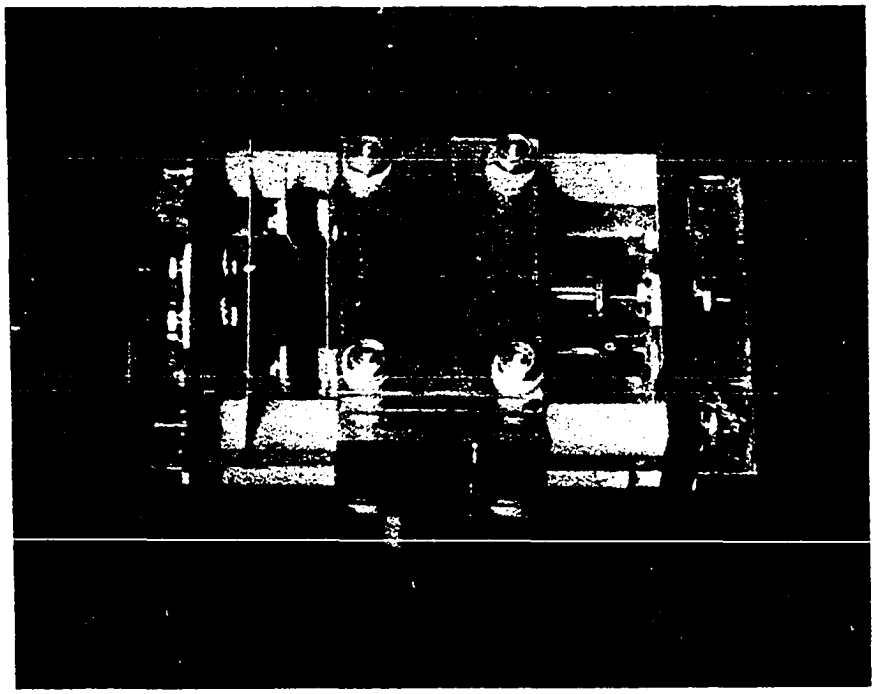

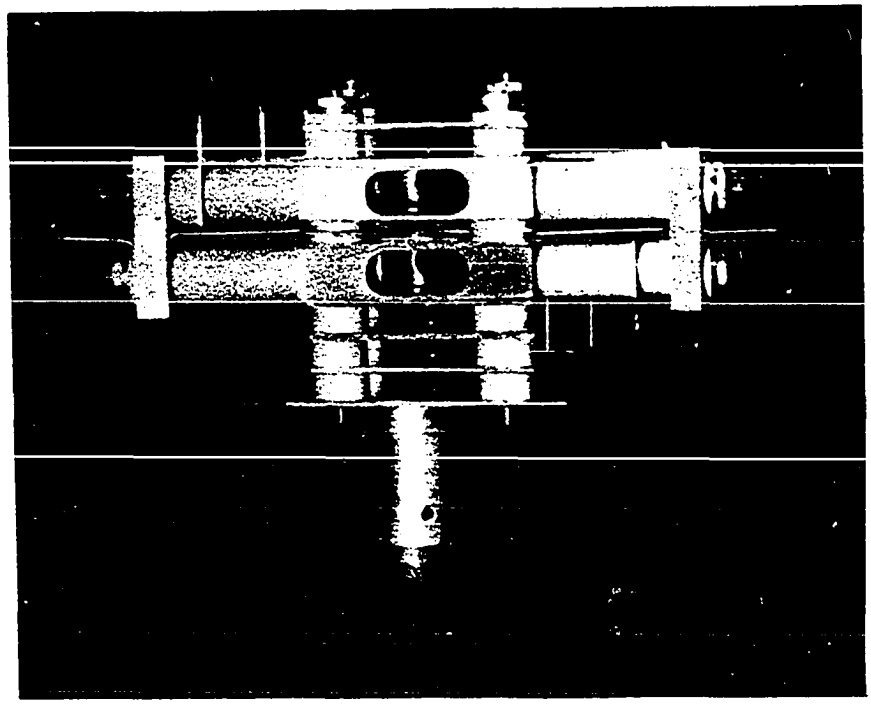

The tungsten mesh grid in ion source I (Figure 16), through which the positive ions formed in the primary reaction chamber are accelerated to the primary drawout plate, has been replaced in ion source II by a solid plate with a 1/8 in. dia. aperture. This permits better control of the electric fields in the primary reaction chamber and results in less distortion of the primary electron beam by the ion drawout field.

The improved design of ion source II succeeded in reducing the pickup problem to a tolerable level. However, problems arising from ion trapping in the secondary electron beam complicated the calibration of the energy of the secondary electron beam, especially at low energies. In order to solve this problem, ion source II was modified, resulting in ion source III (Figure 23). The modification to ion source II consists of removing one of the three tungsten mesh grids which separate the two chambers of the ion source and insulating the remaining two grids from the shield potentials and from each other (Figure 23). By applying the proper potential to the grid closest to the secondary shield (2Y repellor), the ion trapping problem was eliminated.

Ion source III has been successfully utilized to measure neutral fragment mass spectra and neutral fragment ionization potentials and appearance potentials.

Figure 23. Configuration of ion source III. Except for the configuration of tungsten mesh grids between the two ionization chambers, ion source III is identical to ion source II

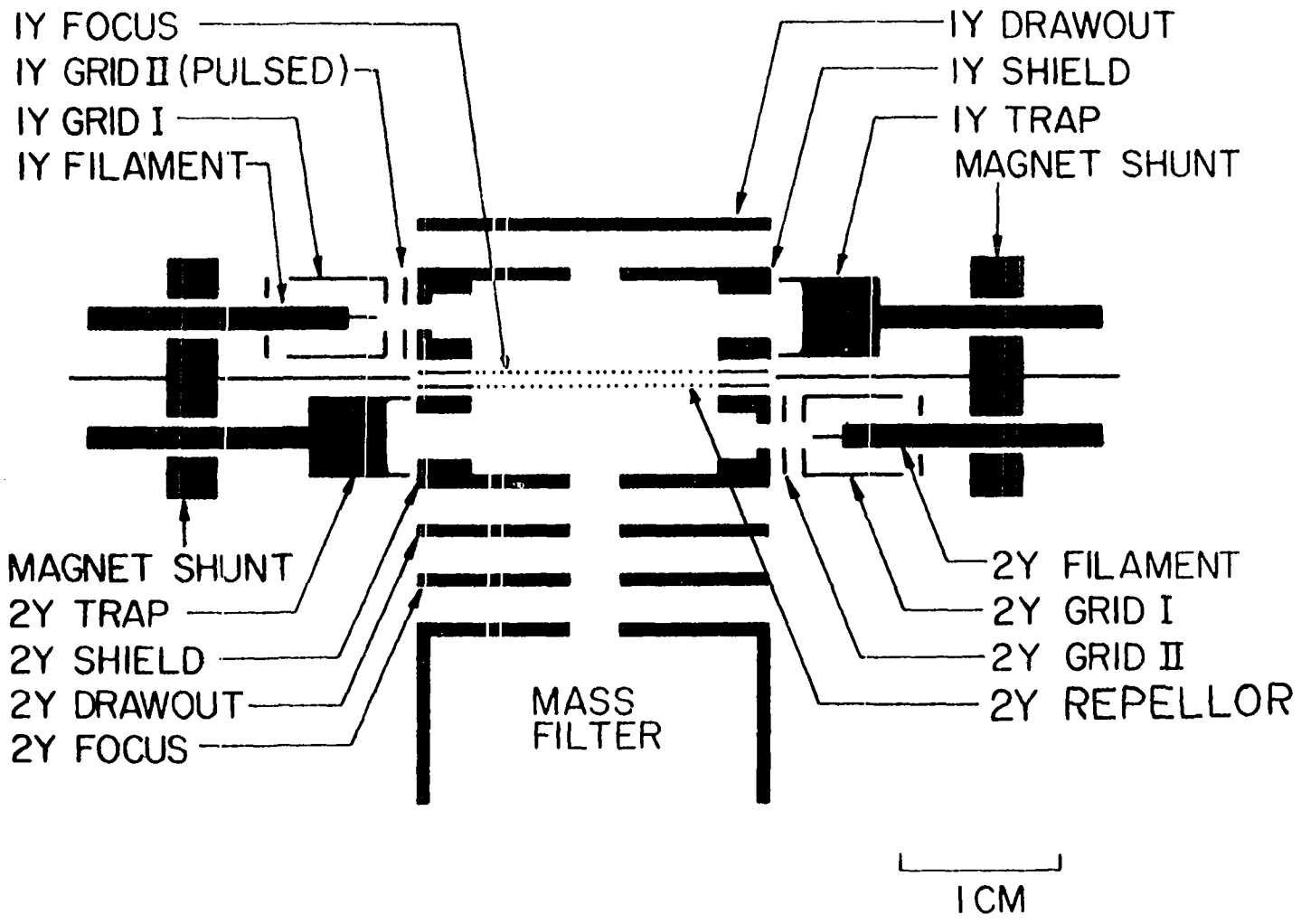
1Y FOCUS
1Y GRID II (PULSED)
1Y GRID I
1Y FILAMENT
1Y DRAWOUT
1Y SHIELD
1Y TRAP
MAGNET SHUNT
MAGNET SHUNT
2Y TRAP
2Y SHIELD
2Y DRAWOUT
2Y FOCUS
MASS FILTER
2Y FILAMENT
2Y GRID I
2Y GRID II
2Y REPELLOR
1 CM

## C. Electronic Components

### 1. Ion pump and pressure protection circuit

The ion pump is powered by a VacIon pump control unit (Varian Model 921-0011) which incorporates an internal protection circuit to shut off its power when the pressure in the vacuum system exceeds $10^{-4}$ Torr. An external relay circuit (Figure 24) activated by the internal protection circuit extends the pressure protection to various additional instrument components, including the two emission regulators. A switch in the external pressure protection circuit provides for bypassing the protection capability so that the components powered by this circuit may be operated when the ion pump is inoperative.

The current generated in the ion pump is displayed by a meter on the pump control unit and provides a direct measurement of the pressure in the vacuum system.

### 2. Ion source power supplies

The ion source power supplies (Figures 25,26) furnish the dc potentials to the various components of the dual ionization chamber ion source, excluding those electron gun components whose potentials are supplied by the emission regulators. In order to eliminate ac pickup between the two chambers of the ion source, two separate dc power supplies are utilized; a primary supply (Figure 25) which

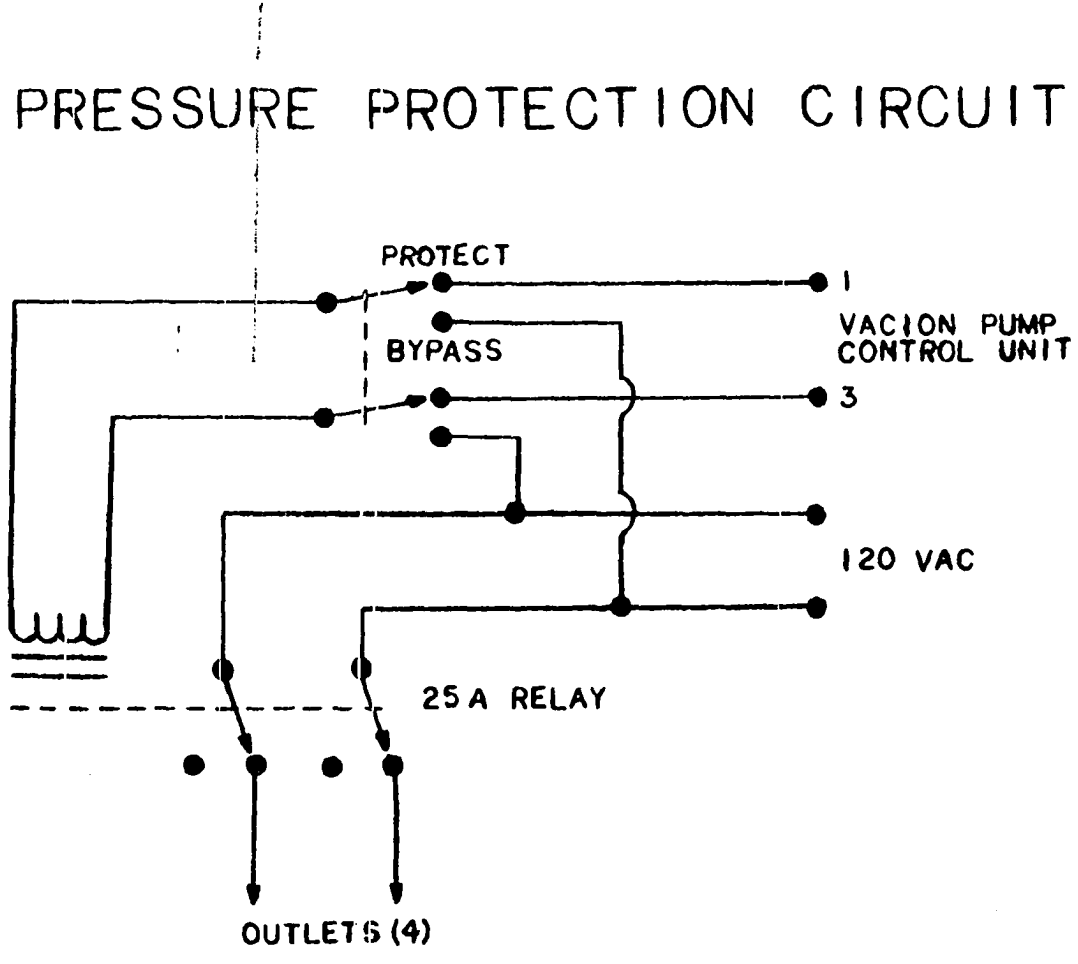


Figure 24. External relay circuit which extends overpressure protection to critical instrument components

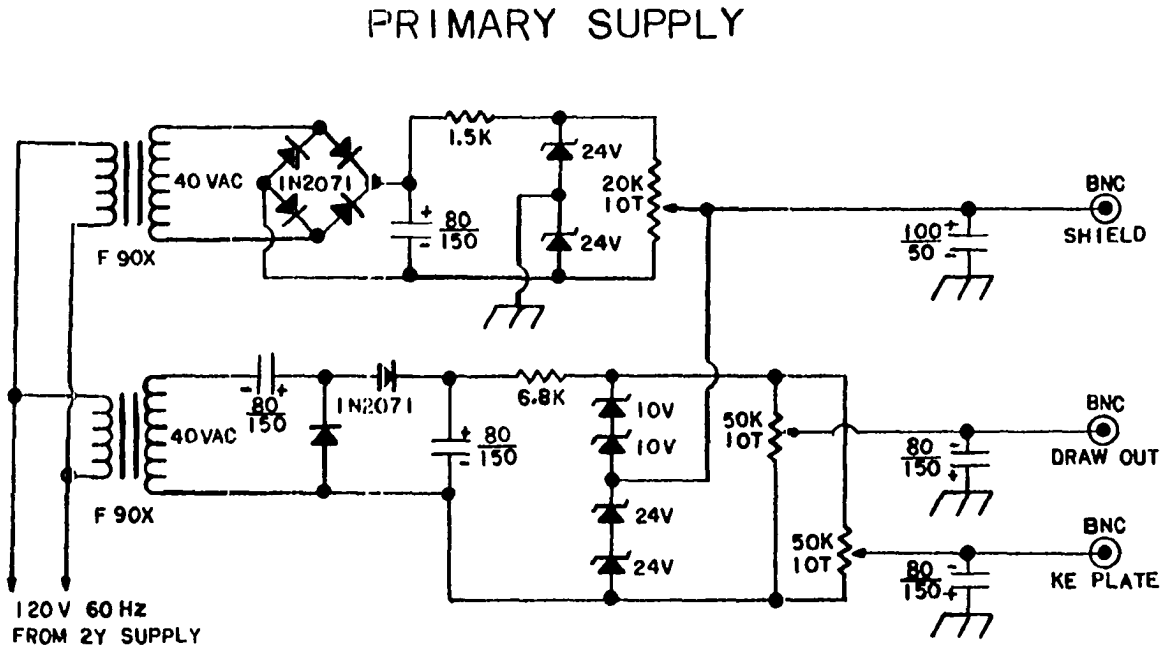


Figure 25. The dc power supply which furnishes the dc potentials to various components of the primary (1Y) reaction chamber of the ion source

Figure 26. The dc power supply which furnishes the dc potentials to various components of the secondary (2Y) ionization chamber

# SECONDARY SUPPLY

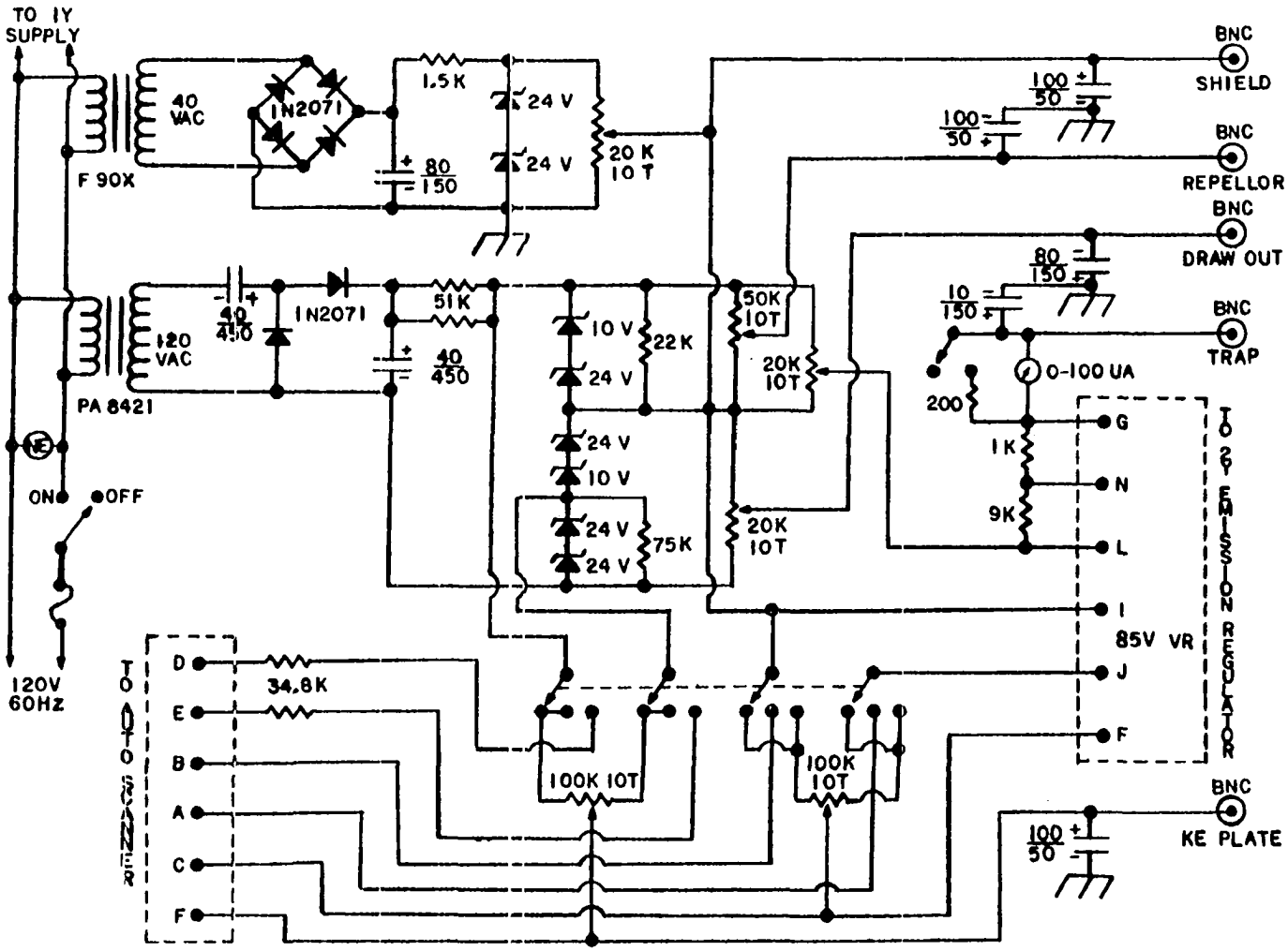

provides the dc potentials for the components of the primary (1Y) reaction chamber, and a secondary supply (Figure 26) which provides the dc potentials for the components of the secondary (2Y) ionization chamber. The 60 Hz noise component on the dc potentials furnished by the zener diode-regulated power supplies is less than 2 mV (rms).

The primary supply furnishes the following ranges of dc potentials to the components of the primary (1Y) reaction chamber.

| Component | Range Available |
|---|---|
| 1Y Shield | -24 V to +24 V (WRT Ground) |
| 1Y Drawout | -48 V to +20 V (WRT 1Y Shield) |
| 1Y KE (Focus) | -48 V to +20 V (WRT 1Y Shield) |

The ranges of dc potentials provided by the secondary supply for the various components of the secondary (2Y) reaction chamber are as follows:

| Component | Range Available |
|---|---|
| 2Y Shield | 0 V to +48 V (WRT Ground) |
| 2Y Repellor | 0 V to +34 V (WRT 2Y Shield) |
| 2Y Drawout | -82 V to 0 V (WRT 2Y Shield) |
| 2Y KE (Focus) | -34 V to +34 V (WRT 2Y Shield) |
| 2Y Trap | 0 V to +34 V (WRT 2Y Shield) |

If the potentials undergo a change of polarity (WRT ground potential) during adjustment, the filter capacitors on the output must be reversed to accommodate the new polarity.

The secondary supply includes provision for automatically scanning the secondary electron accelerating voltage (2Y EAV) or the potential on the 2Y KE plate (Focus). The potential to be automatically scanned is transferred to the automatic scanning circuit (Figure 27) by means of a 3-position switch (Figure 26). The functions corresponding to the various switch positions are as follows:

| Position | Function |
|---|---|
| 1 | 2Y KE manual, 2Y EAV manual |
| 2 | 2Y KE manual, 2Y EAV auto |
| 3 | 2Y KE auto, 2Y EAV manual |

It should be noted that the range of potentials (WRT 2Y Shield) supplied to the 2Y KE plate is reduced to -9 V to +9 V in the automatic scan mode (switch position 3). The ranges of 2Y EAV available in the manual and automatic scan modes (switch position 2) are 0 V to 85 V and 3.3 V to 85 V, respectively. In the case of the 2Y KE plate potentials, the reduced range was necessitated by the power supply design, but in the case of the 2Y EAV, the lower limit of 3.3 V was incorporated in the automatic scanning circuit to prevent filament burnout.

3. Emission regulators

The emission regulators are solid state circuits which were designed and built at Iowa State University and have

been described previously (36). The circuits provide better than one percent regulation in two modes. The current through the filament can be regulated up to 5 amperes (filament regulation) or the emission current to the trap can be regulated from 1 μA to 110 μA (trap regulation).

The secondary emission regulator includes a zener diode-regulated power supply which furnishes a variable dc potential (-12 V to +12 V with respect to 2Y Filament) to 2Y Grid I and a battery which supplies a constant dc potential (+22 1/2 V with respect to 2Y Filament) to 2Y Grid II.

The primary emission regulator includes two zener diode-regulated power supplies which furnish variable dc potentials to 1Y Grid I (-12 V to +12 V with respect to 1Y Filament) and to 1Y Trap (0 V to +50 V with respect to 1Y Shield). The primary electron accelerating voltage (1Y EAV), which is supplied by a 150 V VR tube, can be adjusted manually over the range 0 V to 150 V, or can be transferred by means of a two-position switch to the automatic scanning circuit (Figure 27). When the automatic scanning circuit is utilized, the range over which the 1Y EAV may be varied is reduced to 3 V to 75 V.

4. Grid pulsing and automatic scanning circuits

The grid pulsing circuit (Figure 27) furnishes a square wave potential to 1Y Grid II to pulse the primary electron

Figure 27. Left half: Grid pulsing circuit
Right half: Automatic scanning circuit

# AUTOMATIC SCAN CIRCUIT

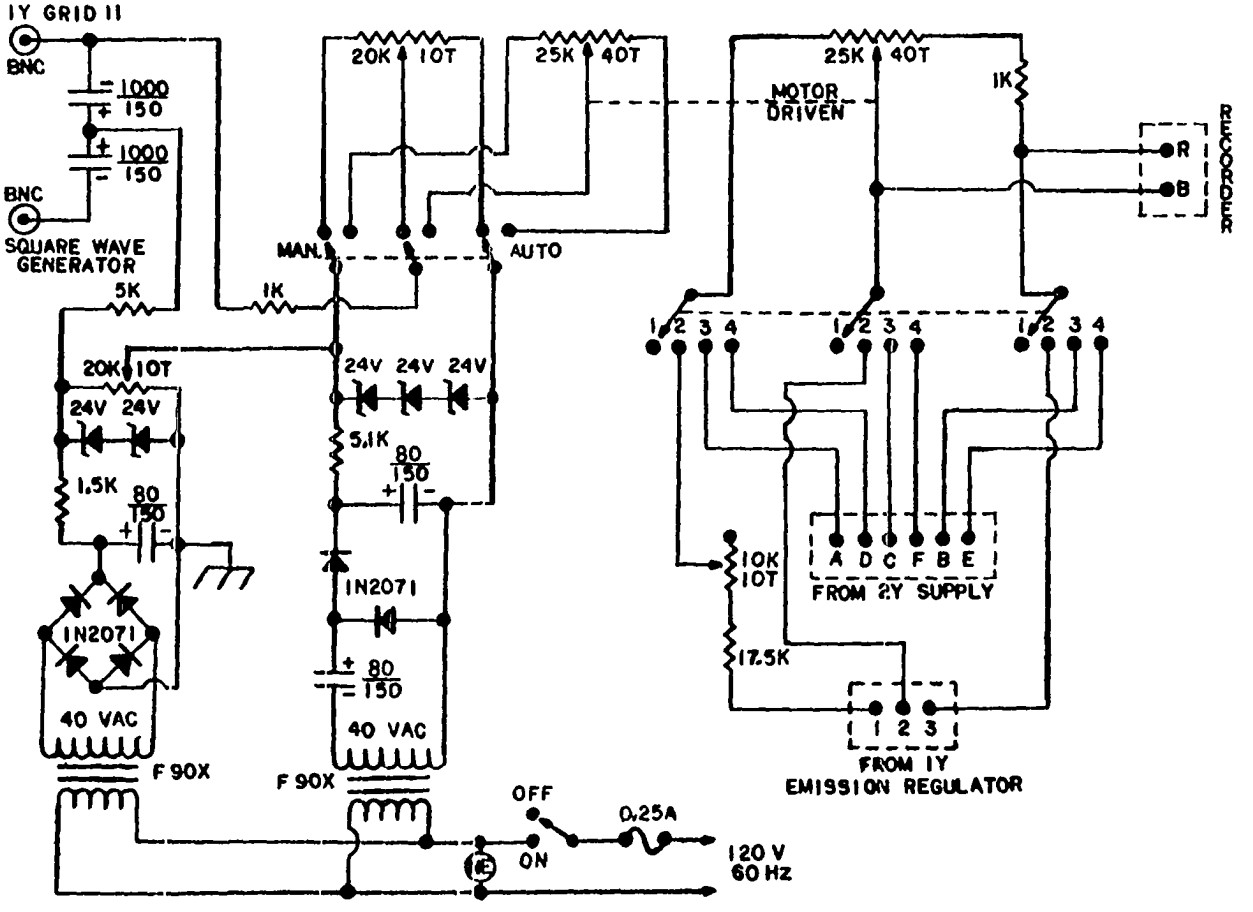

beam. In order to prevent pickup of the pulse signal by other ion source circuitry, the grid pulsing circuit is completely isolated from all other circuits. The circuit consists of a square wave generator (Hewlett-Packard Company, Model 211A) which furnishes a 0 V to -55 V square wave potential with respect to ground at frequencies from 1 Hz to 1 MHz, a zener diode-regulated power supply which furnishes a variable dc potential (-72 V to +48 V with respect to ground), and a pair of 1000 μF capacitors connected in series for mixing the two signals. The utilization of two capacitors connected in series (Figure 27) extends the range of dc potentials available to 1Y Grid II to include both positive and negative potentials with respect to ground. However, losses in the circuit reduce the pulse amplitude supplied to 1Y Grid II to ∿35 V.

The dc potential supplied to 1Y Grid II is normally adjusted manually, but when scanning 1Y EAV, it is adjusted by the automatic scanning circuit which keeps the 1Y filament vs. 1Y Grid II potential constant throughout the range of the scan.

The automatic scanning circuit (Figure 27) consists of two 40-turn potentiometers driven by a common variable-speed motor and a 4-position function switch for selecting the potential to be scanned. The potentials selected at the various switch positions are as follows:

| Position | Potential Scanned |
|---|---|
| 1 | Off |
| 2 | 1Y EAV |
| 3 | 2Y EAV |
| 4 | 2Y KE |

When scanning 2Y EAV and 2Y KE, only one of the motor-driven potentiometers is utilized. However, when 1Y EAV is to be scanned, the 1Y Grid II potential is transferred by means of a two-position switch (Figure 27) to the second potentiometer and scanned simultaneously. The potential across the 1Y EAV potentiometer can be adjusted to match that across the 1Y Grid II potentiometer, so that the 1Y Grid II versus 1Y Filament potential remains constant throughout the scan.

5. Ion source monitor

The ion source monitor (Figure 28) provides a means of monitoring the dc potentials being furnished to various components of the ion source. It is connected between the ion source power supplies and the ion source by means of shielded cables and consists of three components, a 12-position function switch for selecting the potentials to be monitored, a $\pm$50 μA dc meter (zero center scale) upon which the potentials are displayed, and a 4-position range switch for selecting the range in volts which corresponds to full scale on the meter. The meter ranges corresponding to the various range switch positions are as follows:

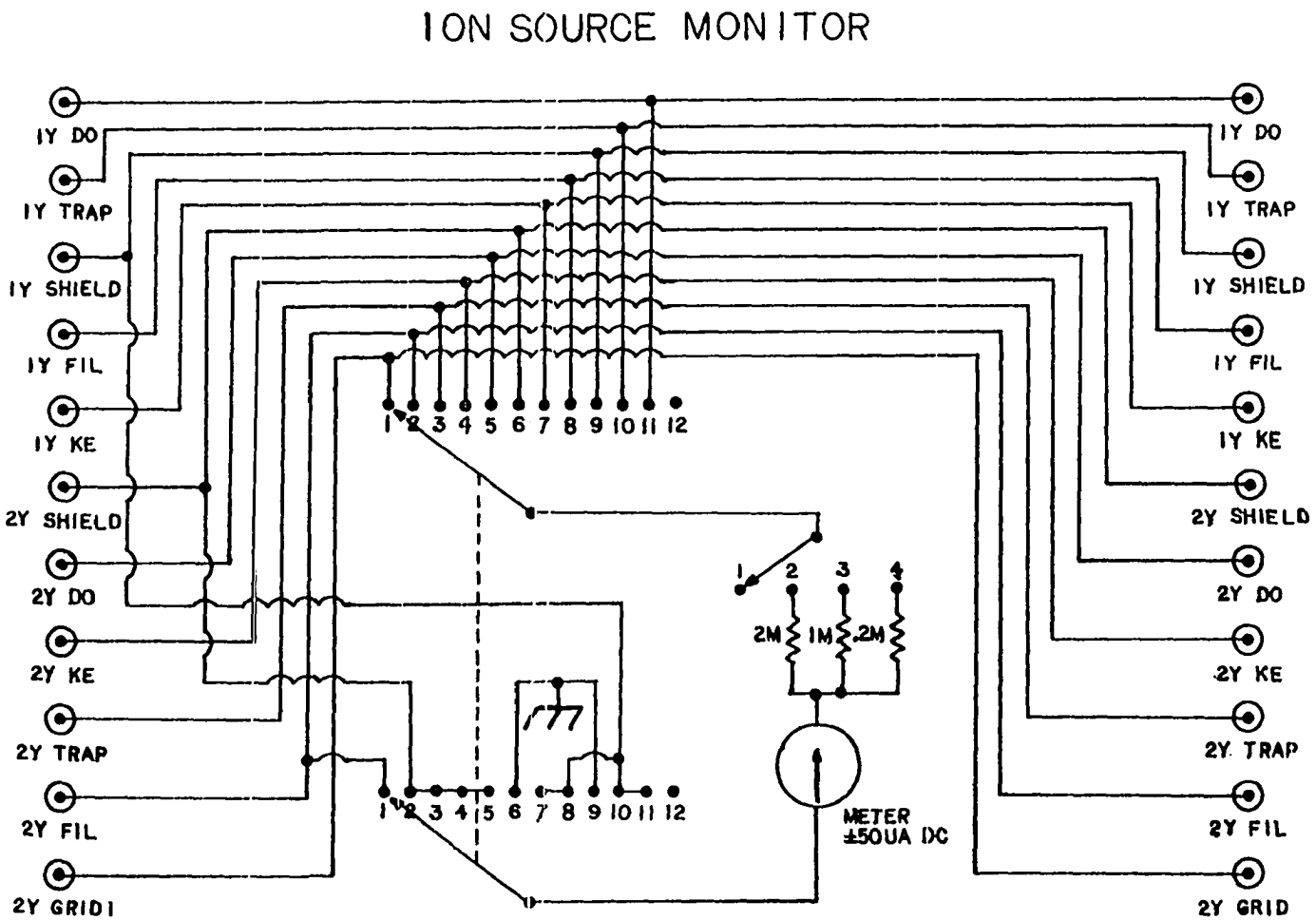


Figure 28. Schematic diagram of the ion source monitor

| Position | Range |
|---|---|
| 1 | Off |
| 2 | ±100 Volts |
| 3 | ±50 Volts |
| 4 | ±10 Volts |

The potentials which are displayed at the various function switch positions are as follows:

| Position | Potential Displayed |
|---|---|
| 1 | 2Y Grid I WRT 2Y Filament |
| 2 | 2Y Filament WRT 2Y Shield |
| 3 | 2Y Trap WRT 2Y Shield |
| 4 | 2Y KE (Focus) WRT 2Y Shield |
| 5 | 2Y Drawout WRT 2Y Shield |
| 6 | 2Y Shield WRT Ground |
| 7 | 1Y KE (Focus) WRT 1Y Shield |
| 8 | 1Y Filament WRT 1Y Shield |
| 9 | 1Y Shield WRT Ground |
| 10 | 1Y Trap WRT 1Y Shield |
| 11 | 1Y Drawout WRT 1Y Shield |
| 12 | Spare |

6. Quadrupole power supply

The quadrupole power supply (Extranuclear Laboratories, Inc., Model QPS with High-Q Head B), which furnishes the rf-dc potentials necessary for operation of the quadrupole mass filter, operates over the frequency range 0.94 MHz to 6.16 MHz with a maximum rf power of 250 W. When in operation, the frequency is adjusted to provide maximum rf power to

the mass filter. The balance ripple suppression and stability of the circuit are adequate to achieve resolutions of 2500 or more, limited only by the mechanical tolerances of the mass filter.

The quadrupole power supply also includes provision for biasing the poles such that the axis of the mass filter is off ground by up to ±8 V. With an external voltage source, the axis of the mass filter can be operated up to ±400 V off ground.

In order to increase the mass range of the instrument, it was necessary to modify the High-Q Head by connecting a 50 pf capacitor (Centralab 850Z-50Z) from each pole to ground.

A sweep generator (Extranuclear Laboratories, Inc. Model 091-5) provides the scanning capability for the quadrupole power supply. Twelve calibrated sweep times from 0.003 sec to 1000 sec are available, with an uncalibrated vernier (1 to 4) on all calibrated times.

7. Deflector power supply

The deflector power supply (Figure 29), a zener diode-regulated, dc power supply, furnishes a continuously variable (0 to +100 V) dc potential to electrode A (Figure 15) of the deflector. The 60 Hz noise component of the dc output is less than 5 mV peak-to-peak.

If, as described previously, deflector electrode C (Figure 15) is to be used as an ion collector in order to establish the gain of the electron multiplier, the deflector power supply can be easily modified to furnish a negative (0 to -100 V) potential to electrode C. This modification consists of grounding the circuit at point G' instead of at point G (Figure 29).

8. Electron multiplier circuit

The electron multiplier circuit (Figure 30) is a simple voltage divider which establishes the potential differences between adjacent dynodes of the electron multiplier. The circuit is powered by a high voltage power supply (Fluke Model 413C) which provides a continuously variable dc potential (0 to -3111 V at 0 to 20 mA) with a resolution of 2 mV and a 60 Hz ripple of less than 150 μV rms. A chain of 17 glass encapsulated resistors (Victoreen RX8, 50 KΩ±1%) fixes the potentials of all of the electron multiplier dynodes with the exception of the first or conversion dynode. The potential ($V_N$) of dynode N (N = 2,17) is given by

$$V_N = \left(\frac{18-N}{17}\right) V_o$$

where $V_o$ is the output of the high voltage power supply. During normal operation, a shielded cable connects BNC-2 and BNC-3 (Figure 30), and the potential of the first dynode ($V_1$) is adjustable to means of a 100 KΩ potentiometer over the

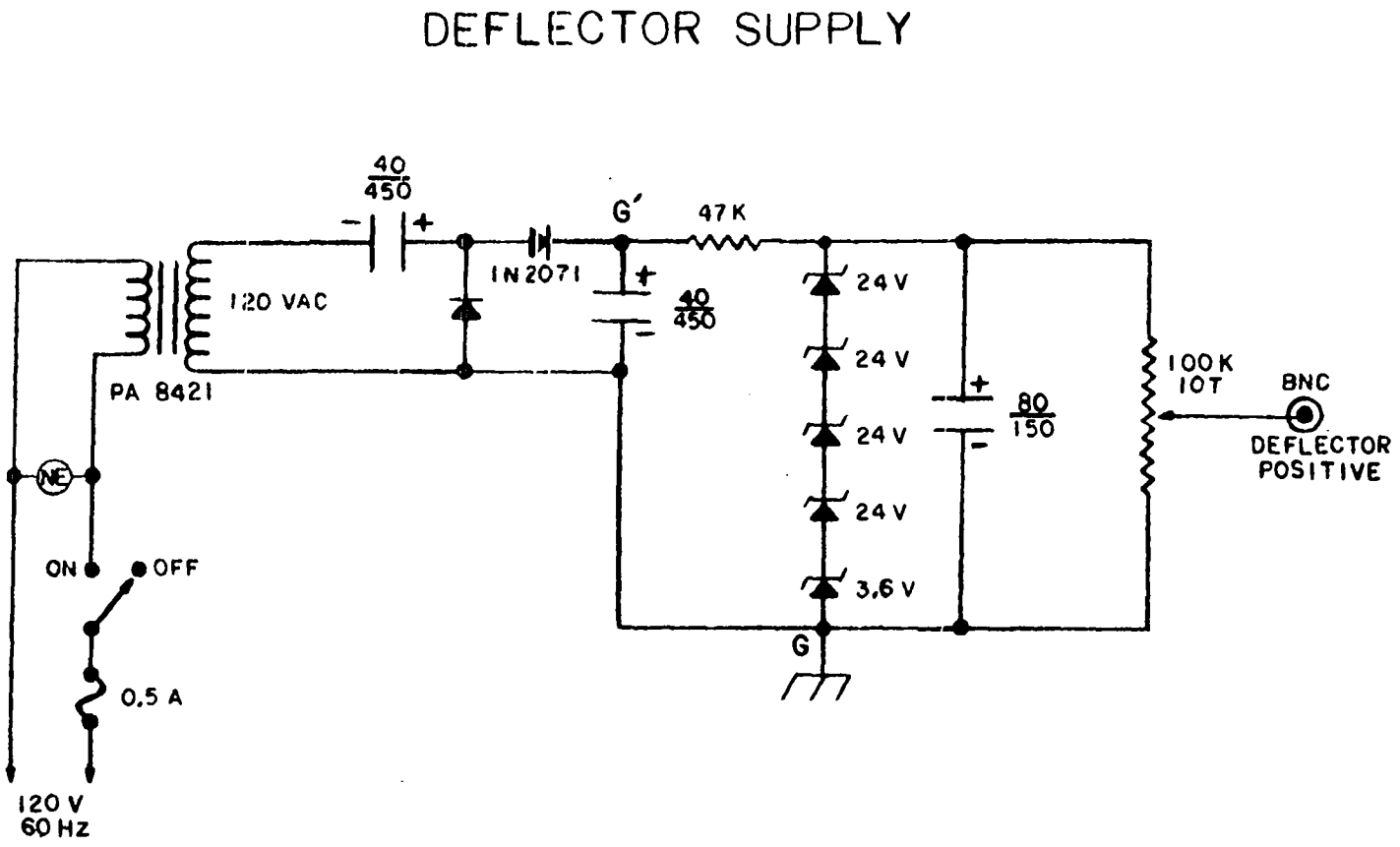


Figure 29. Schematic diagram of the deflector power supply

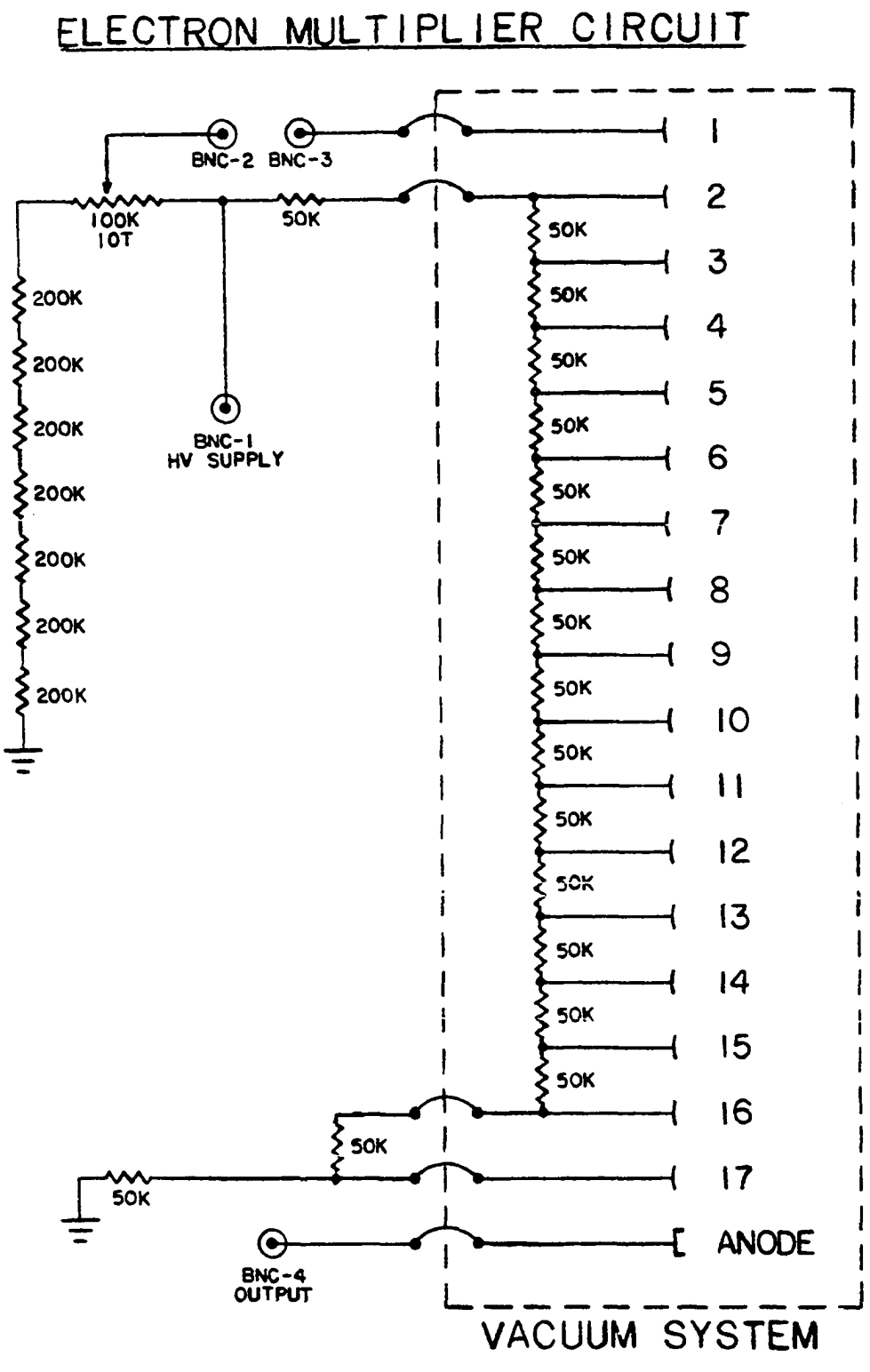


Figure 30. Schematic diagram of the electron multiplier circuit. During normal operation, BNC-2 and BNC-3 are connected by a shielded cable

range $\frac{14}{15} V_0 \leq V_1 \leq V_0$, allowing the gain of the electron multiplier to be varied independently of the high voltage power supply. The gain of the electron multiplier can be measured by adjusting $V_1$ to $\frac{14}{15} V_0$, measuring the current striking the first dynode with an electrometer, and comparing this measured current to the multiplier anode current obtained when $V_1 = V_0$.

9. Preamplifier

The preamplifier (Figure 31), which was designed and built at Iowa State University, amplifies the electron multiplier output and separates the signal into its ac and dc components. The electron multiplier output current is converted to a voltage ($10^8$ V/A), amplified with unity gain by operational amplifier 1 ($OA_1$), and transmitted to a passive filter network ($R_1C_1$ and $R_2C_2$) which separates the signal into its ac and dc components. The dc component is inverted and amplified with unity gain by $OA_2$ and output to a recorder. A feedback loop to the input of $OA_1$ nulls the incoming dc signal. Thus, the dc channel must be overloaded by 100% before $OA_1$ will saturate and affect the ac channel.

The ac component is inverted and amplified with a feedback gain of 10 by $OA_3$ and output to a lock-in amplifier. The gain characteristics of the ac channel as a function of signal frequency (F) are established by resistors $R_1$ and $R_2$

Figure 31. Simplified diagram of preamplifier circuit ($OA_1$: Intersil, Inc., Model 8007 AC $OA_2$, $OA_3$: Intersil, Inc., Model 8007 C)

Figure 32. Gain characteristics of the ac channel of the preamplifier as a function of frequency (F)

## PREAMPLIFIER

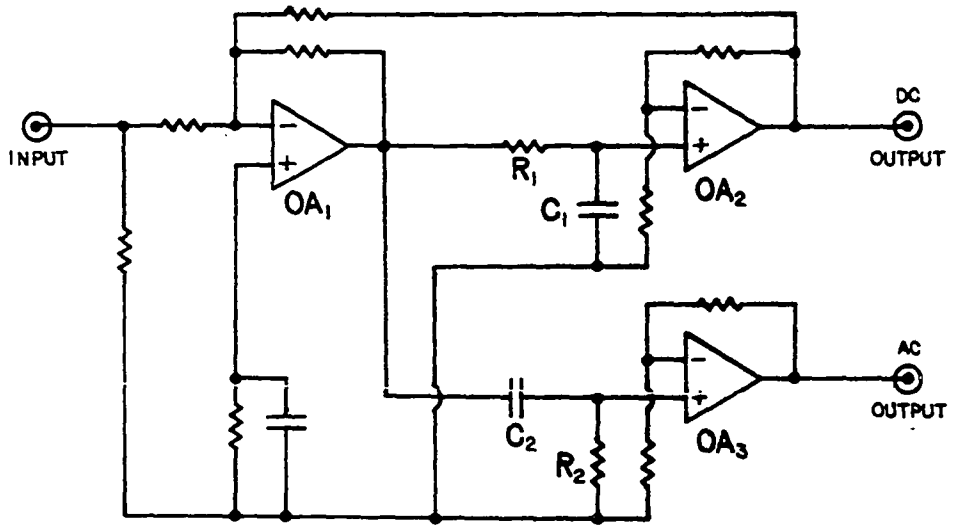


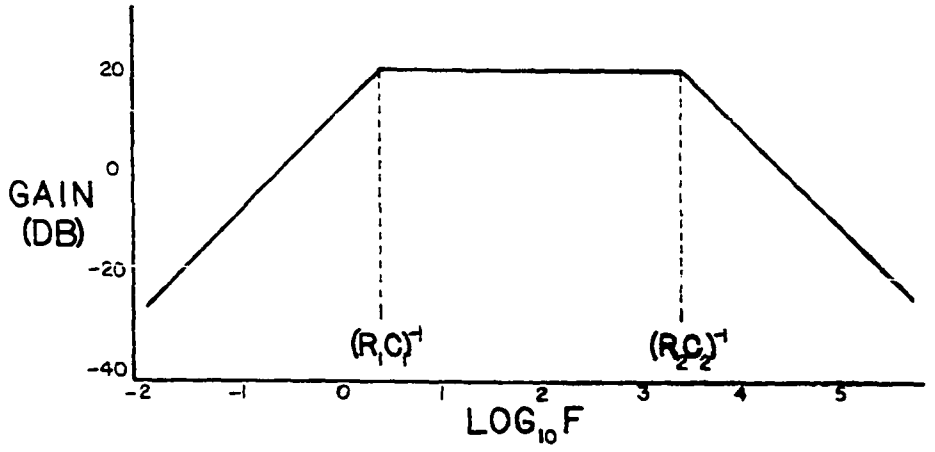

and capacitors $C_1$ and $C_2$ and are presented in graphical form in Figure 32.

10. Lock-in amplifier

The lock-in amplifier (Princeton Applied Research Corporation, Model 122) enables the fundamental frequency component of noisy signals to be measured accurately. It features high sensitivity (100 μV to 50 mV rms), low internal noise, a wide range of operating frequencies (5 Hz to 50 KHz), and filter time constants from 1 msec to 30 sec.

The lock-in amplifier is operated in the "Selective External" mode which requires an externally generated reference signal. This reference signal is furnished by the square wave generator which pulses 1Y Grid II in the ion source.

11. Recorder

The X-Y recorder (Hewlett-Packard, Moseley Division, Model 7030 A) features 17 calibrated dc voltage ranges on each axis (0.1 mV/in. to 20 V/in.) and a continuously adjustable, calibrated zero offset, including 3 full scales on the X-axis and 4 full scales on the Y-axis in 5 in. steps. The accuracy of the recorder is 0.2% of full scale and its linearity is 0.1% of full scale.

# III. DEVELOPMENTAL PROBLEMS

## A. Sensitivity

The relative sensitivity of a mass spectrometer developed for direct detection of neutral fragments depends upon its capability to enhance the ion currents from ionized neutral fragments with respect to the ion currents from other processes and upon its capability to separate the ac and dc components of the ion currents from each other. Several features were incorporated into the design of this instrument to enhance the ion current from ionized neutral fragments with respect to the ion current from other processes. The distance between the centers of the primary and secondary electron beams was minimized (0.3 in.) and high transparency (92%) tungsten mesh grids were utilized to separate the two ion source chambers. Also, the enlarged exit aperture for the sample gas molecules and the short distance ($\sim$4 mm) to the cold surface combine to keep the pressure in the secondary chamber due to a sample to a minimum. The proper choice of operating conditions can also enhance the ion current from ionized neutral fragments. Since the energy required to ionize a neutral fragment is less than that required to produce the same ionic fragment from the parent molecule and since a low ionizing energy favors production of that component of ion current resulting from the lowest energy processes, the ion current from

ionized neutral fragments is enhanced by operating the secondary electron beam at low energy.

The signal/noise ratio (S/N) for detecting the ionized neutral fragments has also been improved by utilizing a pentode electron gun and improved grid pulsing circuitry to improve the pulse shape of the pulsed primary electron beam. However, the biggest improvement in S/N ratio for detecting the ionized neutral fragments resulted from the identification and subsequent elimination of six anomalous phase-correlated output signals. Although these signals were almost certainly generated in earlier instruments (18-31) designed for detection of neutral fragments, they have not been described previously, and may be a source of error in the results obtained with those instruments.

### B. Anomalous Phase-Correlated Output Signals

The various phase-correlated output signals were characterized by focussing the mass filter to transmit ions of a given mass/charge ratio, adjusting the gain of the electron multiplier, and monitoring the output of the lock-in amplifier as a function of various parameters, including the detection phase angle, the sample pressure, the primary electron current, the secondary electron current, the primary Shield potential, and the primary KE (Focus) potential. In all, seven phase-correlated output signals, summarized in Figure 33, were isolated and identified, only one of which is

## PHASE DEPENDENT SIGNALS

| TYPE OF SIGNAL | ORDER OF DEPENDENCE UPON | | | AFFECTED BY ION SOURCE POTENTIALS? |
|---|---|---|---|---|
| | SAMPLE PRESSURE | PRIMARY ELECTRON CURRENT | SECONDARY ELECTRON CURRENT | |
| EXTERNAL PICKUP | 0 | 0 | 0 | NO |
| INTERNAL PICKUP | 1 | 0 | 1 | NO |
| PHOTONS | 1 | 1 | 0 | NO |
| IONS | 1 | 1 | 0 | YES |
| ELECTRONS | 2 | 1 | 0 | YES |
| AUTOIONIZING NEUTRAL SPECIES | 1 | 1 | 0 | NO |
| NEUTRAL FRAGMENTS | 1 | 1 | 1 | NO |

Figure 33. Summary of the characteristics of the seven phase-correlated output signals which were isolated and identified

attributable to ionization of neutral fragments. The characteristics of each of these signals are described below.

1. External pickup

Since this phase-correlated output signal persists when both electron beams are turned off, it was the first anomalous signal to be isolated, identified, and eliminated. Arising from pickup of the 1Y Grid II (see Figure 20) pulse signal by the output cables between the electron multiplier and the preamplifier, its intensity depends only on the amplitude of the 1Y Grid II pulse signal and the detection phase of the lock-in amplifier. This anomalous signal was eliminated by better shielding of the 1Y Grid II pulse circuitry, by double-shielding of the output cable, and by mounting the preamplifier as close as possible to the electron multiplier.

2. Photons

The interaction of the pulsed primary electron beam with sample gas molecules yields photons which are of sufficient energy to eject electrons from the first dynode of the electron multiplier, resulting in a phase-correlated output signal. Because it is eliminated by offsetting the electron multiplier, this signal was not a problem with this instrument. However, its presence as a potential phase-correlated output signal was verified. After removing the deflector and locating the entrance slit of the electron multiplier

directly opposite the exit aperture of the mass filter, a phase-correlated output signal with a first-order dependence on primary electron current and sample pressure and a zero-order dependence on secondary electron current, 1Y KE (Focus) potential, and 1Y Shield potential (Figure 33) was observed. When the instrument was returned to its offset configuration, the signal could no longer be detected.

3. Positive ions

If a sufficient potential barrier is not established between the primary and secondary chambers of the ion source, positive ions formed in the primary chamber may enter the secondary chamber, be focussed through the mass filter, and be observed as a phase-correlated output signal. The intensity of this signal is characterized by a first-order dependence on sample pressure and primary electron current and a zero-order dependence on secondary electron current. It is eliminated by setting the 1Y Shield potential at least 8 V negative with respect to the 2Y Shield potential.

4. Electrons

This phase-correlated output signal is characterized by a second-order dependence on sample pressure, a first-order dependence on primary electron current, and a zero-order dependence on secondary electron current. Since the intensity of this anomalous signal increases as the 1Y KE

(Focus) potential is adjusted to be more positive with respect to the 1Y Shield potential, it is attributed to the transmission of negatively-charged particles (concluded to be electrons, which are much more abundant than negative ions) from the primary chamber to the secondary chamber. Since the 2Y Shield potential is kept 8 V positive with respect to the 1Y Shield potential, the electrons are accelerated to sufficient energy to ionize sample gas molecules. Because the signal intensity has a second-order dependence on sample pressure, the electrons which are transmitted from the primary chamber to the secondary chamber are produced by the interaction of the primary electron beam with sample gas molecules. They could be secondary electrons produced by the ionization of sample gas molecules, or they could be electrons which are scattered by the sample gas molecules, as there is no way to differentiate the two processes. This anomalous phase-correlated signal was eliminated by setting the 1Y KE (Focus) potential 6 V negative with respect to the 1Y Shield potential.

5. Internal pickup

A phase-correlated output signal arising from pickup of the 1Y Grid II pulse signal by ion source components associated with the secondary ionization chamber is characterized by a first-order dependence on secondary electron current and sample pressure and a zero-order dependence on

primary electron current. Measures taken to prevent this pickup included shielding the 1Y Grid II lead inside the vacuum system, opposing the electron guns, installing grounded plates between the electron guns, and installing filter capacitors on the ion source power supply. Although these measures have succeeded in reducing the resulting anomalous signal to a barely detectable level, they have not completely eliminated it.

6. Autoionizing neutral species

When a sample gas molecule interacts with an electron in the primary chamber of the ion source, autoionizing neutral species may be formed. If these species have a sufficiently long lifetime, they may diffuse to the secondary chamber where ionization occurs, resulting in a phase-correlated output signal which is characterized by a first-order dependence on primary electron current and sample pressure and a zero-order dependence on secondary electron current. Because the particles diffuse to the secondary chamber as excited neutral species, this signal is impossible to eliminate. However, the contribution to neutral mass spectra attributed to autoionizing neutral species is usually small, and can be determined by simply recording the apparent neutral mass spectra with no electron current in the secondary chamber.

7. Neutral fragments

The phase-correlated output signal attributed to ionization of neutral fragments by the secondary electron beam is characterized by a first-order dependence on primary electron current, secondary electron current, and sample pressure. Its intensity is not affected by changes in the 1Y KE (Focus) potential or the 1Y Shield potential.

# IV. EXPERIMENTAL

## A. Ion Source Conditions

### 1. Sample pressure

At present, the VacIon pump control unit provides the only measure of the total pressure in the main vacuum chamber of the instrument. Since most of the sample gas molecules are condensed on a liquid $N_2$-cooled surface immediately after they traverse the primary ionization region, the pump control unit provides a poor measure of the sample pressure in the ion source. However, due to the limited efficiency of the glass nozzle for confining the stream of sample gas molecules toward the cold surface, the sample pressure in the primary reaction chamber can be assumed to be less than $\sim$100 times the pressure indicated by the VacIon pump control unit. Thus, an upper limit of the sample pressure in the primary reaction chamber is easily established.

In practice, a quantity of sample which yields a pressure of 0.1-1.0 Torr in the final expansion volume of the inlet system is sufficient to obtain its neutral mass spectrum. For most organic liquids the sample size utilized is about 5-25 microliters. When obtaining neutral fragment ionization potentials and appearance potentials, the sample size may be increased to yield a pressure of up to 5.0 Torr in the final expansion volume of the inlet system.

2. Electrode potentials

The electrode potentials which were utilized in the three ion sources are presented in Table 1. These potentials were arrived at by first meeting the criteria for preventing transmission of positive ions and electrons from the primary chamber to the secondary chamber of the ion source (i.e., 1Y Shield 8 V negative with respect to 2Y Shield and 1Y KE (Focus) ∿6 V negative with respect to 1Y Shield), and then adjusting the 2Y KE (Focus) and 2Y Drawout potentials to maximize the collected ion current. Likewise, the 1Y Drawout potential was adjusted to extract the positive ions from the primary chamber. The potentials of the electron gun components were adjusted independently to maximize the electron current to the trap electrodes.

3. Electron current

Because of the low ion drawout fields in the ion source, severe ion trapping (Figure 34) occurs in the secondary ionization chamber at trap currents greater than 40 μA. Thus, the secondary electron beam is normally operated at a maximum trap current to 40 μA. However, in the primary reaction chamber, higher trap currents (up to 200 μA) may be utilized to produce neutral fragments, since they are not trapped by the electron beam (Figure 35).

Table 1. Electrode potentials utilized in the various ion sources

| Electrodes | Electrode potentials[a] Ion source I | Ion source II | Ion source III |
|---|---|---|---|
| 1Y Shield | +1 | +1 | +1 |
| 1Y Drawout | -45 | -45 | -45 |
| 1Y KE (Focus) | -5 | -5 | -4 |
| 1Y Filament | -EAV1 + 1 | -EAV1 + 1 | -EAV1 + 1 |
| 1Y Grid I | -EAV1 + 9 | -EAV1 + 9 | -EAV1 + 9 |
| 1Y Grid II[b] | -EAV1 + 12 | -EAV1 + 12 | -EAV1 + 12 |
| 1Y Trap | +45 | +45 | +45 |
| 2Y Shield | +9 | +9 | +9 |
| 2Y Drawout | -61 | -61 | -41 |
| 2Y KE (Focus) | +3 | +3 | +5 |
| 2Y Repellor | ---- | ---- | +10 |
| 2Y Filament | -EAV2 + 9 | -EAV2 + 9 | -EAV2 + 9 |
| 2Y Grid I | -EAV2 + 16 | -EAV2 + 16 | -EAV2 + 16 |
| 2Y Grid II | -EAV2 + 31.5 | -EAV2 + 31.5 | -EAV2 + 31.5 |
| 2Y Trap | +42 | +42 | +42 |

[a]Potentials are given in volts with respect to ground.

[b]A 0 to -35 V square wave potential is superimposed on the potential listed for this electrode.

Figure 34. Plot of ion current versus 2Y trap current. Decrease in ion current due to ionization of neutral fragments at trap currents greater than 40 μA is attributed to ion trapping

Figure 35. Plot of ion current due to ionization of neutral fragments versus 1Y trap current. This plot shows no evidence of ion trapping effects

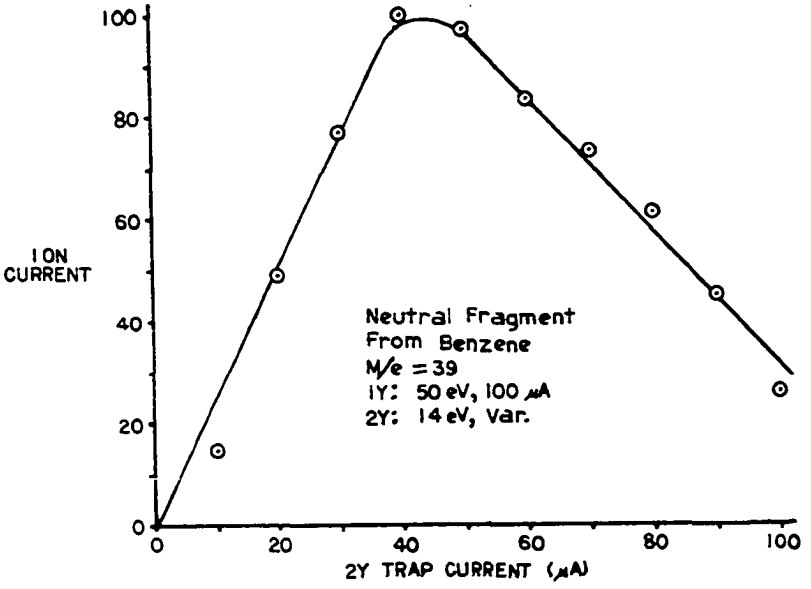
ION CURRENT
100
80
60
40
20
0
0
20
40
60
80
100
2Y TRAP CURRENT (μA)
Neutral Fragment
From Benzene
M/e = 39
1Y: 50 eV, 100 μA
2Y: 14 eV, Var.

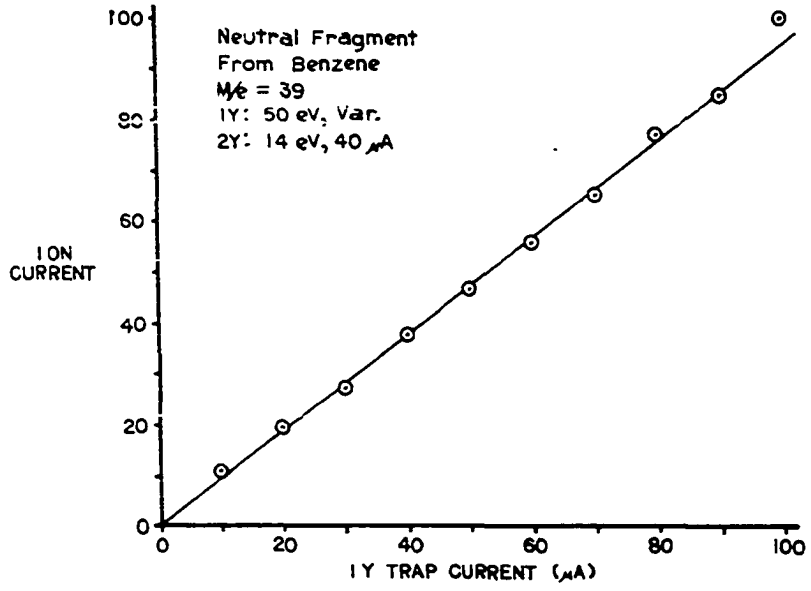
ION CURRENT
100
80
60
40
20
0
0
20
40
60
80
100
1Y TRAP CURRENT (μA)
Neutral Fragment
From Benzene
M/e = 39
1Y: 50 eV, Var.
2Y: 14 eV, 40 μA

4. Pulse frequency

A frequency of 260 Hz was chosen for pulsing the primary electron beam because this frequency yields the highest signal/noise ratio (S/N) for detecting neutral fragments. At lower frequencies, harmonics of the 60 Hz line current reduce the S/N significantly. At higher frequencies, a significant phase shift effect results because neutral fragments of different mass require different times to diffuse to the secondary chamber and to traverse the mass filter after ionization. This phase shift can be calculated using the results of the kinetic-molecular theory of gases. According to the kinetic-molecular theory, the rms velocity ($\sqrt{\bar{u}^2}$) of gas molecules with mass M is given by

$$\sqrt{\bar{u}^2} = \sqrt{\frac{3RT}{M}} \quad (17)$$

where T is the temperature and R is the gas constant. If the temperature in the ion source is assumed to be 300°K, and if the mass range of interest is 12 amu to 120 amu, the rms velocities are as follows:

$$M = 12; \sqrt{\bar{u}^2} = 7.9 \times 10^4 \text{ cm/sec} \quad (18)$$

$$M = 120; \sqrt{\bar{u}^2} = 2.5 \times 10^4 \text{ cm/sec} \quad (19)$$

Since the distance between the centers of the two electron beams in the ion source is $\sim$0.8 cm, the time (t) required

for the neutral fragments to diffuse is as follows:

$$M = 12;\ t_{12} = 1 \times 10^{-5} \text{ sec} \tag{20}$$

$$M = 120;\ t_{120} = 3.2 \times 10^{-5} \text{ sec} \tag{21}$$

If the energy of the ionized neutral fragments is 10 eV, the time (t') required for the ionized neutral fragments to reach the first dynode of the electron multiplier (15 cm) is given by the following:

$$M = 12;\ t'_{12} = 1.2 \times 10^{-5} \text{ sec} \tag{22}$$

$$M = 120;\ t'_{120} = 3.7 \times 10^{-5} \text{ sec} \tag{23}$$

The total time between formation of the neutral fragments and their collection as ions is given by

$$M = 12;\ t_{12} + t'_{12} = 2.2 \times 10^{-5} \text{ sec} \tag{24}$$

$$M = 120;\ t_{120} + t'_{120} = 6.9 \times 10^{-5} \text{ sec} \tag{25}$$

For a pulsing frequency of 260 Hz, the difference in the total times ($t_{120} + t'_{120} - t_{12} - t'_{12}$) results in a phase shift of 4.4 deg. If this phase shift is not taken into account, an error in sensitivity of $\sim$0.3% results, which is well within the limits of accuracy of the instrument. However, at higher frequencies, this error can become significant. For example, at a pulsing frequency of 1 KHz, the phase shift is 17.5°, resulting in a sensitivity

difference of ∿5% between masses 12 and 120.

The difference in sensitivity caused by this phase shift is easily calculated and can thus be corrected. However, a second problem exists at higher pulsing frequencies (>260 Hz). Since the neutral fragments do not all travel at the same velocity, but have a distribution of velocities, the shape of the square wave output signal due to ionized neutral fragments deteriorates at higher frequencies, resulting in a serious loss in sensitivity. In order to avoid this problem, the pulse frequency which is utilized should be chosen as low as possible, but unique with respect to any possible ac pickup from any source present in the laboratory.

## B. Data Acquisition

### 1. Conventional mass spectra

The conventional mass spectrum of a compound is normally obtained by monitoring the dc channel of the output circuitry with only the secondary electron beam activated, although the conventional mass spectrum may be obtained when both electron beams are activated. Since the liquid $N_2$ cooled surface minimizes the sample pressure in the secondary chamber, its use reduces the sensitivity for obtaining conventional mass spectra. Therefore, it is generally maintained at ambient temperature when operating the instrument in this mode.

The conventional mass spectrum of a compound is obtained as follows: after achieving the desired sample pressure and adjusting the 2Y EAV and the 2Y electron current, the voltage applied to electrode A of the deflector (see Figure 15) is adjusted to maximize the output at m/e = 28. After adjusting the gain of the multiplier to yield a preamplifier output (dc) of ∿9 V for the most intense peak, the preamplifier output is recorded directly as a function of the mass/charge ratio. In order to eliminate clipping of the intense peaks by the recorder, a maximum scan rate of 1 sec/amu is utilized.

After obtaining its raw mass spectrum, the sample gas is removed from the final expansion volume of the inlet system by opening valve $V_1$ (Figure 10). As soon as the pressure in the main vacuum chamber stabilizes (∿2-3 min.), the mass spectrum of the background gases is obtained utilizing the same conditions under which the raw sample mass spectrum was obtained. This background mass spectrum is later subtracted from the raw sample mass spectrum to correct for any background contributions.

2. Neutral fragment mass spectra

The neutral fragment mass spectrum of a compound is obtained by monitoring the output of the lock-in amplifier (ac channel of the output circuitry) with both the primary and secondary electron beams activated. In order to obtain

the best sensitivity, the liquid $N_2$ cooled surface is utilized to minimize the flow of sample into the secondary chamber. In addition, high electron currents (up to 200 μA) and an electron accelerating voltage of 50 V are utilized in the primary chamber. In the secondary chamber, the electron current is limited to 0-40 μA because of ion trapping, and a low electron accelerating voltage (10 to 20 V) is utilized to enhance the ion current from ionized neutral fragments with respect to the ion current from other sources.

With two exceptions, the procedure used for obtaining a neutral fragment mass spectrum is the same as that used for obtaining a conventional mass spectrum. First, the multiplier gain is adjusted to yield a lock-in amplifier output of ∿9 V with the most intense ac ion current focussed through the mass filter. Secondly, the scan rate is adjusted according to the time constant of the lock-in amplifier. With a time constant of 1 sec , a maximum scan rate of 1/7 amu/sec is utilized. When a 3 sec time-constant is utilized, the maximum scan rate is 1/20 amu/sec.

### 3. Conventional ionization efficiency curves

Conventional ionization efficiency curves are obtained by focussing ions with a given m/e through the mass filter and recording the dc channel output as a function of the energy of the secondary electron beam. Only the secondary electron beam is normally activated and its energy is scanned

automatically by means of the automatic scanning circuit (Figure 28). When obtaining ionization efficiency curves, a maximum trap current of 30 μA is utilized in the secondary electron beam, since utilization of higher trap currents results in significant ion trapping. Since the ion trapping problem becomes more severe at low electron energies, the observed energy scale deviates from the predicted energy scale (Figure 36) when ion trapping is occurring. When a trap current of 30 μA is utilized, the ion trapping problem is eliminated. Normally, two calibrants, a rare gas (argon or xenon) and the parent ion of the compound being studied, are utilized to calibrate the energy of the secondary electron beam.

The ionization efficiency curve for each ion of interest is normalized by adjusting the multiplier gain to obtain a constant output current at an energy 2 V above the energy at which the ion current vanishes.

4. Neutral fragment ionization potentials

Neutral fragment ionization potentials are measured by activating both the primary and secondary electron beams, focussing ions with a given m/e through the mass filter, and recording the ac channel output as a function of the energy of the secondary electron beam. In general, high trap currents (up to 200 μA) are utilized in the primary chamber to enhance the component of ion current due to ionization

Figure 36. Plot of measured I.P.'s versus literature I.P.'s showing deviation at low energies due to ion trapping. The 2Y trap current was 40 μA. When the 2Y trap current was reduced to 30 μA, the experimental points fell on the dashed line within the expected experimental error

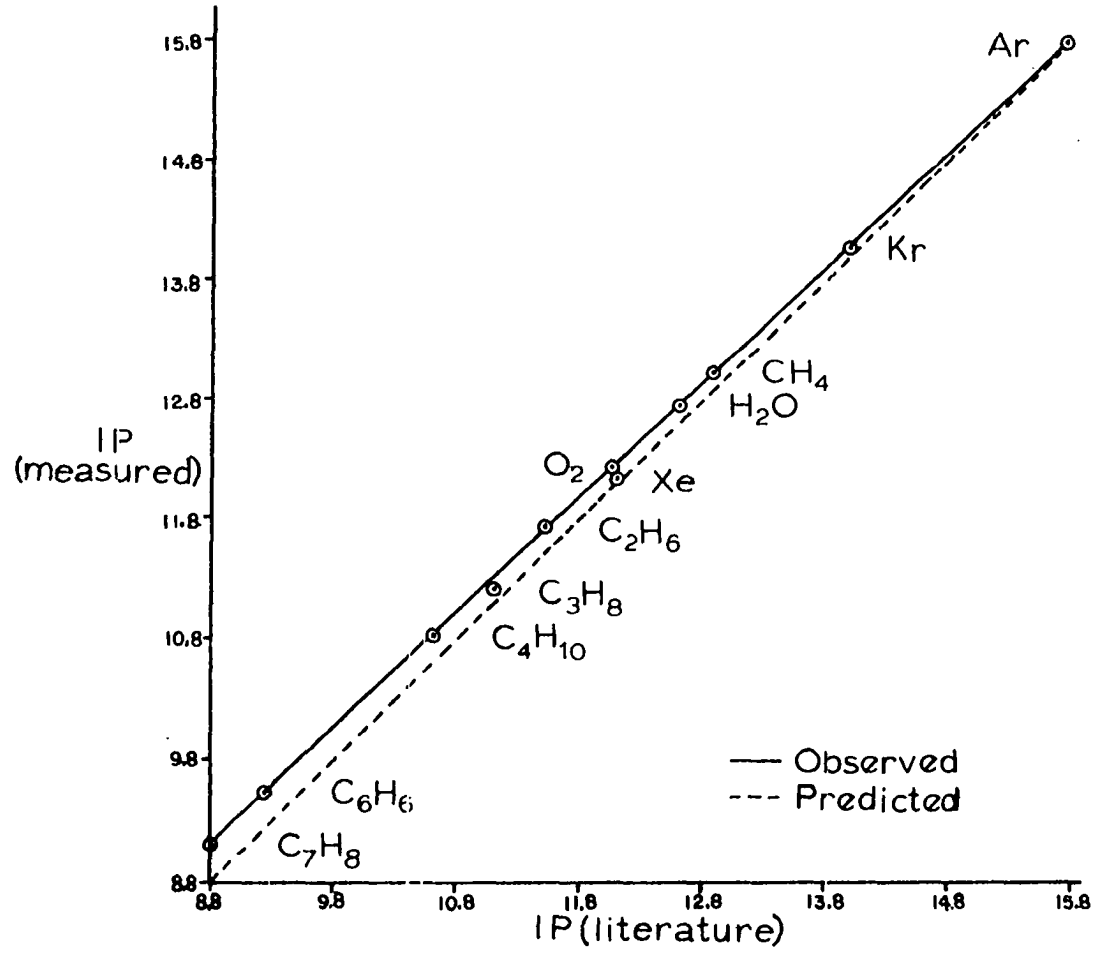
15.8
14.8
13.8
12.8
11.8
10.8
9.8
8.8
IP
(measured)
8.8
9.8
10.8
11.8
12.8
13.8
14.8
15.8
IP(literature)
Ar
Kr
$CH_4$
$H_2O$
$O_2$
Xe
$C_2H_6$
$C_3H_8$
$C_4H_{10}$
$C_6H_6$
$C_7H_8$
Observed
Predicted

of neutral fragments with respect to that from other sources. A maximum trap current of 30 μA is utilized in the secondary chamber to minimize ion trapping. Normally, conventional ionization efficiency curves are utilized to calibrate the energy of the secondary electron beam. The neutral fragment ionization efficiency curves are normalized in the same fashion as conventional ionization efficiency curves.

The measurement of neutral fragment ionization potentials is a very important function of the instrument, since relatively few neutral fragment ionization potentials are known.

5. Neutral fragment appearance potentials

Neutral fragment appearance potentials are measured by activating both electron beams, focussing ions with the m/e of interest through the mass filter, and recording the ac channel output as a function of the primary electron energy. Calibration of the primary electron beam energy is accomplished by introducing separate reference gas samples and recording the total ion current striking the primary drawout plate as a function of the energy of the primary electron beam.

Due to the inefficiency of the present grid pulsing circuit, a maximum pulse amplitude of 35 V can be obtained on 1Y Grid II. This limits the trap current which can be maintained in the primary electron beam to a maximum of 50 μA

over the energy range of 6 eV to 15 eV, resulting in a reduced S/N for detecting the neutral fragments. The S/N for detecting the neutral fragments is also reduced because fewer neutral fragments are produced as the energy of the primary electron beam is reduced, while the ion current produced from other sources in the secondary ionization chamber remains constant. On the other hand, when measuring neutral fragment ionization potentials, the number of neutral fragments entering the secondary chamber remains constant, and the S/N actually improves as the energy of the secondary electron beam is reduced, since the production of ion current from sources other than ionization of neutral fragments requires more energy than the ionization of neutral fragments. Thus, the S/N obtained when measuring neutral fragment appearance potentials is 1 to 2 orders of magnitude less than the S/N obtained when measuring neutral fragment ionization potentials.

# V. TREATMENT OF DATA

## A. Conventional Mass Spectra

Conventional positive ion mass spectra are tabulated in raw form by measuring and recording the ion current obtained at each m/e and subtracting any contributions from residual (background) gases present in the mass spectrometer. However, because of mass discrimination by the quadrupole mass filter, the sensitivity for detection of positive ions varies with m/e, being lowest for detecting ions with high m/e. Thus, in order for the detected ion current to be truly representative of the ions formed in the ion source, the raw mass spectra must be corrected to account for this mass discrimination.

### 1. Correction for mass discrimination

The mass discrimination of the quadrupole mass filter arises from two sources. First, the quadrupole mass filter is capable of operation in two extreme modes, with resolution constant throughout the mass range or with resolution proportional to m/e. The filter is normally operated somewhere between these two extreme modes. A magnetic sector instrument, on the other hand, operates with resolution constant throughout the mass range. Thus, the choice of an operating mode other than that with resolution constant throughout the mass range results in reduced

sensitivity for ions with high m/e. The second source of mass discrimination is the fringe fields at the entrance to (and to a lesser extent at the exit of) the quadrupole mass filter (37). These fringe fields cause some of the ions which would normally acquire a stable trajectory through the mass filter, to strike the quadrupole rods and be neutralized. Since the extent to which an ion is affected by the fringe fields is directly related to the amount of time the ion spends in traversing them, the slower travelling (i.e., higher m/e) ions will be affected most. Thus, both sources of mass discrimination result in lower sensitivity for detecting ions with higher m/e.

The relative sensitivities for detecting ions with different m/e can be determined by comparing the mass spectra of pure compounds obtained from the quadrupole mass spectrometer with reference spectra obtained from a magnetic sector instrument. A graph of m/e versus the sensitivity correction factors by which the ion currents obtained with the quadrupole mass spectrometer described herein must be multiplied to obtain the relative ion currents which would be observed in a magnetic sector instrument is shown in Figure 37. Since the relative values of the sensitivity correction factors are dependent on various instrument settings (chiefly the ion energy and the Δm, pole bias, and resolution controls on the Extranuclear

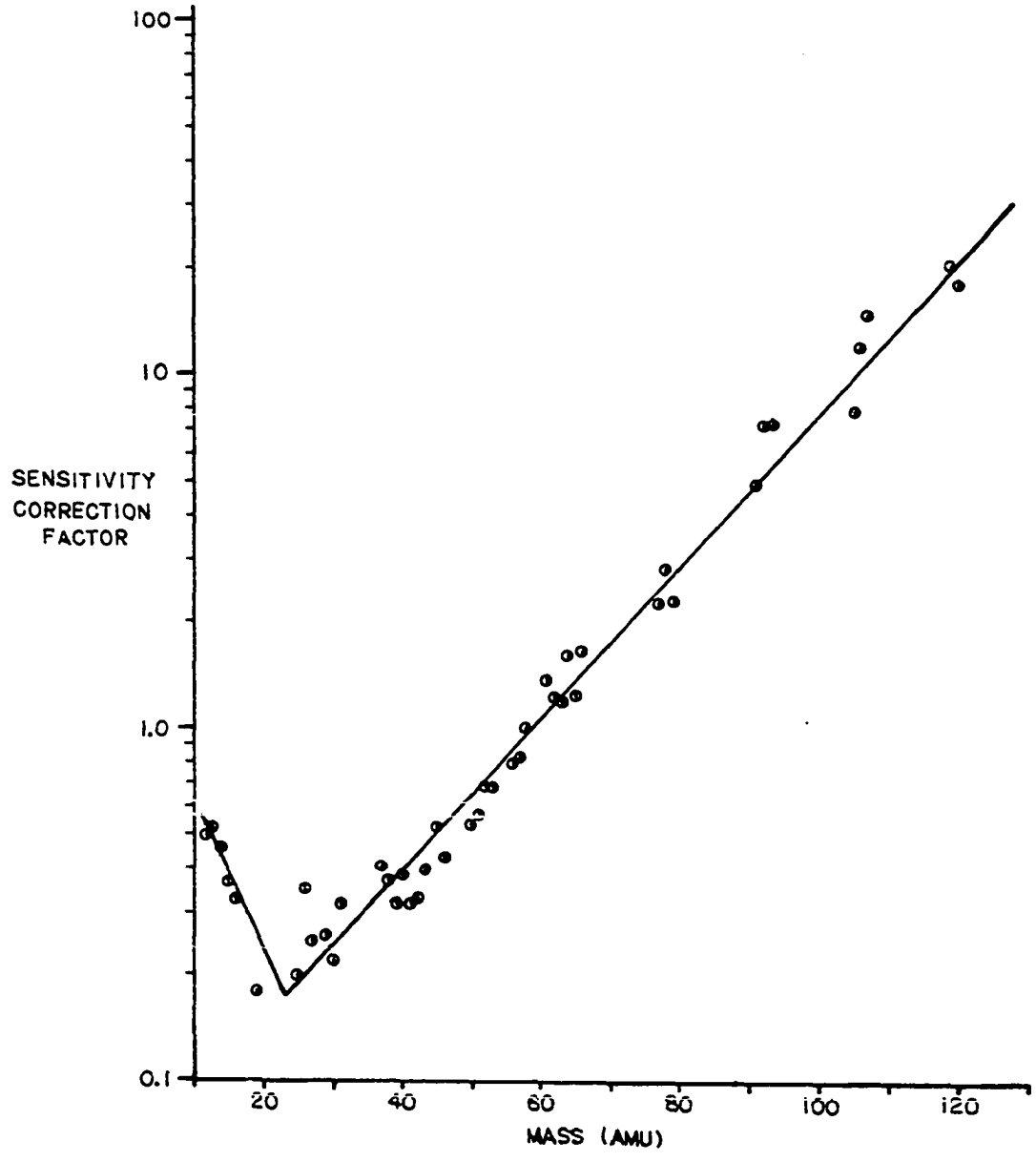


Figure 37. Plot of sensitivity correction factors ($\alpha$ sensitivity$^{-1}$) versus m/e. Experimental points were determined by comparing relative peak intensities obtained from various compounds with tabulated reference spectra

quadrupole power supply), the sensitivity correction factors must be redetermined anytime these instrument settings are changed. It should also be noted that this method of calibrating the relative sensitivity of the instrument for detecting ions of differing m/e corrects for the effects of mass discrimination by the electron multiplier and the ion deflector as well as those arising from the mass filter.

## B. Neutral Fragment Mass Spectra

### 1. Correction for mass discrimination

The same sensitivity correction factors used for correcting for the effects of mass discrimination in conventional mass spectra obtained with a quadrupole instrument were utilized to correct the raw peak intensities of neutral fragment mass spectra.

### 2. Ionization cross-section corrections

Since a neutral fragment mass spectrum should represent the relative abundances of the neutral fragments produced in the primary reaction chamber, the different cross-sections for ionization of the various neutral fragments must be also taken into account. Thus, the ion currents produced by ionization of the various neutral fragments in the secondary chamber must be divided by the corresponding ionization cross-sections. Since ionization cross-sections have not been measured for most of the neutral fragments,

relative ionization cross-sections were calculated by summing the cross-sections of the atoms constituting the neutral fragments. Otvos and Stevenson (38) have shown this method of approximating relative ionization cross-sections to be valid for a wide range of compounds, including hydrocarbons.

### C. Ionization Efficiency Curves

The neutral fragment ionization efficiency curves obtained were evaluated by both linear extrapolation (LE) and Warren's (39) extrapolated voltage difference (EVD) techniques.

# VI. RESULTS AND DISCUSSION

## A. Neutral Fragment Mass Spectra

### 1. Raw neutral fragment mass spectra

The raw neutral fragment mass spectra of benzene, toluene, m-xylene, and mesitylene as obtained by direct recording from the mass spectrometer are shown in Figures 38-41. These raw spectra illustrate the excellent signal/noise ratios obtained for direct detection of the neutral fragments.

The negative signals which are observed are attributed to an instrumental artifact and occur only at those m/e's at which the dc output of the secondary chamber is much larger than the ac output. If the dc output current at a given m/e is large, but not sufficient to cause a negative signal, the ac output signal at that m/e may be attenuated. An example of the occurrence of this phenomenon is the attenuation of the signal due to ionization of $CH_3O^{\cdot}$ (m/e = 31) from ethanol (Figure 42). Such attenuated peaks are readily recognizable because they are characterized by a much higher noise level than that of normal peaks in the same neutral fragment mass spectrum.

Since the energy required to produce a given fragment ion from a parent molecule is always greater than the energy required to produce the same ion by ionization of a neutral fragment, this problem can be eliminated by selecting the

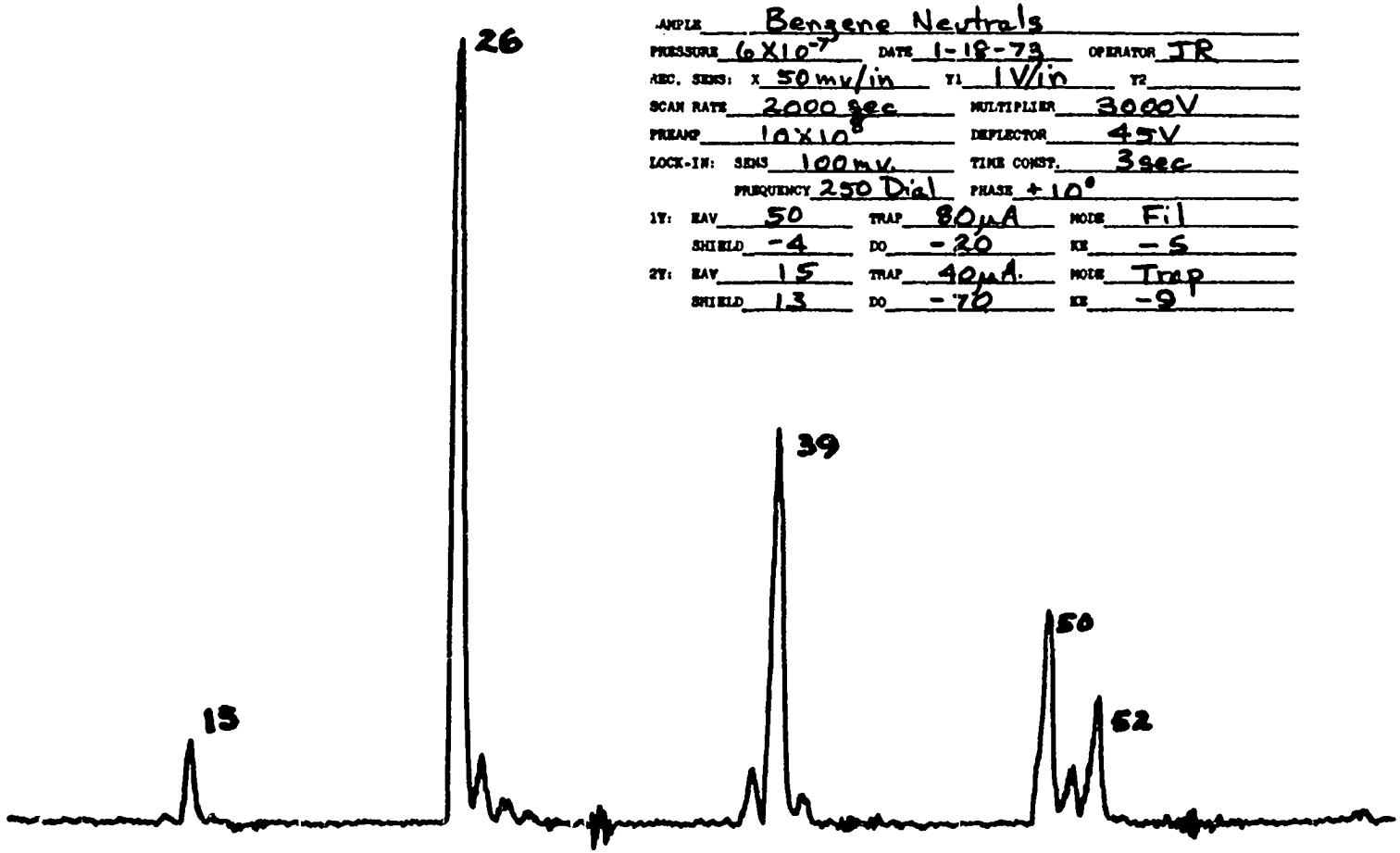


Figure 38. Direct recording of the neutral fragment mass spectrum of benzene

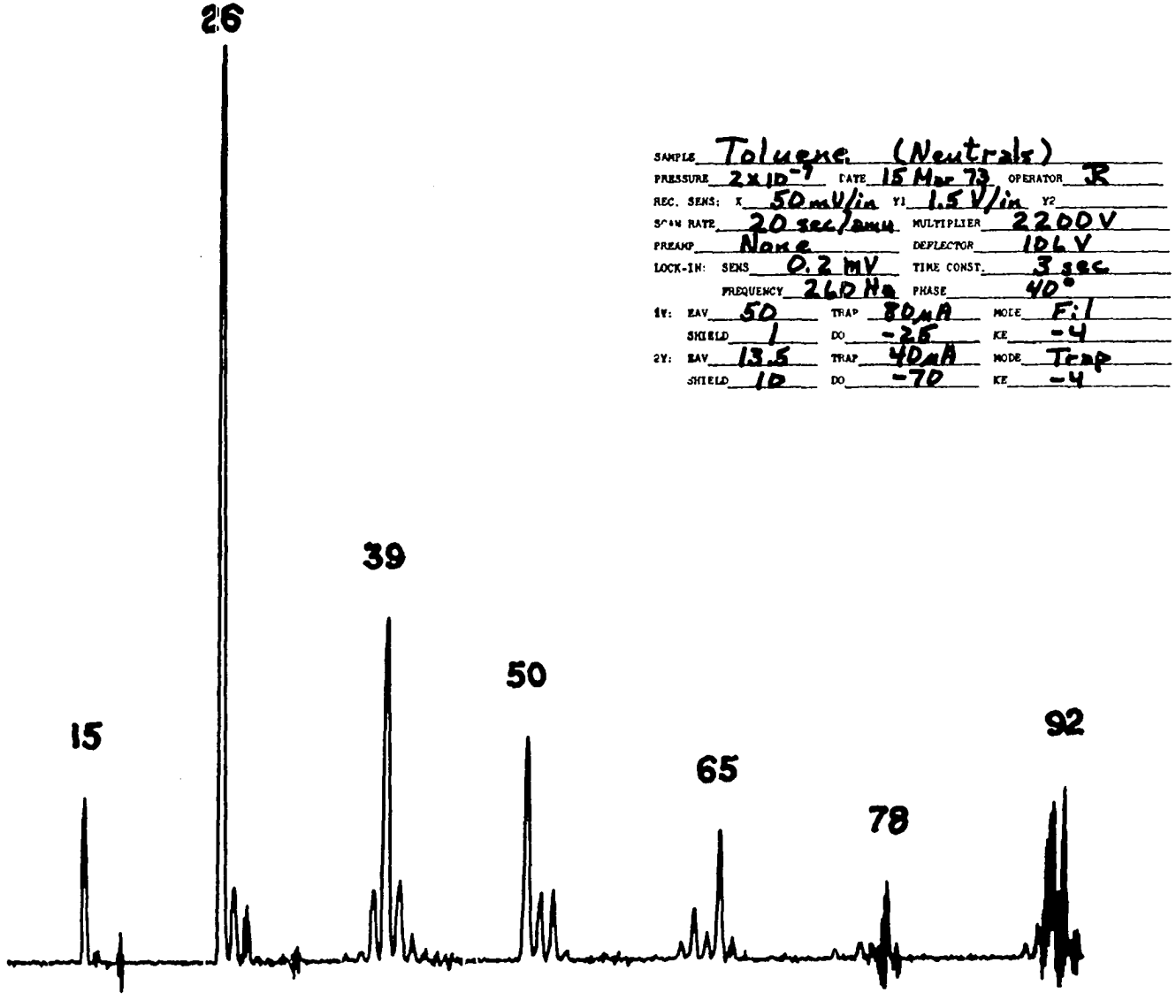


Figure 39. Direct recording of the neutral fragment mass spectrum of toluene

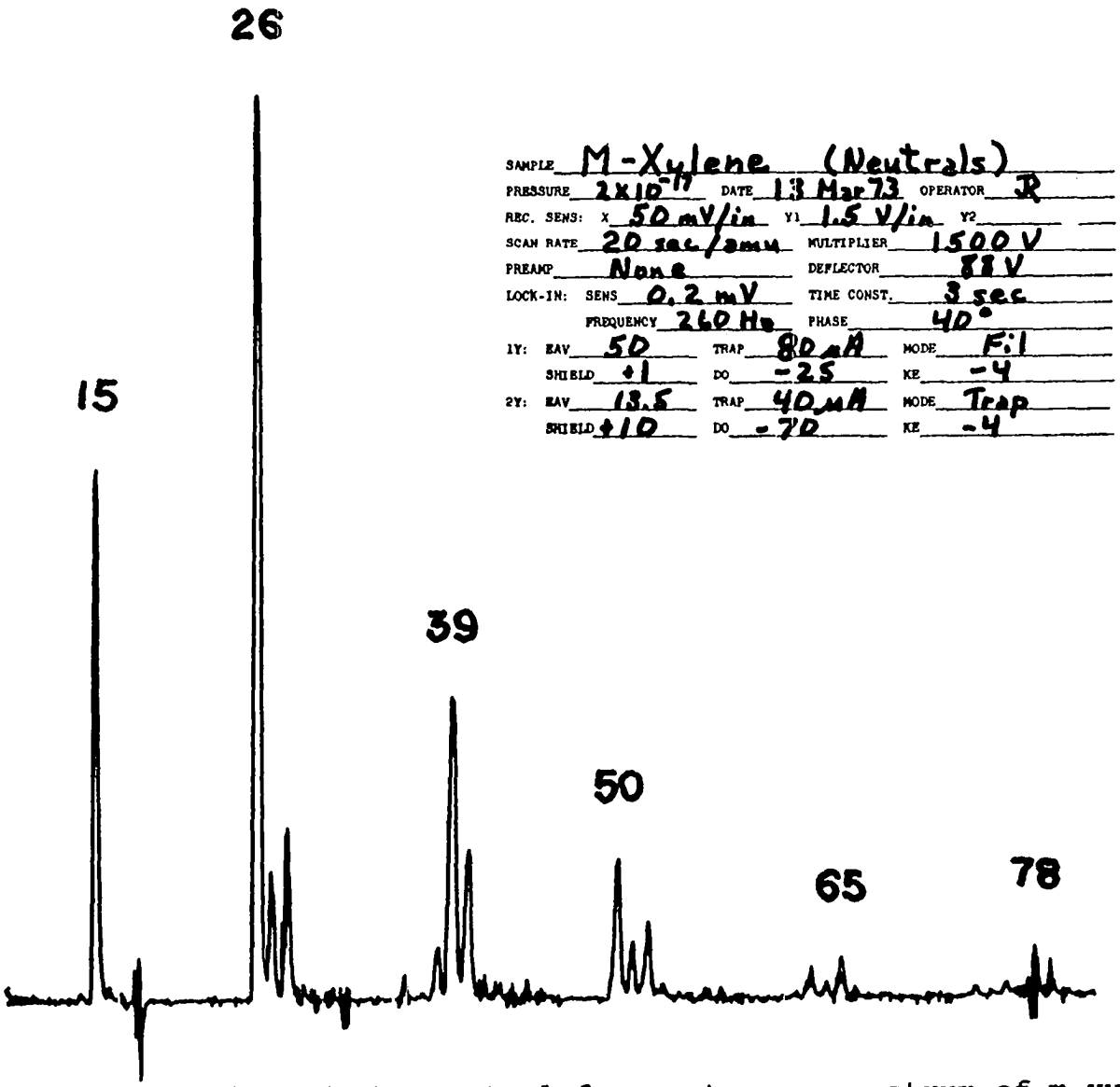


Figure 40. Direct recording of the neutral fragment mass spectrum of m-xylene

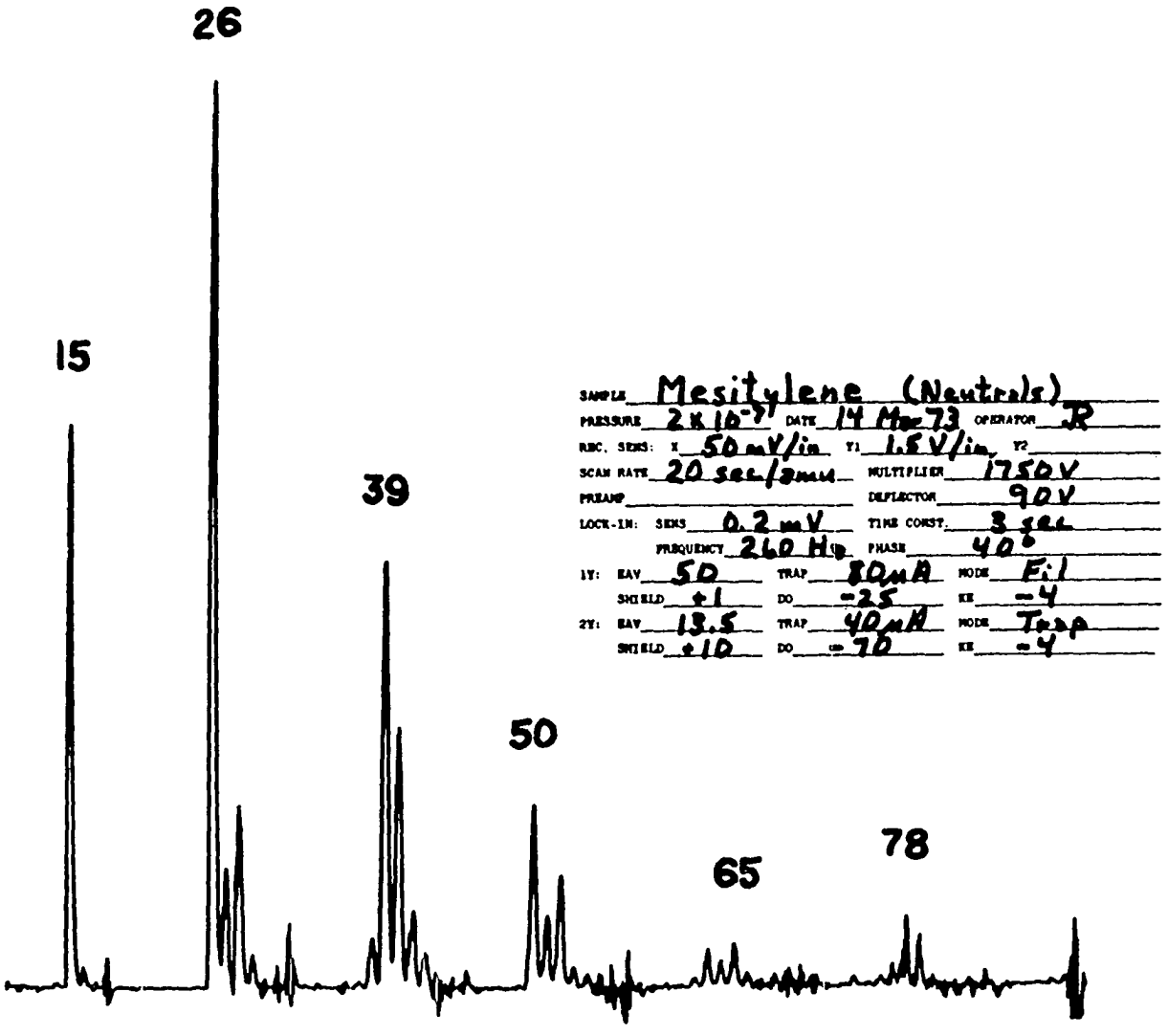


Figure 41. Direct recording of the neutral fragment mass spectrum of mesitylene

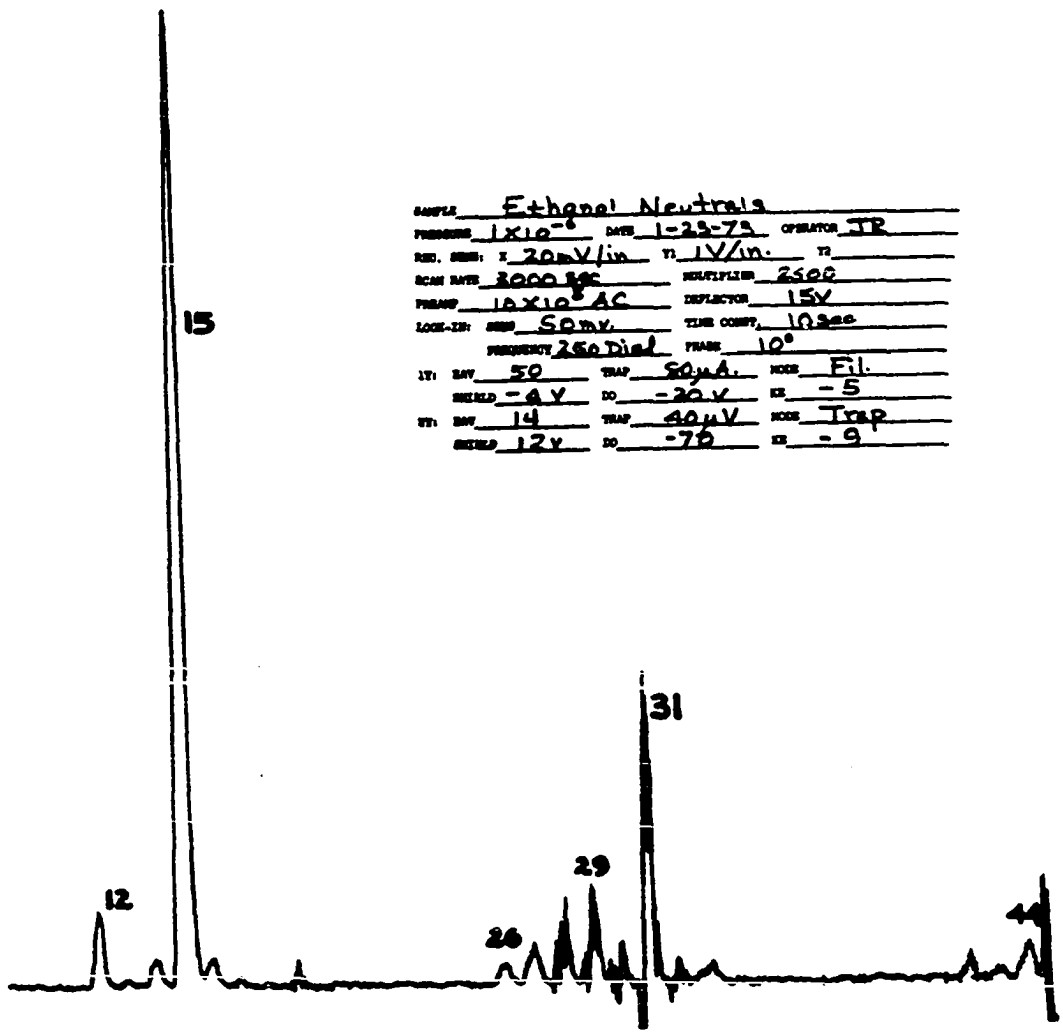


Figure 42. Raw neutral fragment mass spectrum of ethanol. The m/e = 31 peak is severely attenuated because the dc output at m/e = 31 is very large. Such attenuated peaks are characterized by high noise levels

proper electron energy in the secondary chamber. However, if too low a value of ionizing energy is required to eliminate this artifact, discrimination against those neutral fragments with higher ionization potentials results. Thus, a compromise in choosing the proper ionizing energy is often necessary, and it is best to scan the neutral fragment mass spectra at several ionizing energies.

2. Aromatic compounds

The neutral fragment mass spectra of benzene, toluene, o-xylene, m-xylene, p-xylene, and mesitylene, corrected for ionization cross-section and mass discrimination in the quadrupole mass filter, are presented in Figures 43-48. The neutral fragment mass spectra are given for various ionizing energies in the secondary chamber. As expected, the neutral fragments with high ionization potentials (see, for example m/e = 26) make up a greater portion of the spectra as the ionizing energy in the secondary chamber is increased, while those neutral fragments with low ionization potentials (see, for example m/e = 15,39) make up a proportionately lower portion of the spectra at the higher energies.

The observation of a neutral fragment at m/e = 78 from benzene at 13 eV, but not at higher energies is an example of the effect of the electronic artifact described previously. Excited parent molecules have been observed for all of these compounds, but because of signal attenuation by the large dc

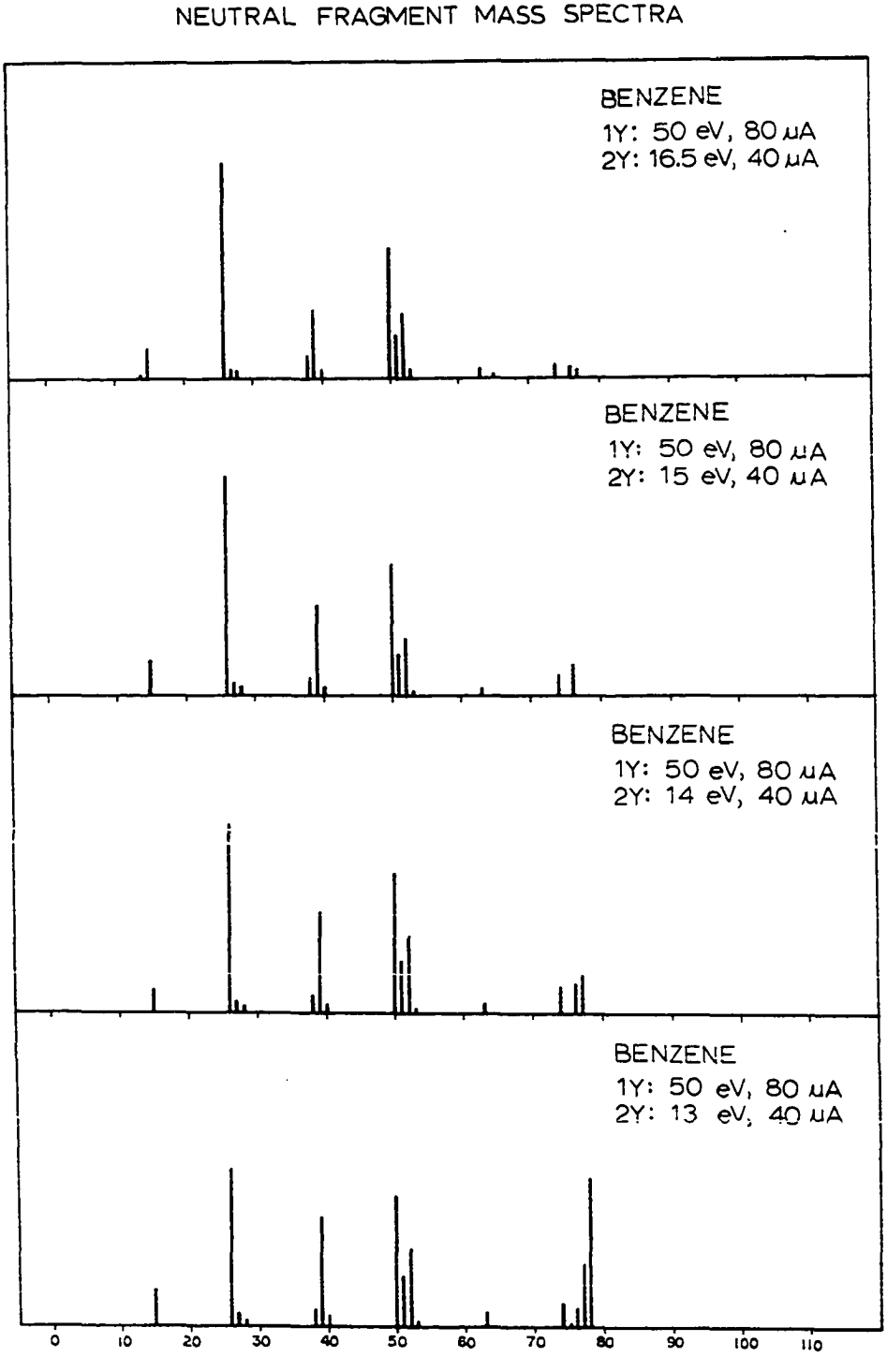


Figure 43. Neutral fragment mass spectra of benzene at various ionizing energies in the secondary chamber

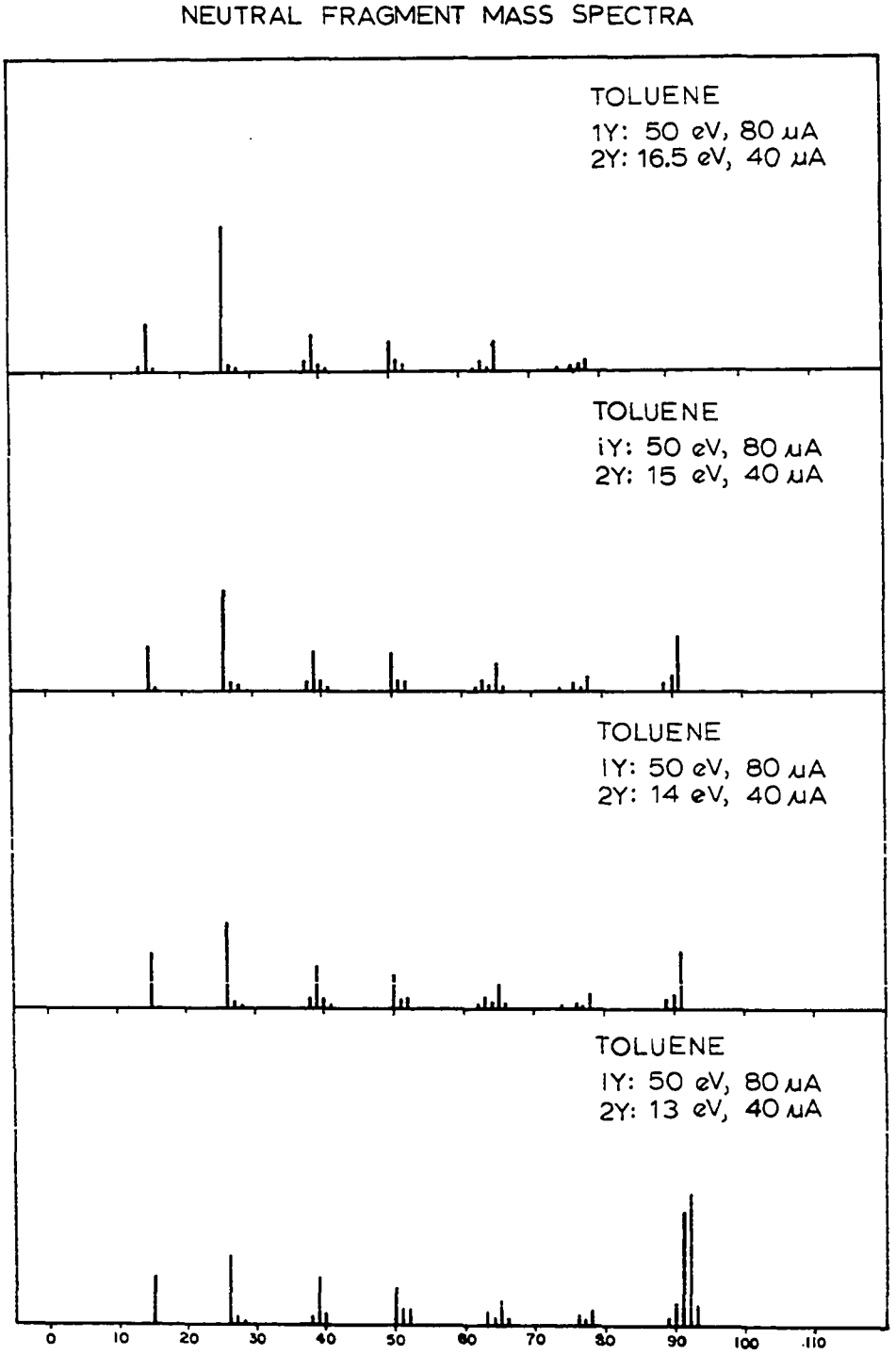


Figure 44. Neutral fragment mass spectra of toluene at various ionizing energies in the secondary chamber

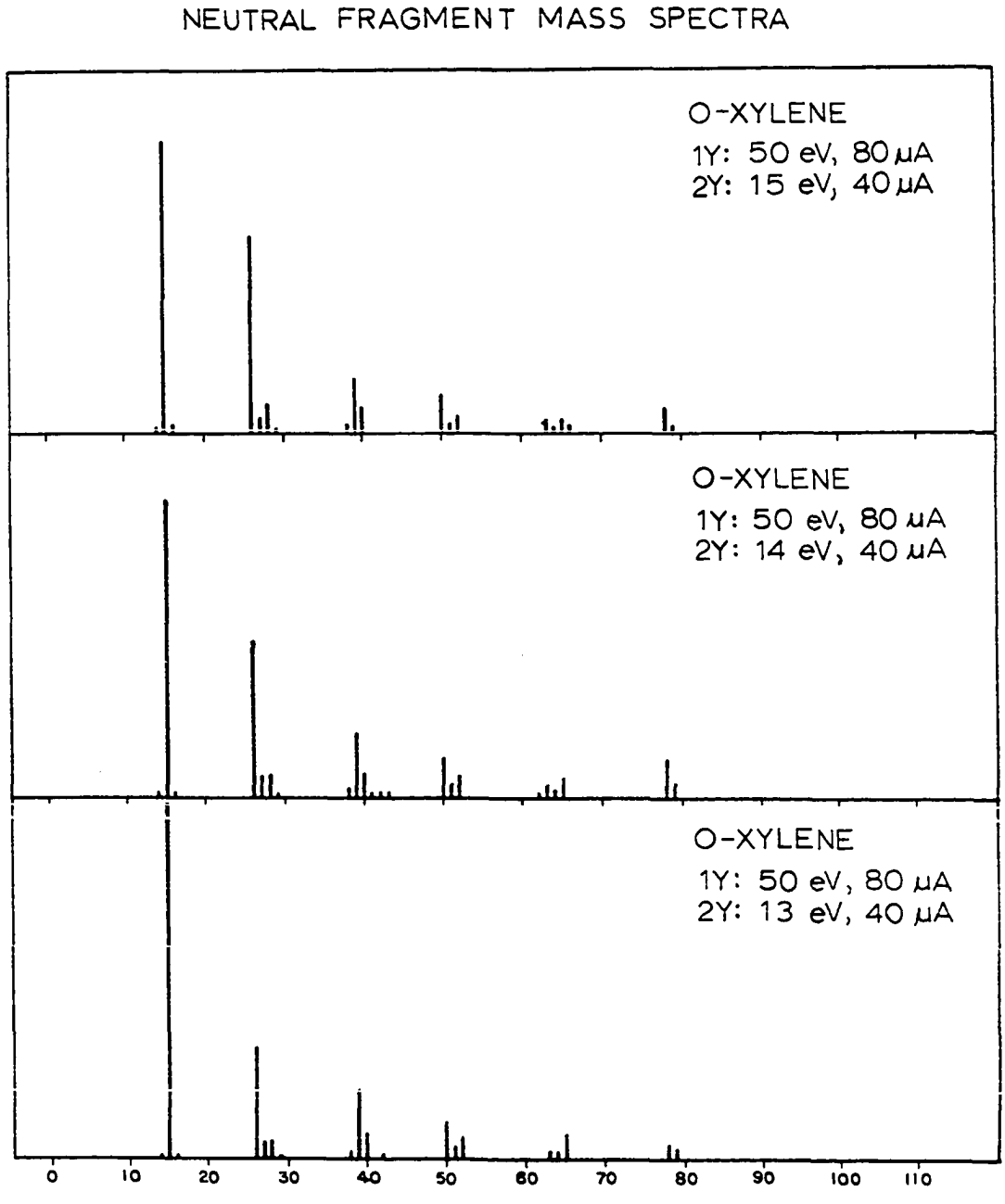


Figure 45. Neutral fragment mass spectra of o-xylene at various ionizing energies in the secondary chamber

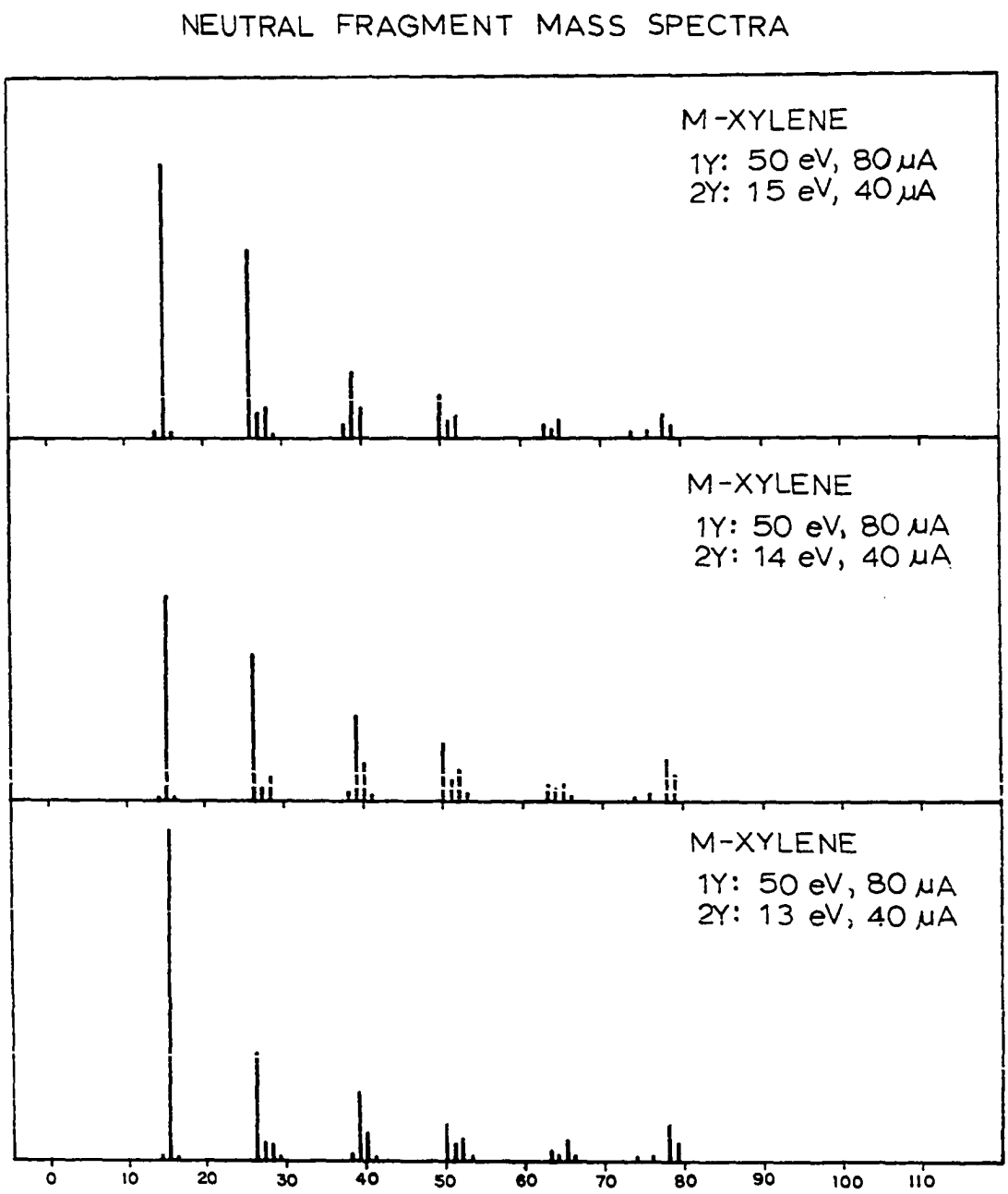


Figure 46. Neutral fragment mass spectra of m-xylene at various ionizing energies in the secondary chamber

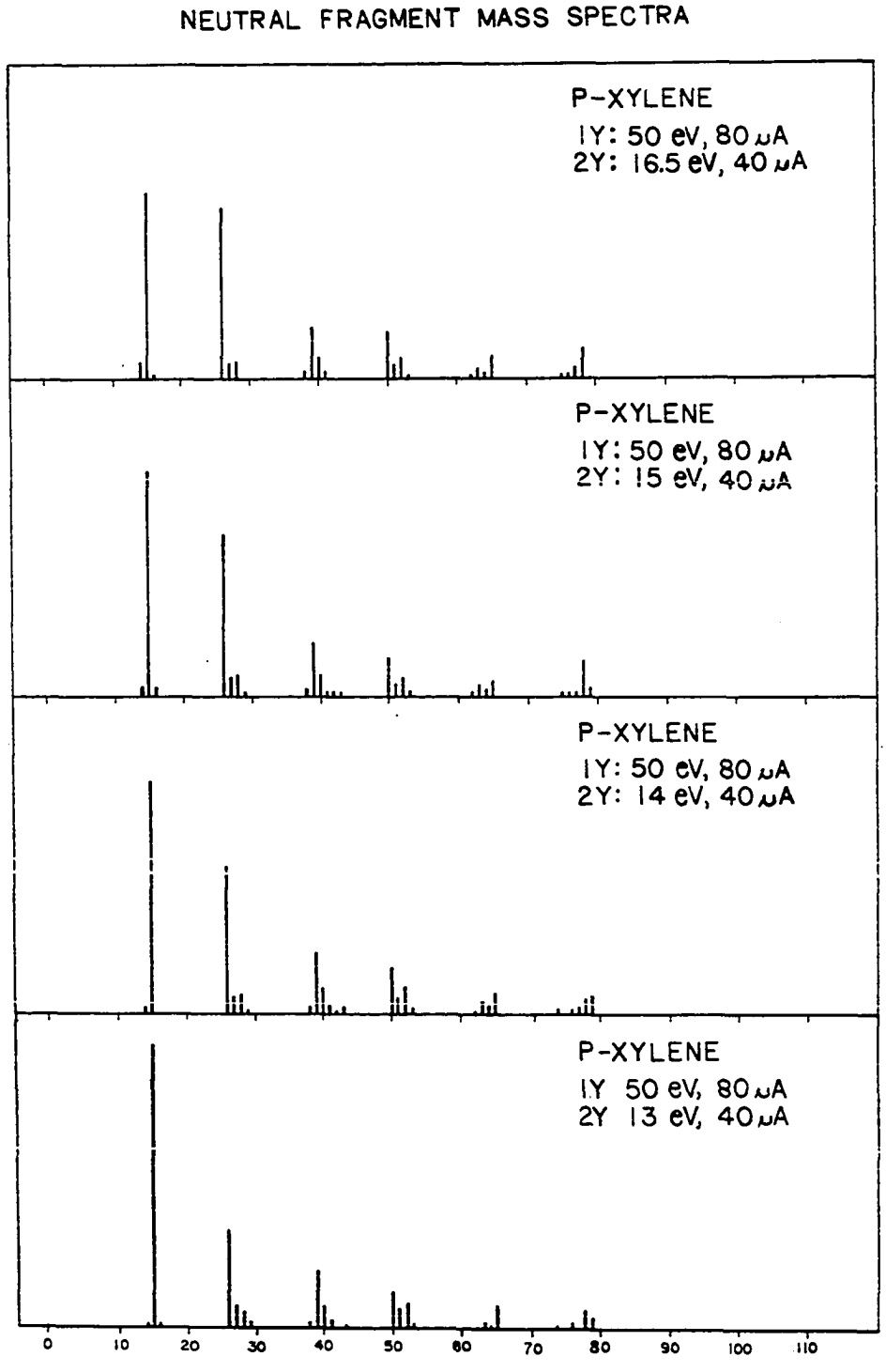


Figure 47. Neutral fragment mass spectra of p-xylene at various ionizing energies in the secondary chamber

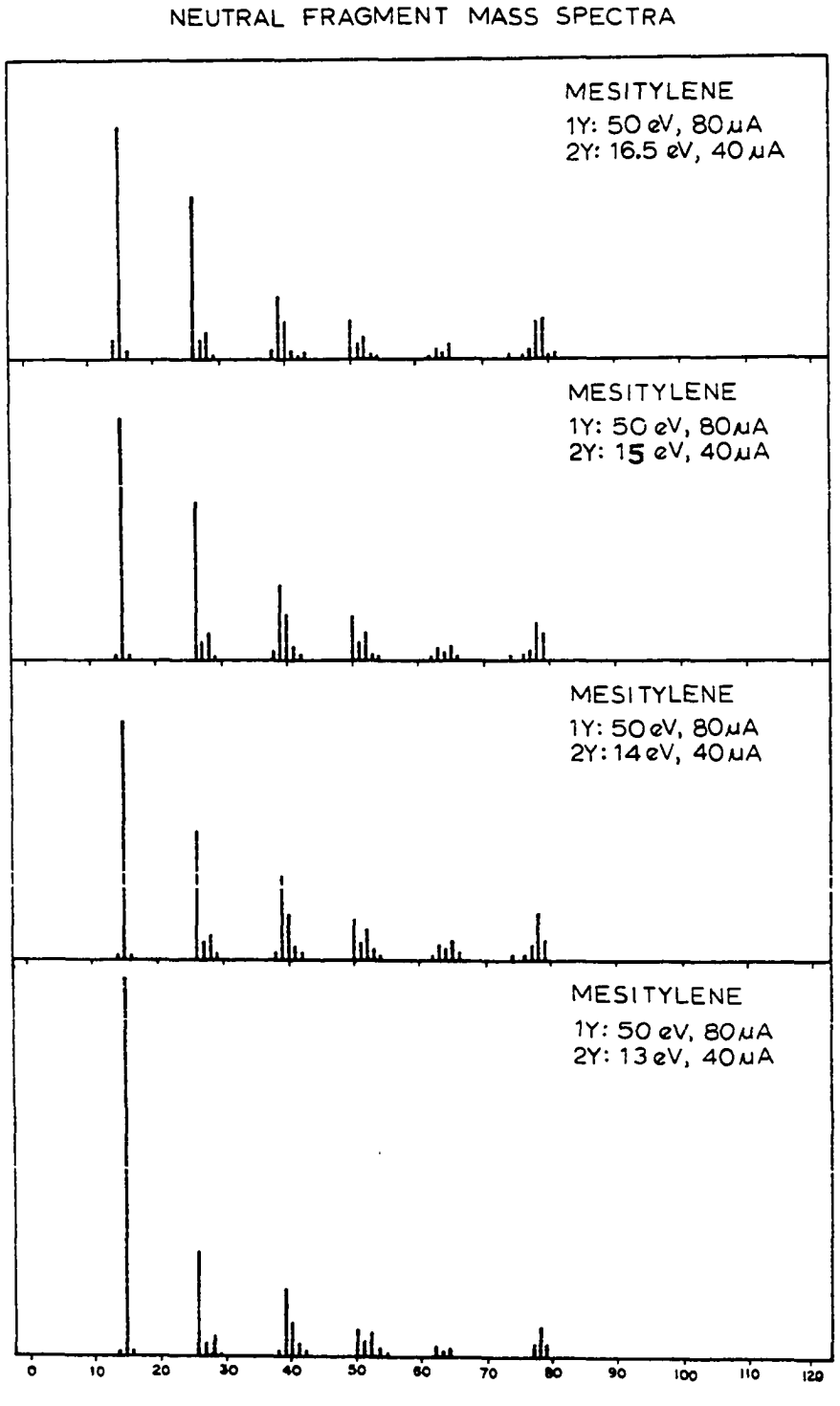


Figure 48. Neutral fragment mass spectra of mesitylene at various ionizing energies in the secondary chamber

component at the parent m/e, they are observed only over a very narrow range of secondary electron energy.

If sufficient electron energy is utilized in the secondary chamber, fragmentation of the neutral fragments occurs, as evidenced by the increase in the relative abundance of the m/e = 14 ($CH_2^+$) ion current in the neutral fragment mass spectra in Figures 43-48 as the secondary electron energy is increased. Since there is generally a complex mixture of neutral fragments present, it is very difficult to identify the specific fragmentation reactions which are occurring. Thus, utilization of a high enough energy to cause significant fragmentation of the neutral fragments in the secondary ionization chamber merely complicates the interpretation of the resulting neutral fragment mass spectra.

The neutral fragment mass spectra of benzene (Figure 43) agree very well with that reported by Beck (19), who detected benzene neutral fragments with m/e's of 1,2,15,26,28,39,40, 50,52,74, and 76. The agreement is even more remarkable when one considers that the two spectra were obtained at much different electron energies. No data is available in the literature for comparison with the remainder of the neutral fragment mass spectra described herein.

The neutral fragment mass spectra of benzene, toluene, m-xylene, and mesitylene are compared in Figure 49. Note the striking similarity of the spectra, with the expected increase

Figure 49. Comparison of the neutral fragment mass spectra of benzene, toluene, m-xylene, and mesitylene

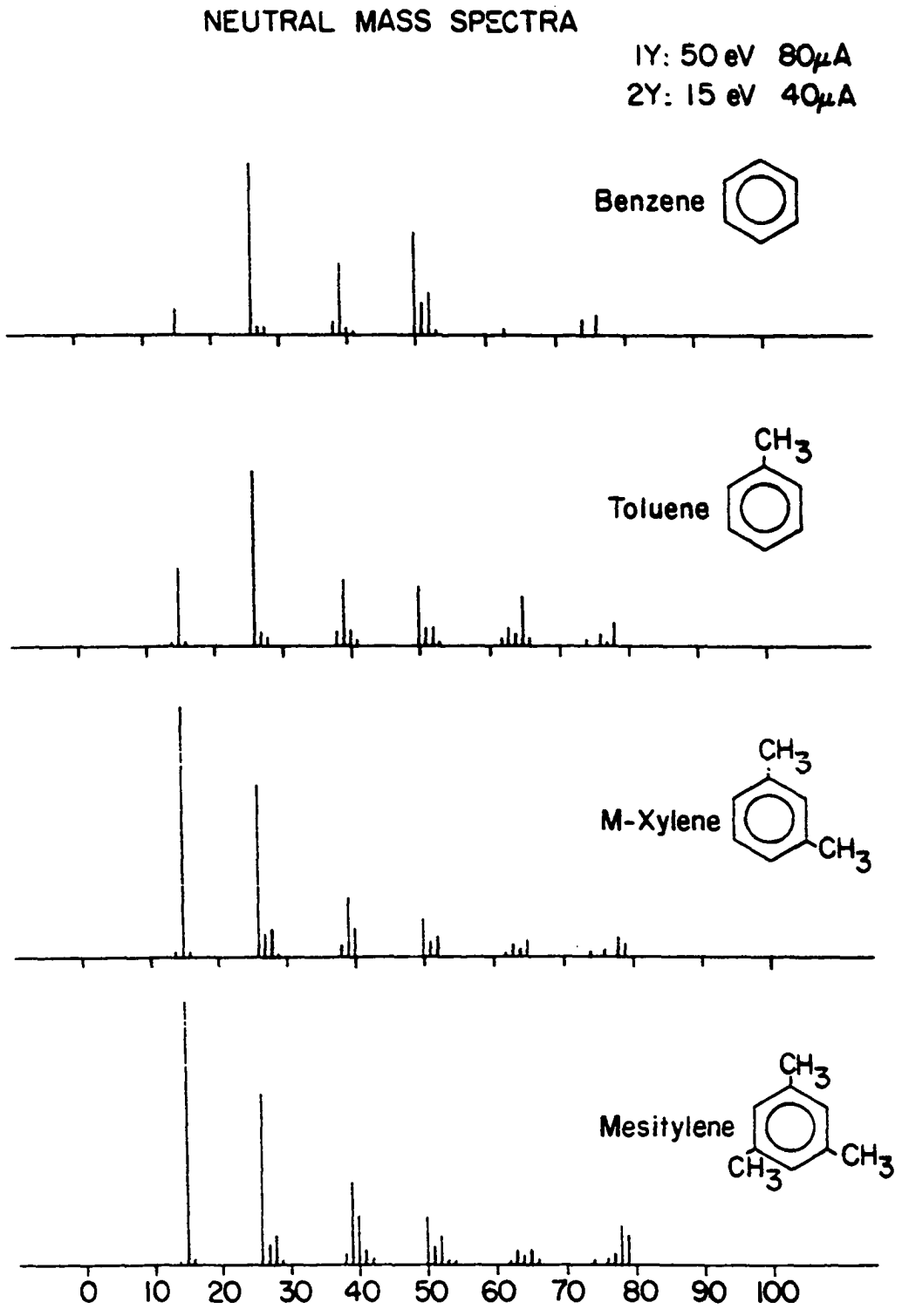
NEUTRAL MASS SPECTRA
1Y: 50 eV 80μA
2Y: 15 eV 40μA
Benzene
Toluene
CH3
M-Xylene
CH3
CH3
Mesitylene
CH3
CH3
CH3
0 10 20 30 40 50 60 70 80 90 100

in relative abundance of $CH_3^{\cdot}$ (m/e = 15) as additional methyl groups are substituted on the ring. Note also the increased abundance of higher mass neutral fragments as the complexity of the molecules increases. The fact that $CH_3^{\cdot}$ (m/e = 15) is observed as a neutral fragment from benzene and that $C_2H_2$ (m/e = 26) and $C_3H_3^{\cdot}$ (m/e = 39) are relatively abundant neutral fragments in the neutral fragment mass spectrum of mesitylene indicates that the hydrogen atoms on these molecules scramble after interaction with an election and before the molecule-ion fragments. These neutral fragments cannot be formed by simple, straightforward fragmentation reactions. The conclusion that hydrogen scrambling is prevalent in aromatic hydrocarbon ions has been reached by numerous other authors (2-9) using different types of mass spectrometric data.

3. Heterocyclic compounds

The neutral fragment mass spectra of pyridine, pyrrole, and thiophene are presented in Figures 50-52. It is interesting to note that many of the neutral fragments common to all of the aromatic hydrocarbon spectra, chiefly $CH_3^{\cdot}$ (m/e = 15), $C_2H_2$ (m/e = 26), $C_3H_3^{\cdot}$ (m/e = 39), $C_4H_2$ (m/e = 50), $C_4H_3^{\cdot}$ (m/e = 51), and $C_4H_4$ (m/e = 52), are also prevalent in the mass spectra of these heterocyclic compounds. Nitrogen- and sulfur- containing neutral fragments are also abundant:

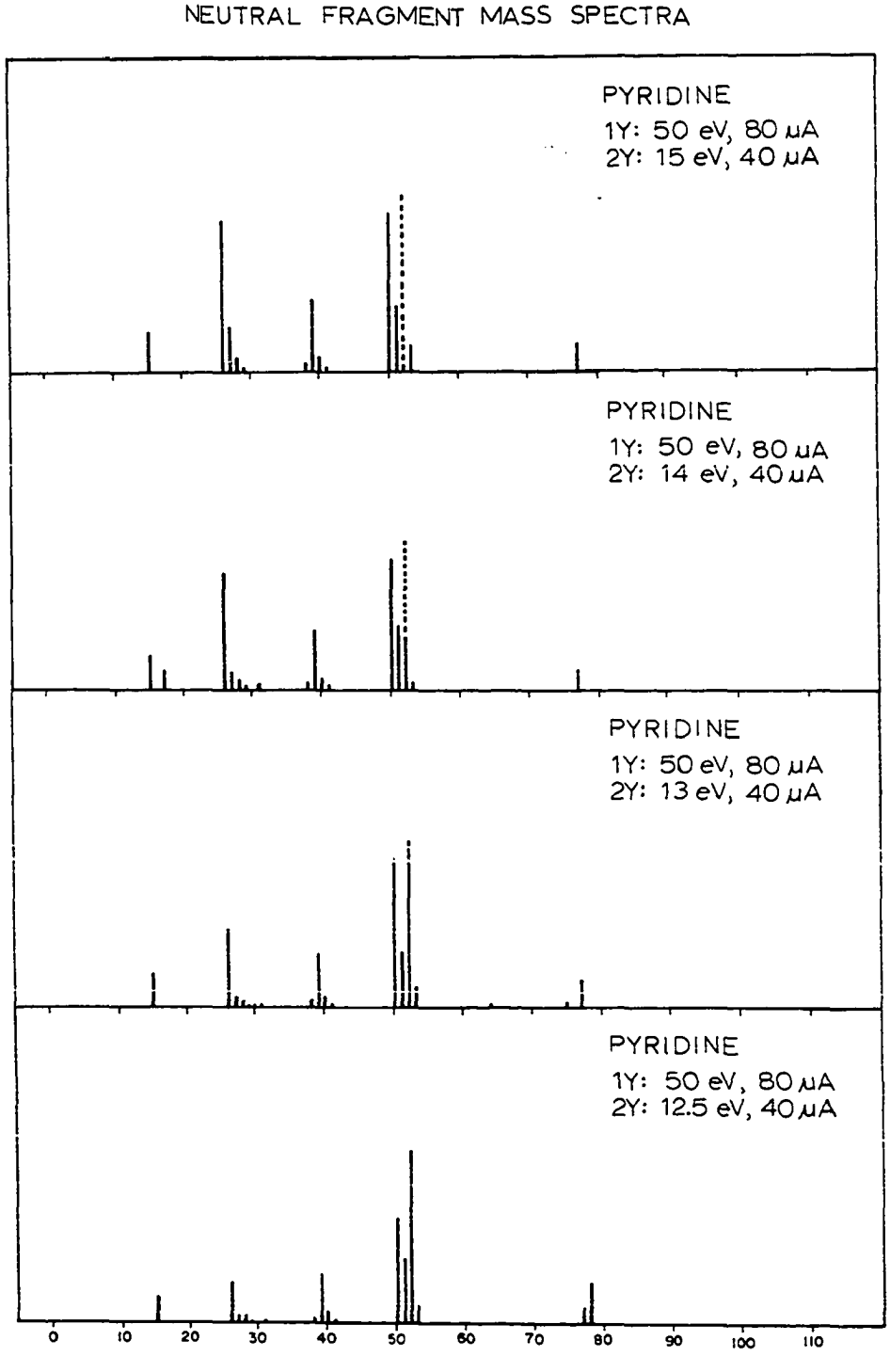


Figure 50. Neutral fragment mass spectra of pyridine. Dashed lines indicate attenuation due to large dc signals

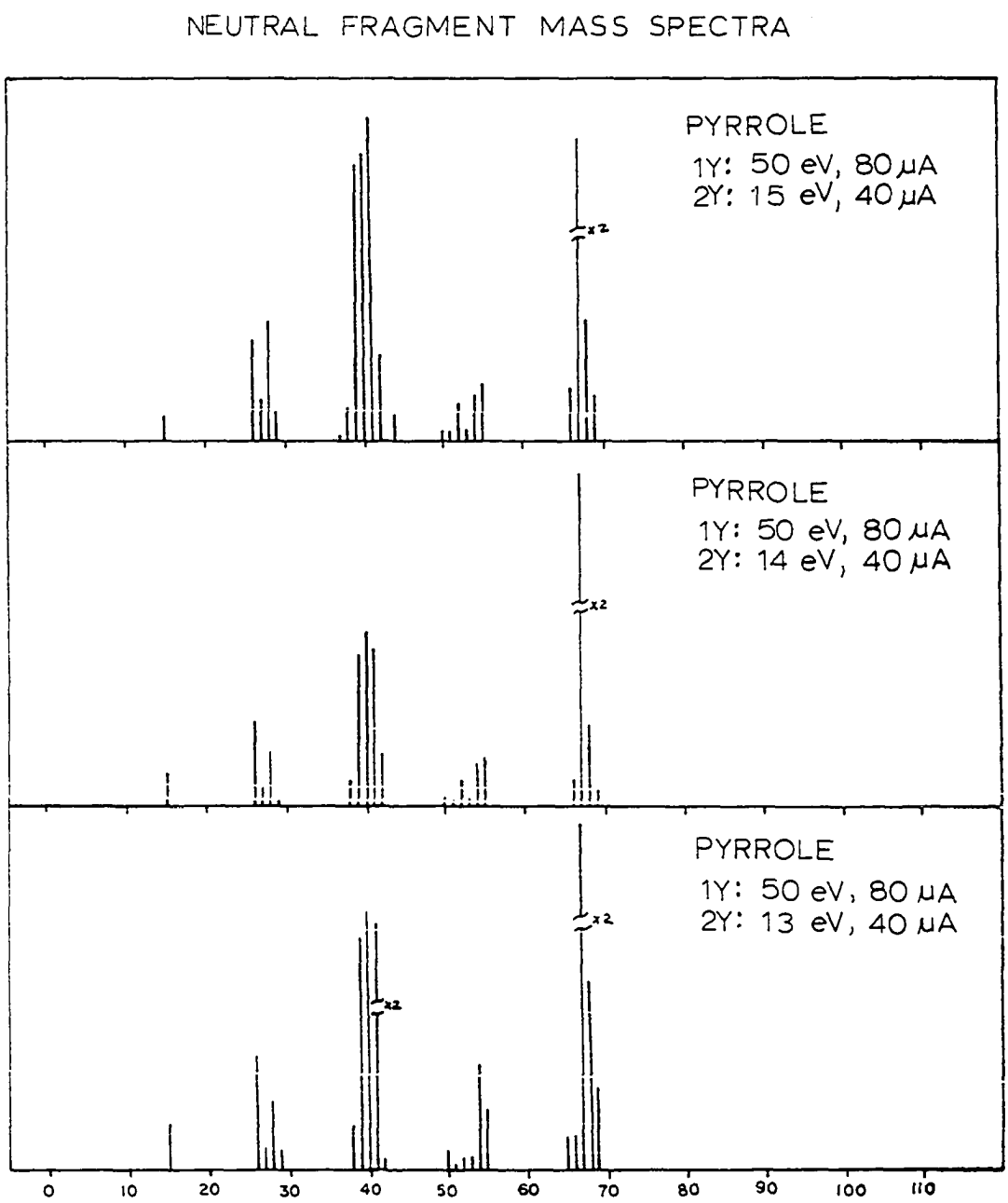


Figure 51. Neutral fragment mass spectra of pyrrole. Dashed lines indicate attenuation due to large dc signals

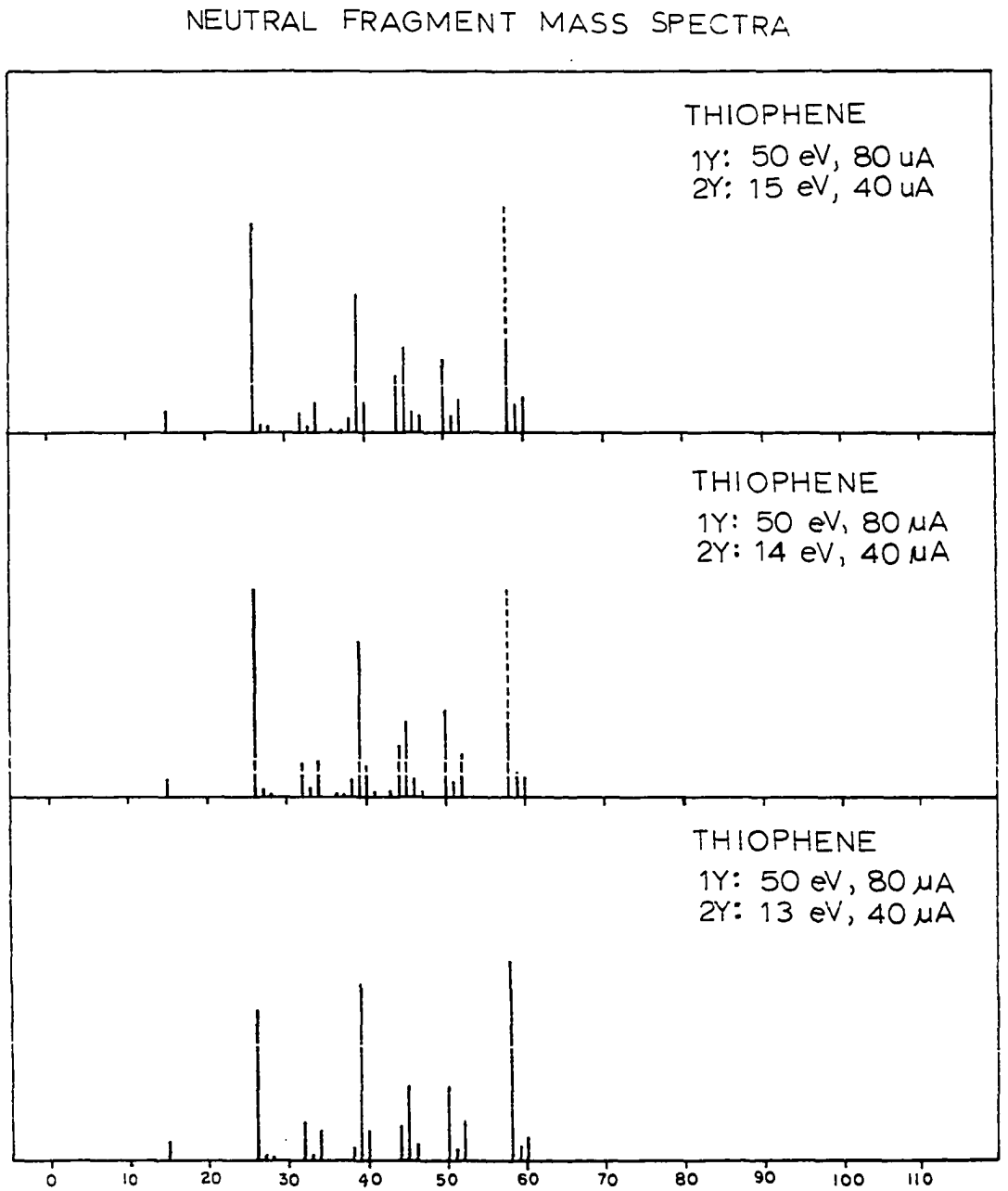


Figure 52. Neutral fragment mass spectra of thiopene. Dashed lines indicate attenuation due to large dc signals. The signal at m/e = 32 was found to have a zero order dependence on the 2Y electron beam, and is attributed to long-lived excited sulfur atoms which autoionize in the secondary chamber

$CNH^{\cdot}$ (m/e = 27) and $C_3H_2N$ (m/e = 52) from pyridine, $CH_2N$ (m/e = 28), $C_2H_2N$ (m/e = 40), $C_3H_3N^{\cdot}$ (m/e = 41), $C_3H_4N$ (m/e = 54), and $C_4H_4N$ (m/e = 66) from pyrrole, and S (m/e = 32), $H_2S$ (m/e = 34), $CH_2S$ (m/e = 44), $CH_3S^{\cdot}$ (m/e = 45), $CH_4S$ (m/e = 46), and $C_2H_2S$ (m/e = 58) from thiophene.

The signal observed at m/e = 32 in the neutral fragment mass spectrum of thiophene was found to have a zero-order dependence on the secondary electron beam, and is attributed to long-lived (> $10^{-5}$ sec) excited sulfur atoms which autoionize in the secondary chamber. This excited species generates the most intense signal of this type observed to date.

## B. Neutral Fragment-Positive Ion Correlations

The neutral fragment mass spectra of benzene, toluene, o-xylene, m-xylene, p-xylene, and mesitylene are compared with their corresponding 50 eV positive ion mass spectra in Figures 53-58. The neutral fragment mass spectra are plotted with ascending mass, while the corresponding positive ion mass spectra are plotted above them with descending mass, so that correlations between neutral fragments and their complimentary positive ions can be observed more readily. The neutral fragment mass spectrum and the positive ion mass spectrum of each compound are normalized so that the sum of the ion currents from m/e = 12 to m/e = (Parent-12) in both spectra are equal. The range over which the normalization was

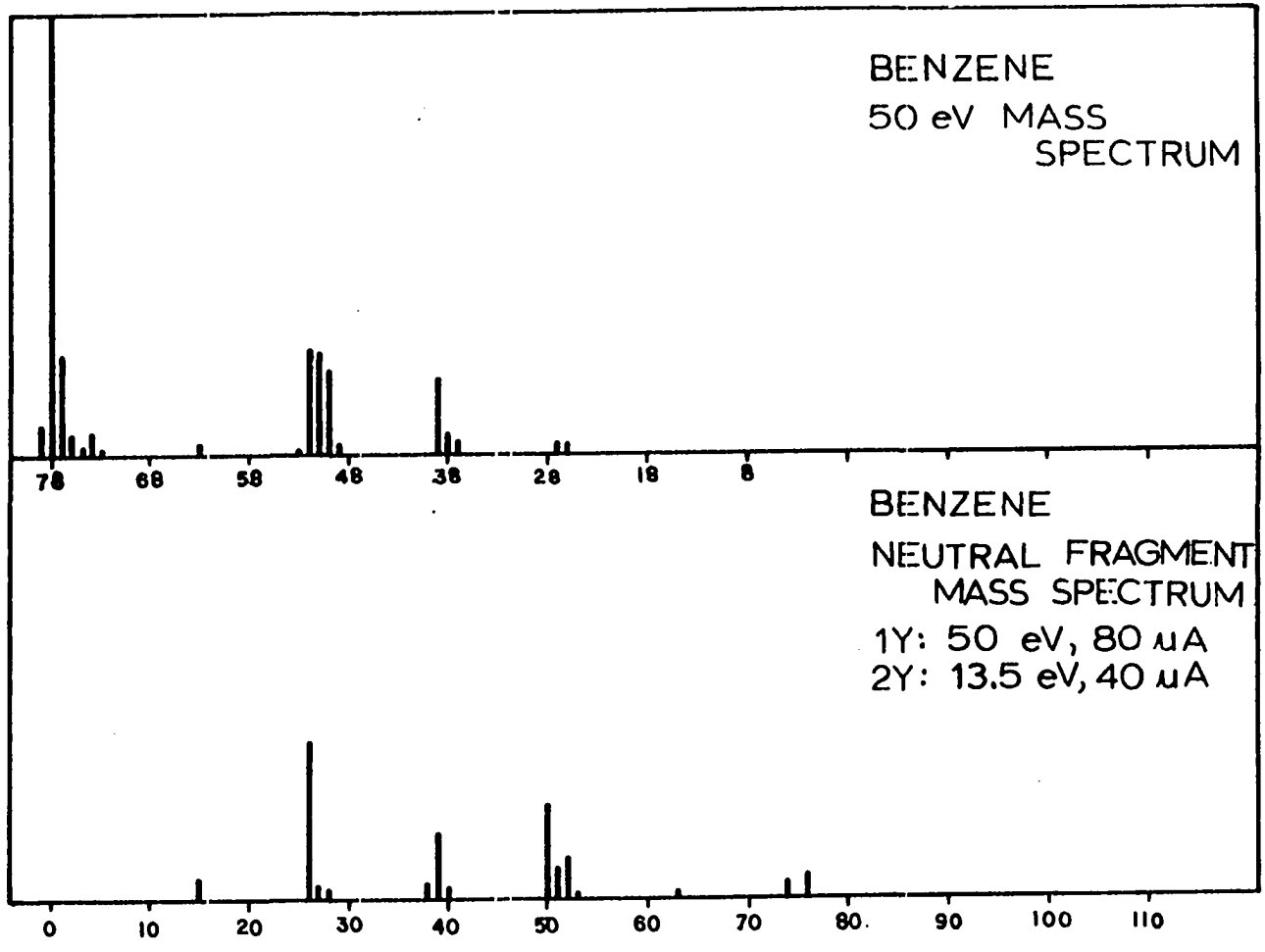


Figure 53. Comparison of the neutral fragment mass spectrum of benzene with its complementary 50 eV positive ion mass spectrum

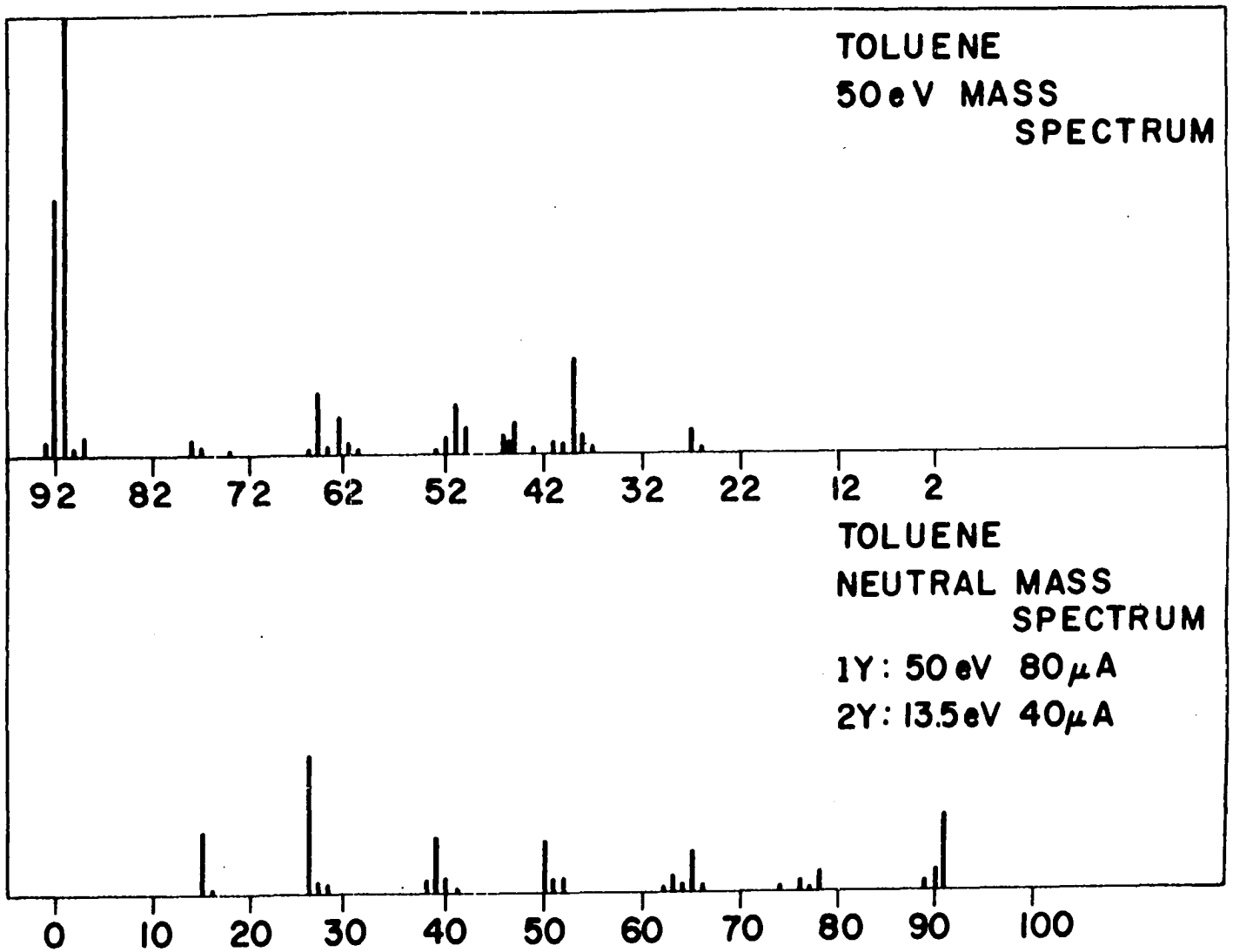


Figure 54. Comparison of the neutral fragment mass spectrum of toluene with its complementary 50 eV positive ion mass spectrum

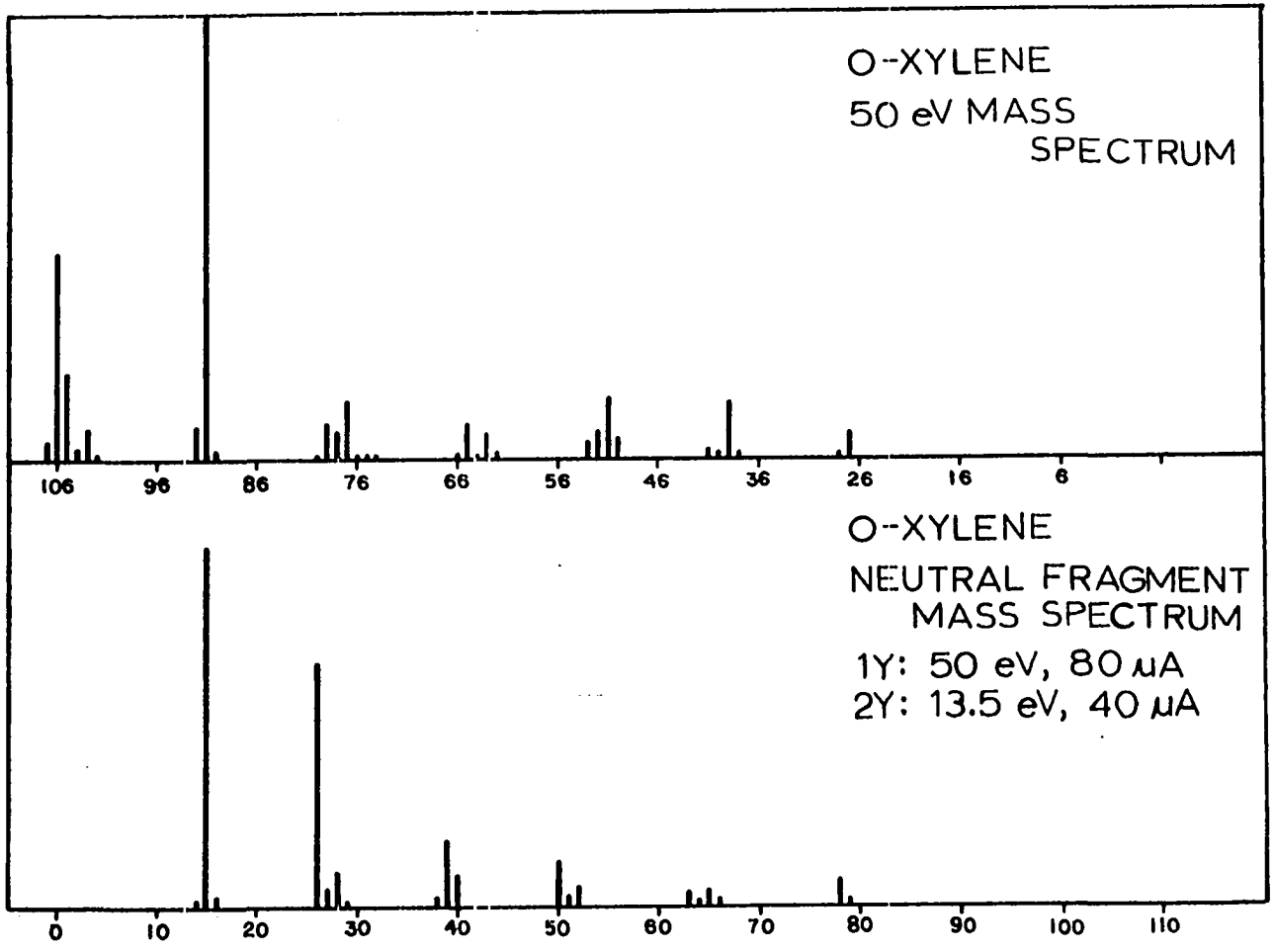


Figure 55. Comparison of the neutral fragment mass spectrum of o-xylene with its complementary 50 eV positive ion mass spectrum

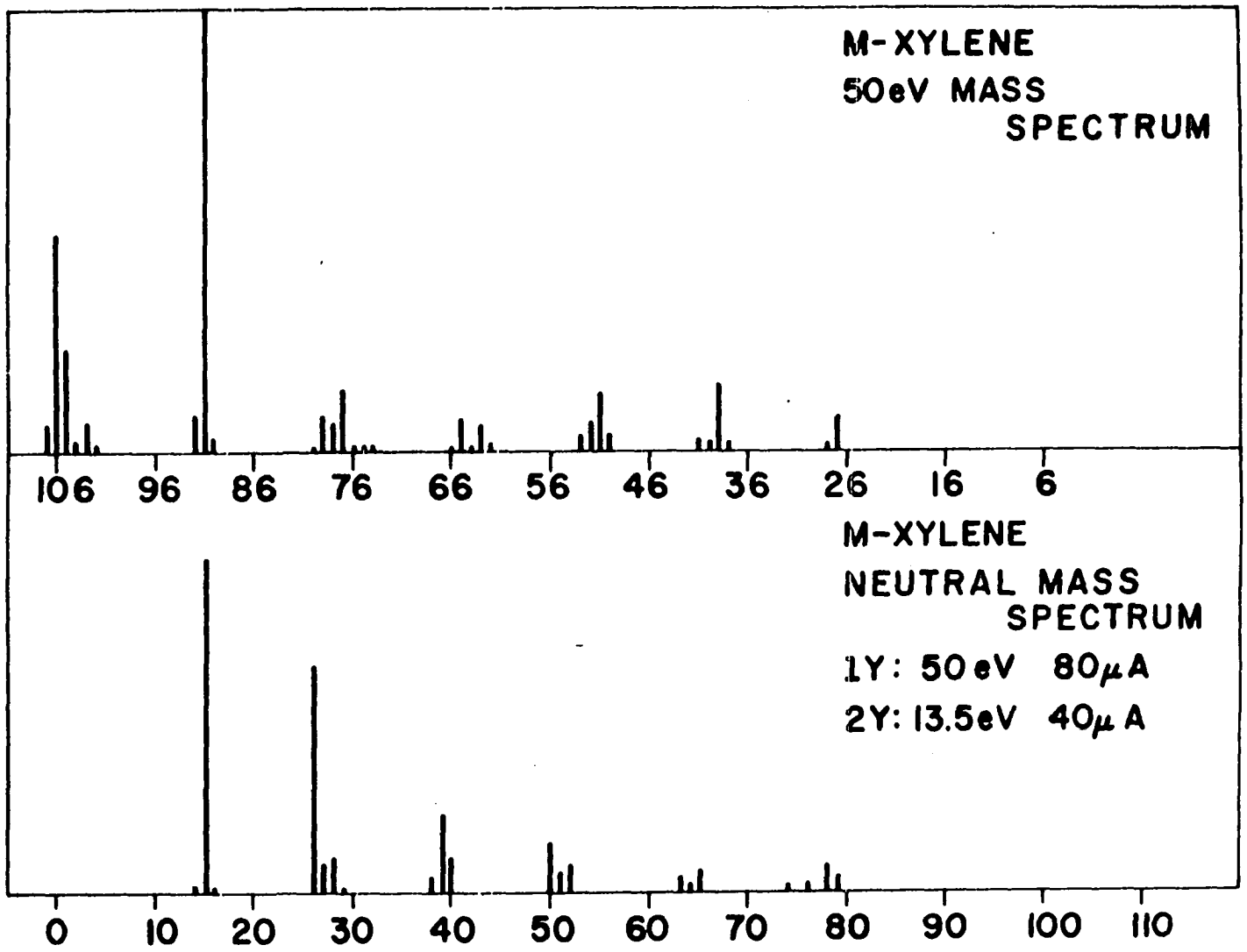


Figure 56. Comparison of the neutral fragment mass spectrum of m-xylene with its complementary 50 eV positive ion mass spectrum

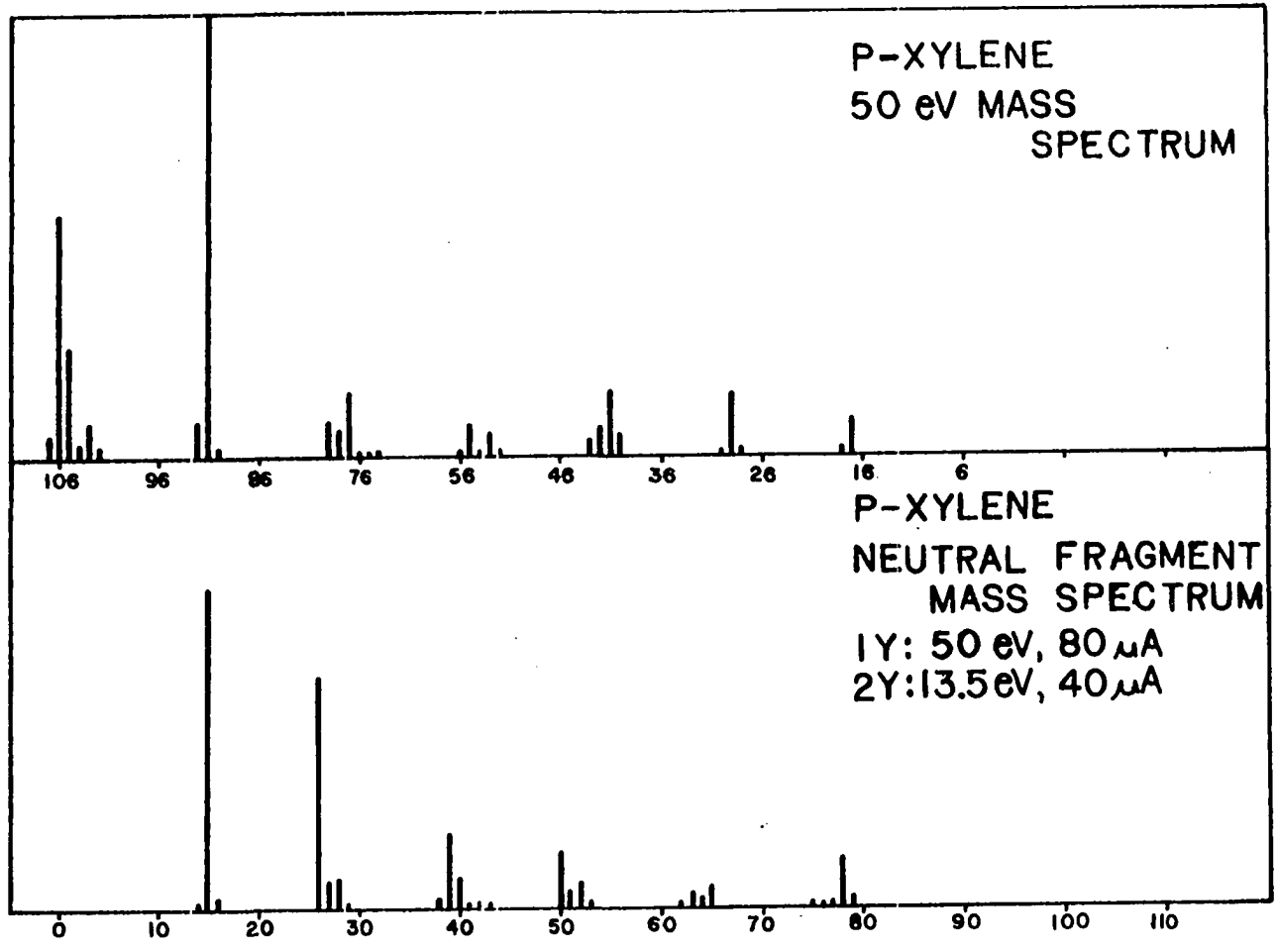


Figure 57. Comparison of the neutral fragment mass spectrum of p-xylene with its complementary 50 eV positive ion mass spectrum

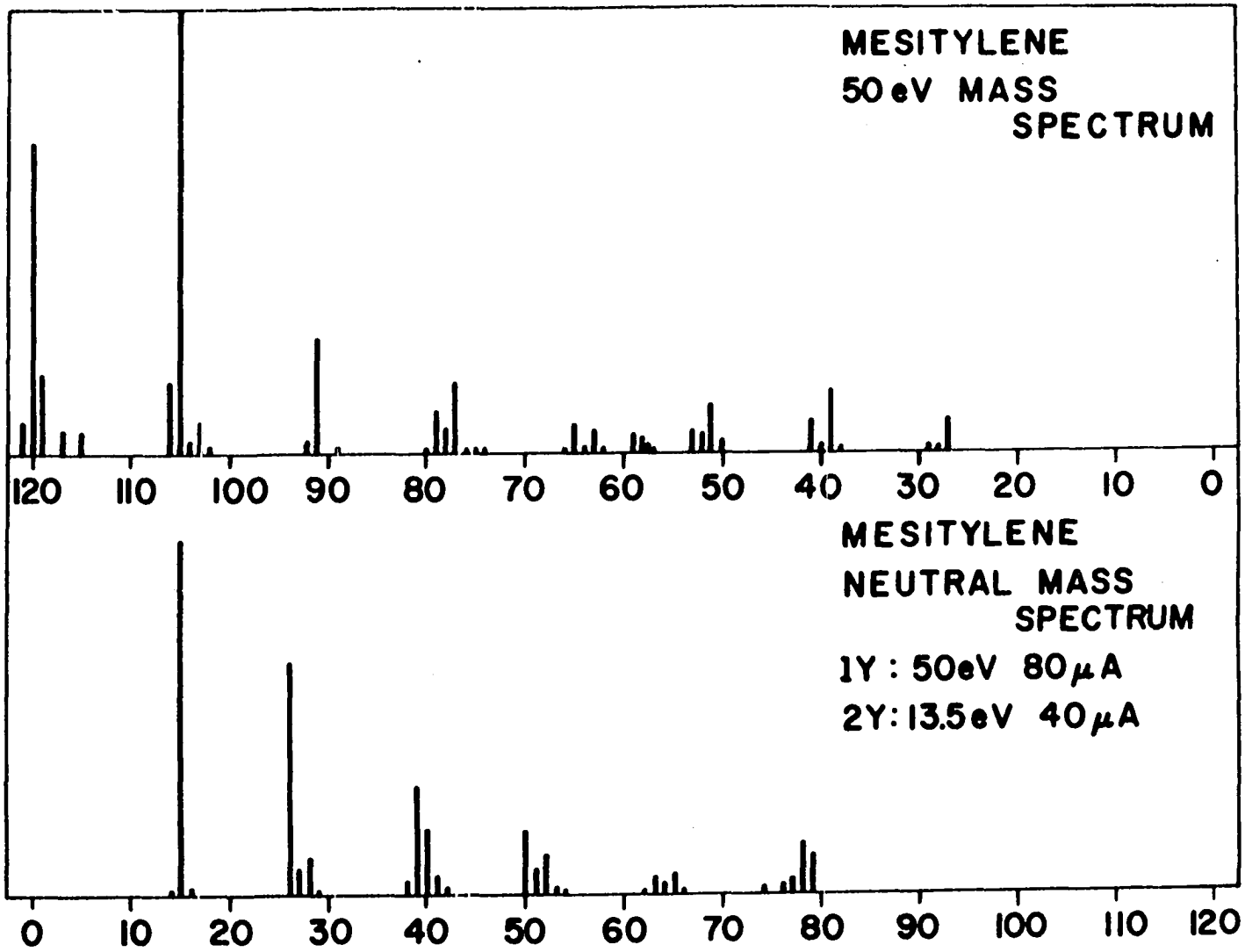


Figure 58. Comparison of the neutral fragment mass spectrum of mesitylene with its complementary 50 eV positive ion mass spectrum

performed was limited for two reasons:

1. The limited dynamic range of the quadrupole power supply prevented focussing of m/e = 1,2 through the mass filter when the desired upper limit of mass range was achieved. Since m/e = 1,2 ($H^{\cdot}$,$H^+$,$H_2$,$H^+_2$) are the only species with m/e < 12 attributed to the samples, species with m/e < 12 were not observed and thus could not be included in the normalization. Also, since a correlation between a neutral fragment and its complementary positive ion is to be made, and since species with m/e < 12 are not included in the normalization, it follows that their complementary species should not be included, i.e., those with m/e > (Parent-12).

2. The electronic artifact described earlier prevented a reliable measurement of the abundances of excited parent molecules ($P^*$) and neutral fragments $(P-H)^{\cdot}$ with m/e = (Parent-1), since $P^+$ and $(P-H)^+$ are the two most abundant species in the low-energy positive ion mass spectra of the compounds studied. Where neutral fragments and positive ions with m/e > (P-12) were detected, they were included in the spectra, but were not included in the sums of ion currents upon which the normalization was based.

Although exact correlation of the positive ion mass spectra with the neutral fragment mass spectra of these aromatic compounds was not observed, it should be noted that the shape of the envelopes of the two types of spectra correspond, especially in the case of the spectra of the xylenes and mesitylene. The correlation seems to be better as the molecules become more complex, with many more fragmentation pathways. Even in the case of benzene, however, where the shapes of the envelopes of the two types of spectra are somewhat different, reasonable correlations can be made if one considers fragmentation processes yielding a positive ion and two or more neutral fragments (including $H^{\cdot}$ and $H_2$). For

example, the processes leading to formation of $C_4H_4^+$ (m/e = 52), $C_4H_3^+$ (m/e = 51), and $C_4H_2^+$ (m/e = 50) in the positive ion mass spectrum could be considered to yield chiefly $C_2H_2$ (m/e = 26), $C_2H_2+H^\cdot$ (m/e = 26,1), and $C_2H_2+H_2$ (m/e = 26,2) respectively.

Another possible contribution to the differences in the two types of spectra concerns significant contributions to the neutral fragment mass spectrum by processes of the type

$$AB \xrightarrow{e^-} A^\cdot + B^\cdot \qquad (26)$$

which do not produce ionic fragments. Such processes would require less energy, and it should thus be possible to identify them, if they are sufficiently abundant, on the basis of neutral fragment appearance potential measurements. In fact, all of the correlations between positive ions and neutral fragments should be supported by correlation of the appearance potentials of the two species wherever possible. Unfortunately, the appearance potential measurements made in this study, to be discussed later, did not furnish any convincing evidence regarding the relative abundances of simple low energy dissociation reactions of the type represented in Equation 26. Thus no conclusions can be drawn regarding their presence or absence.

The neutral fragment mass spectra of pyridine, pyrrole, and thiophene are compared with their complimentary positive

ion mass spectra in Figures 59-61. As in the case of benzene (Figure 53) the correlation between the neutral fragments and positive ions from pyridine is reasonably good, with the exception of the abundant neutral fragments at m/e = 50,51, and 52 which are not balanced by abundant complementary positive ions. The correlation between the two types of spectra from pyrrole is similar, with large differences in the shapes of the envelopes of the two spectra. However, in the case of pyrrole, there are clusters of abundant peaks in the neutral fragment mass spectrum to complement those in the positive ion mass spectrum, even though the relative intensities do not quite match.

In the case of thiophene (Figure 61), on the other hand, the shapes of the envelopes of the two spectra are very similar, and good correlation is realized. At present, it is not understood why some compounds yield much better correlation between positive ion and neutral fragment mass spectra. Further studies of the appearance potentials of the neutral fragments should yield some clues as to whether simple or complex dissociation processes contribute significantly to the formation of neutral fragments.

It is also possible that measurement of neutral fragment abundances at such low ionizing energy in the second chamber introduces significant errors. As stated before, utilization of too great an ionizing energy in the secondary chamber can

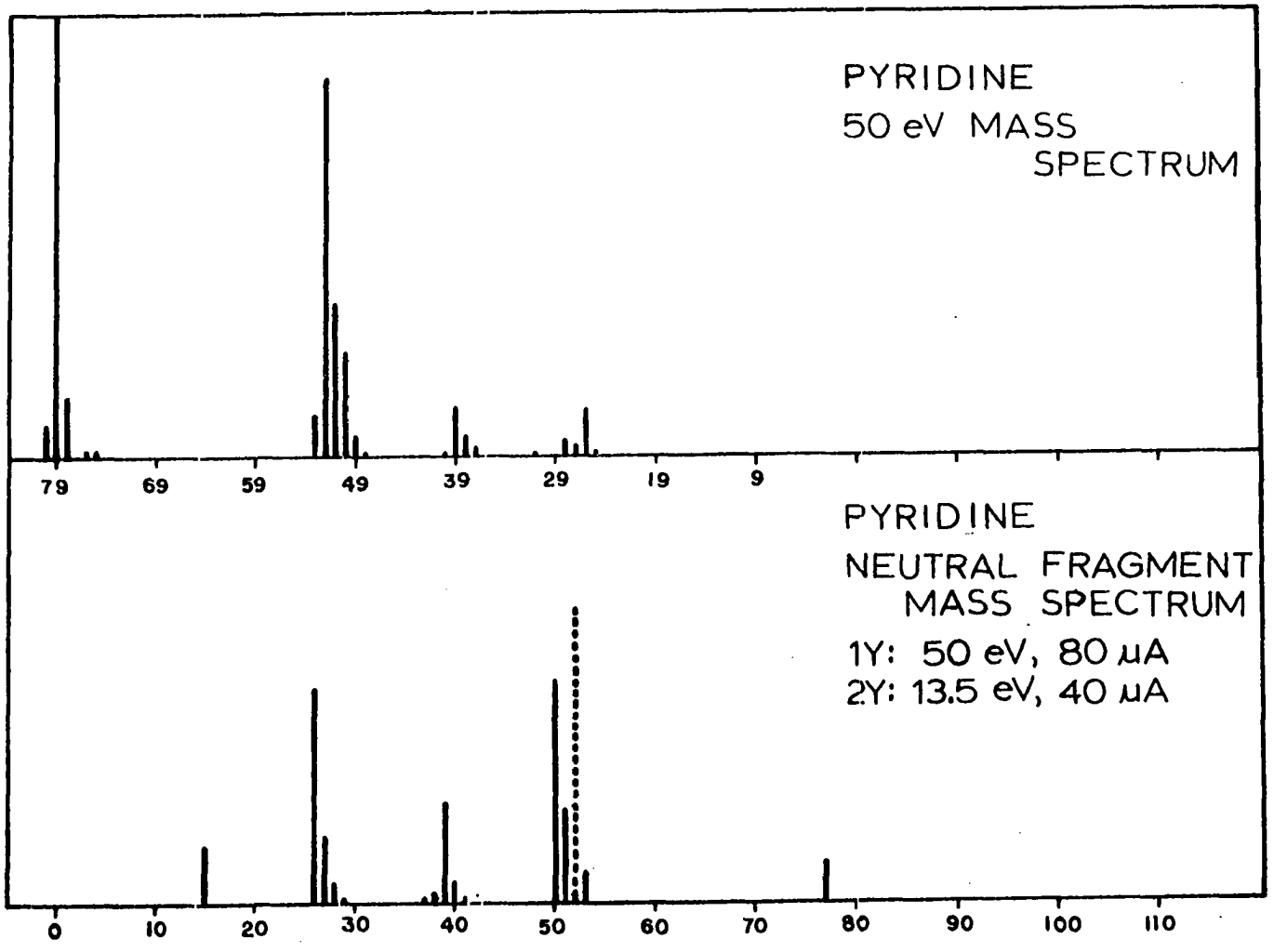


Figure 59. Comparison of the neutral fragment mass spectrum of pyridine with its complementary 50 eV positive ion mass spectrum

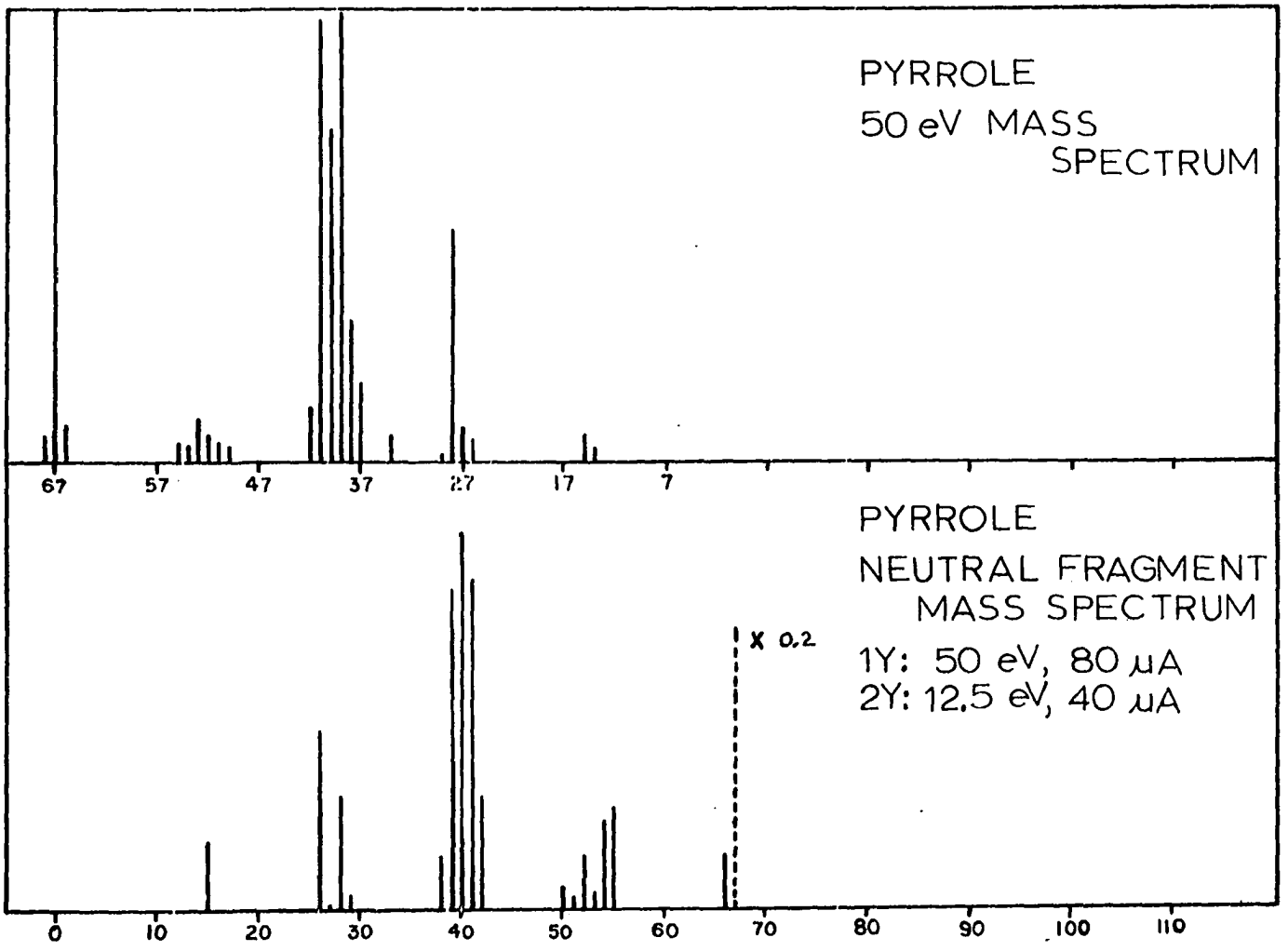


Figure 60. Comparison of the neutral fragment mass spectrum of pyrrole with its complementary 50 eV positive ion mass spectrum

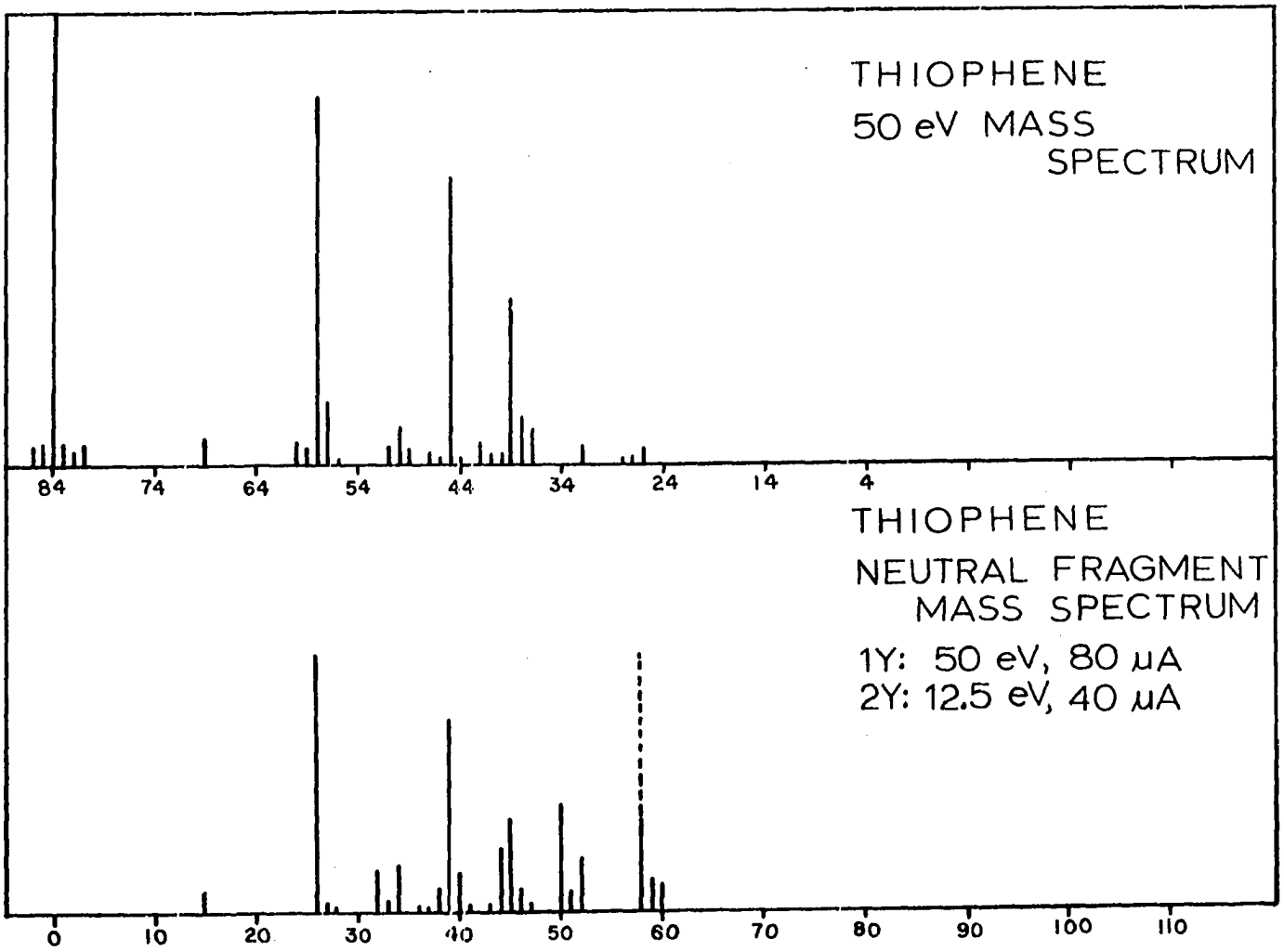


Figure 61. Comparison of the neutral fragment mass spectrum of thiophene with its complementary 50 eV positive ion mass spectrum

lead to fragmentation of the neutral fragments, and, as a consequence, erroneous conclusions as to the neutral fragments present. On the other hand, utilization of too little ionizing energy can discriminate against ionization of those neutral fragments with high ionization potentials. In order to eliminate this problem, the abundance of each neutral fragment could be measured more accurately by measuring the ion current produced by ionization of that neutral fragment at a fixed increment of energy above its ionization potential (for example, by measuring the ion current produced by each neutral fragment at a secondary electron energy one volt greater than the ionization potential of that neutral fragment). The main problem in measuring neutral fragment abundances in this fashion is that it is extremely tedious and time-consuming.

The neutral fragment mass spectra of several isotopically-labelled aromatic hydrocarbons, including those of 1,2-$^{13}$C-3, 4,5,6-$d_4$-benzene, $d_8$-toluene, ring-$d_5$-toluene, $\alpha$-$d_1$-toluene, and 0,0-$d_2$-toluene, are compared with their complementary positive ion mass spectra in Figures 62-66. It was hoped that the neutral fragment mass spectra of these compounds (with the exception of $d_8$-toluene) might yield some insight regarding the abundant scrambling processes resulting from interactions of aromatic molecules with energetic electrons. In the case of the 1,2-$^{13}$C-3,4,5,6-$d_4$-benzene, however, the sample was not

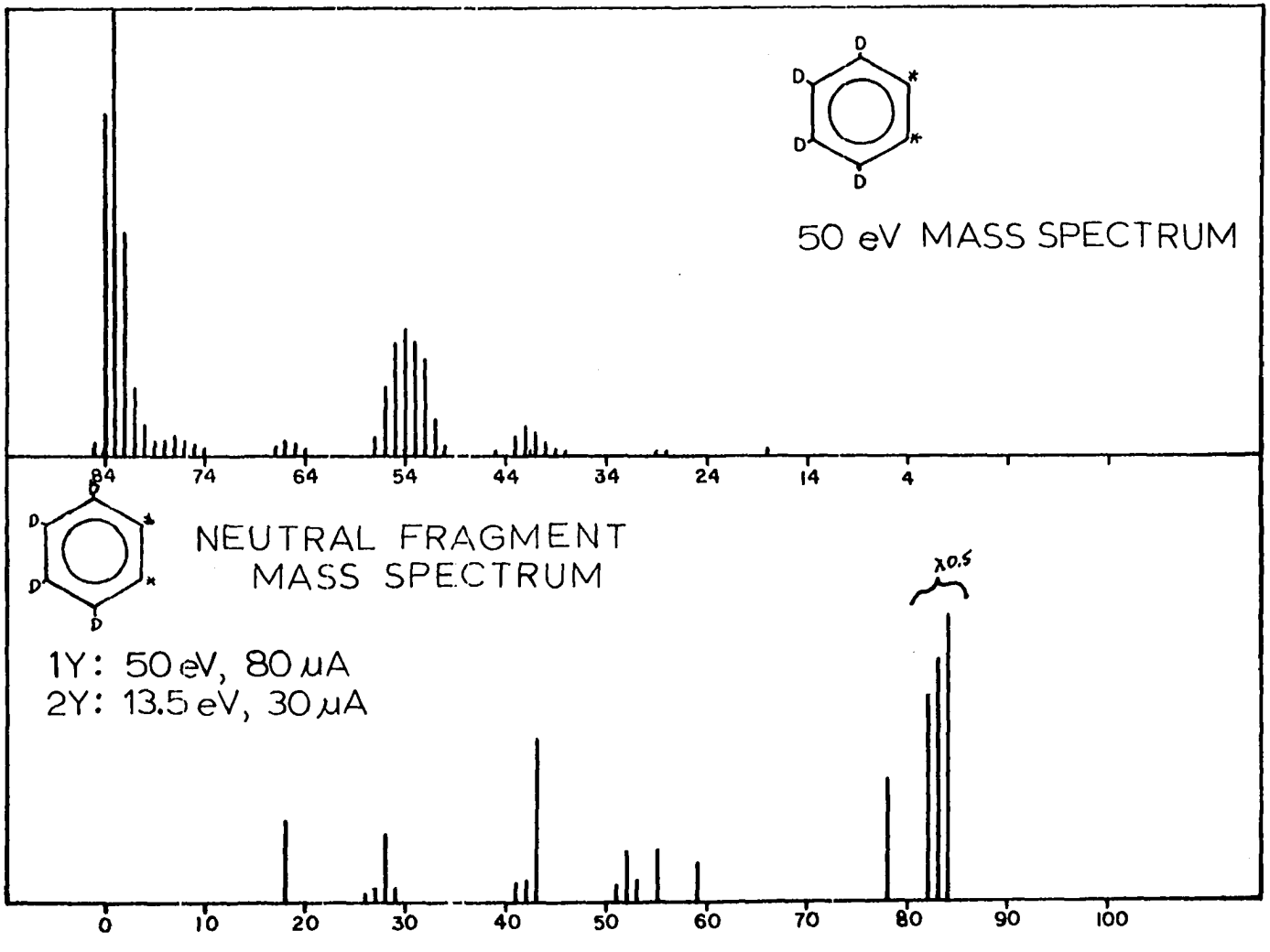


Figure 62. Comparison of the neutral fragment mass spectrum of 1,2-$^{13}$C-3,4,5,6-$d_4$-benzene with its complementary positive ion mass spectrum

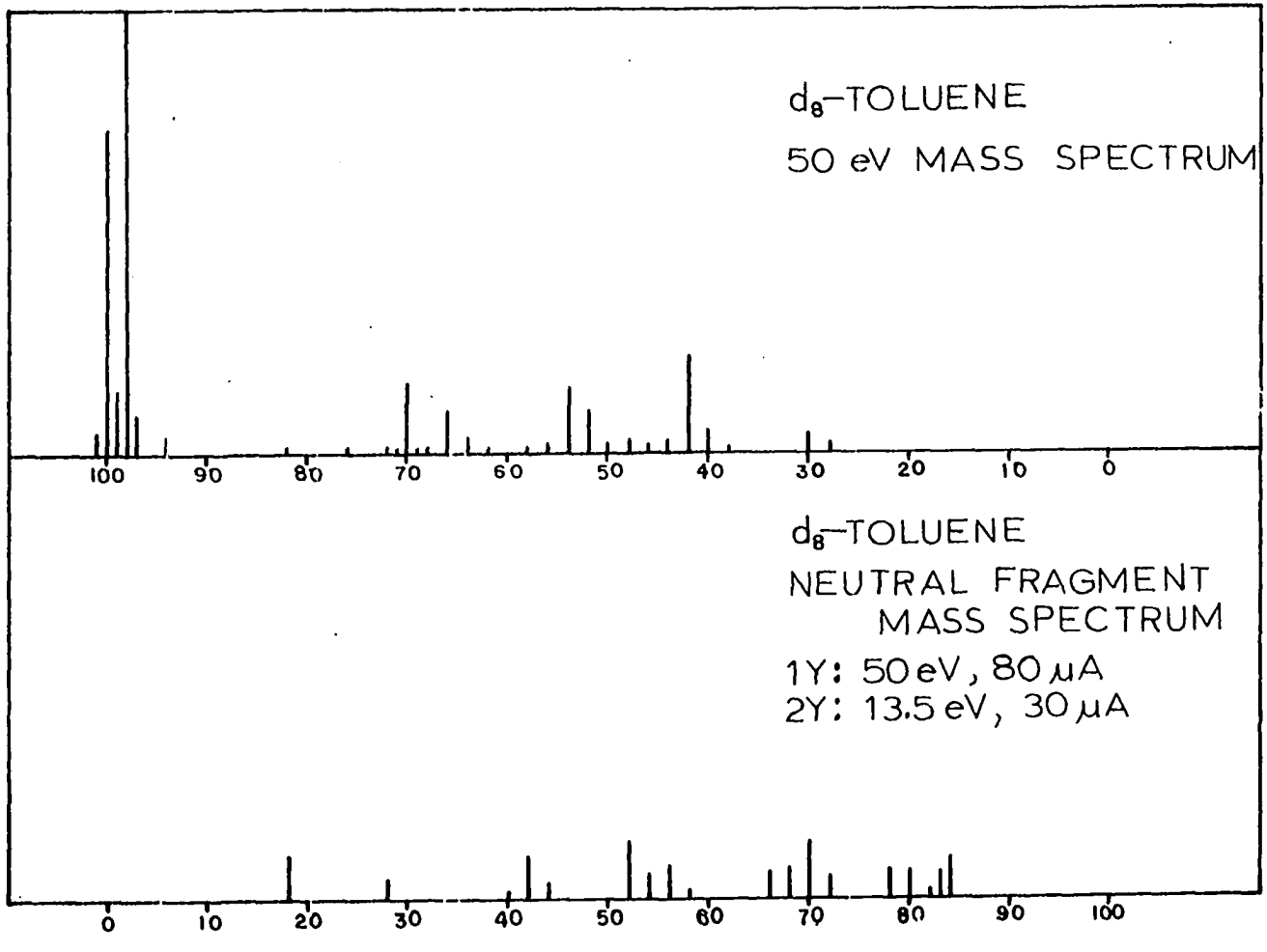


Figure 63. Comparison of the neutral fragment mass spectrum of $d_8$-toluene with its complementary positive ion mass spectrum

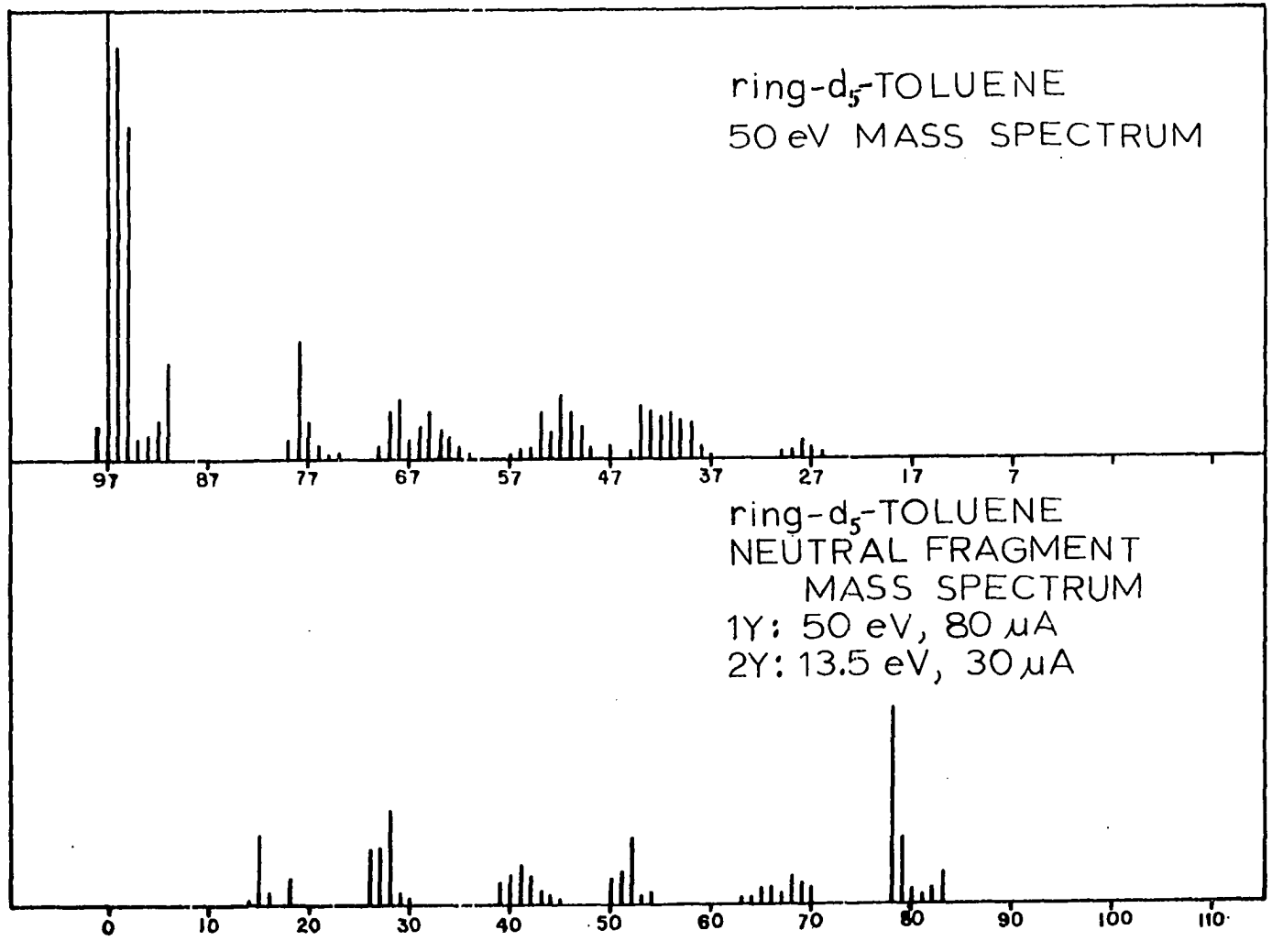


Figure 64. Comparison of the neutral fragment mass spectrum of ring-$d_5$-toluene with its complementary neutral fragment mass spectrum

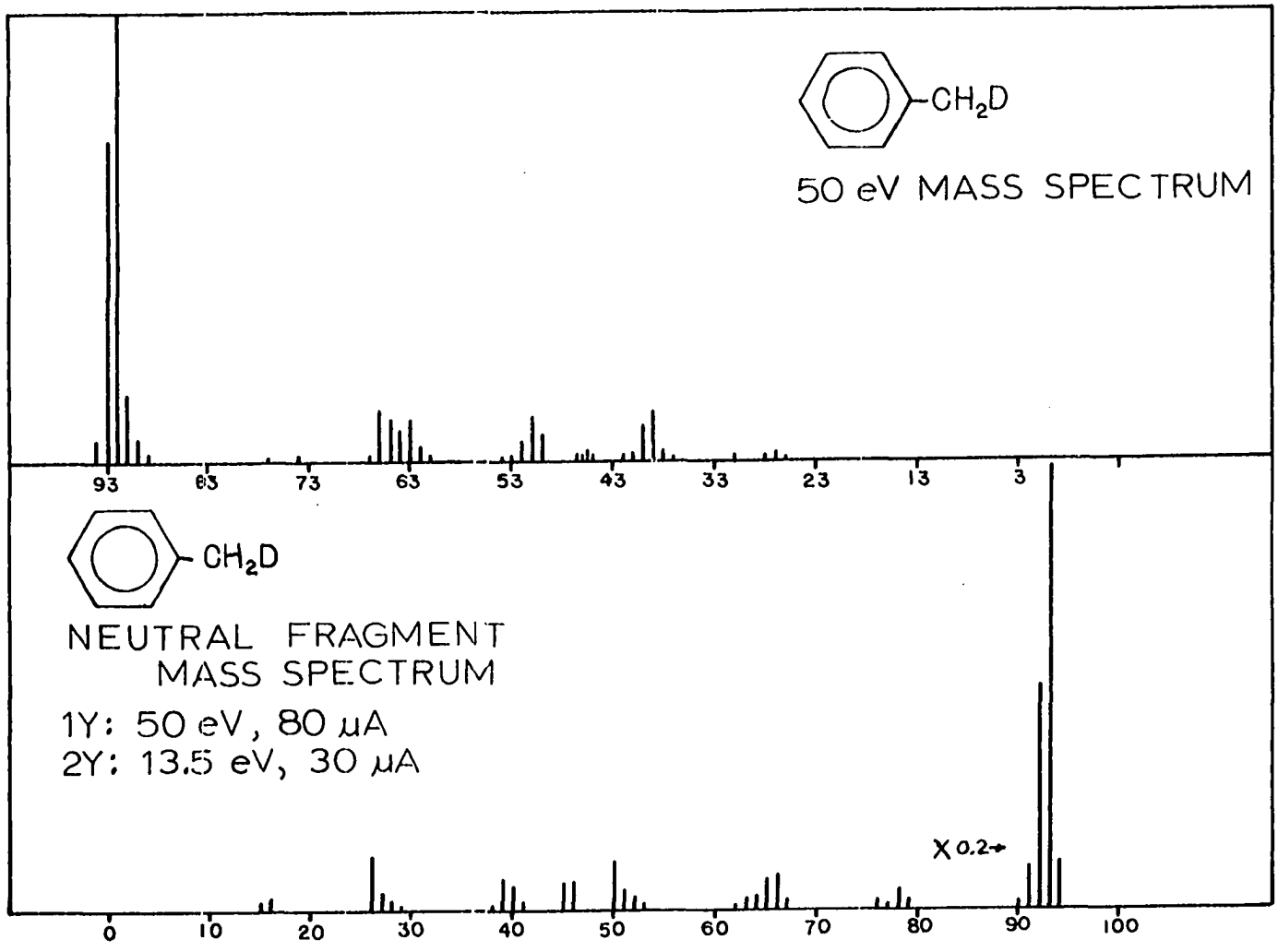


Figure 65. Comparison of the neutral fragment mass spectrum of $\alpha$-$d_1$-toluene with its complementary positive ion mass spectrum

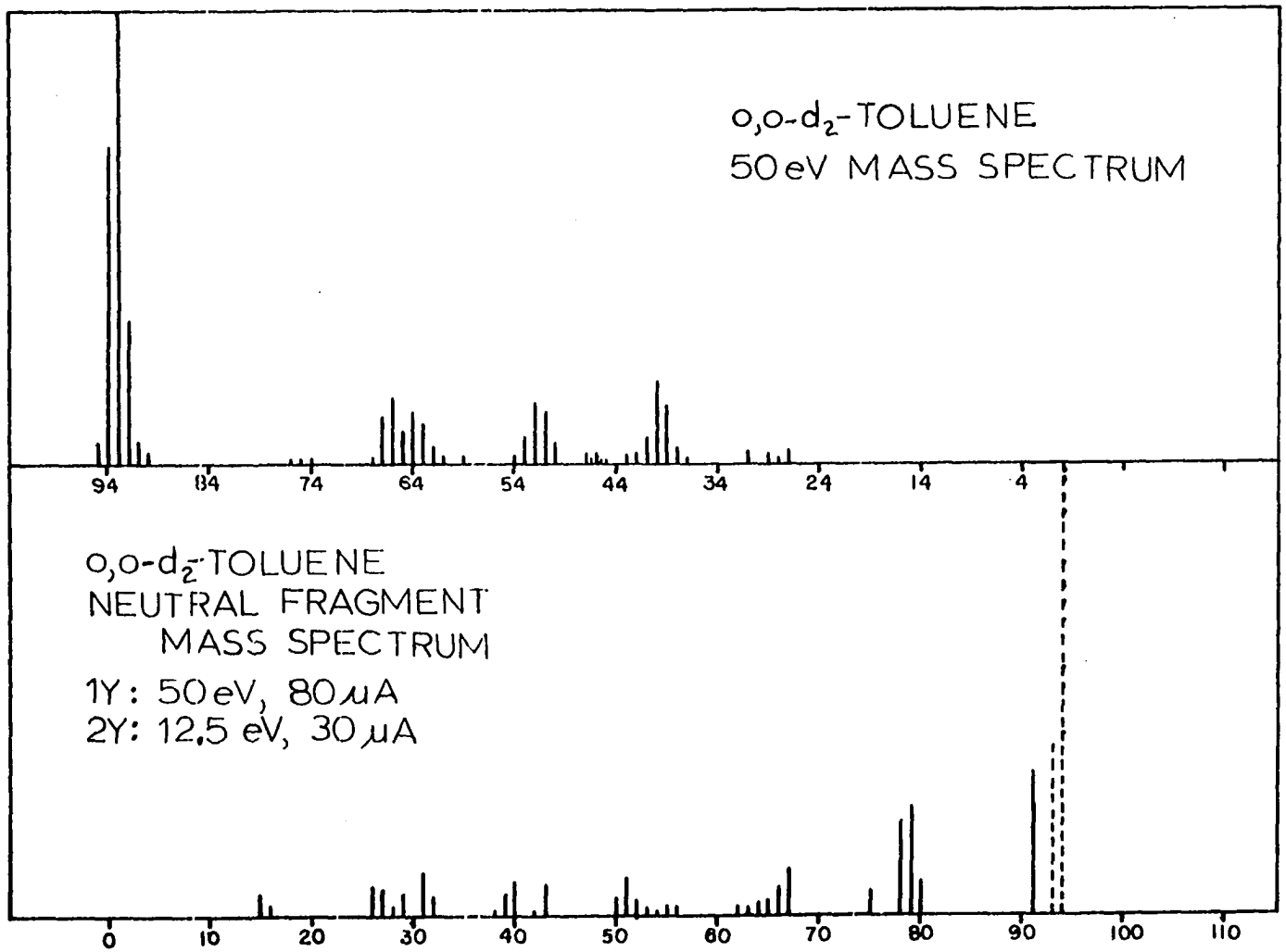


Figure 66. Comparison of the neutral fragment mass spectrum of 0,0-$d_2$-toluene with its complementary positive ion mass spectrum

of sufficient isotopic purity (as evidenced by the distribution of ion intensities in the vicinity of the parent m/e of 84) for any conclusions to be drawn.

The neutral fragment mass spectrum of ring-$d_5$-toluene yielded some striking results regarding the origin of methyl radicals from the parent molecule. Two distinct types of methyl radicals were observed, those arising due to loss of the methyl group from toluene (m/e = 15) and those arising from the ring structure ($CD_3^{\bullet}$, m/e = 18). Surprisingly few hybrid methyl fragments (m/e = 16,17) arising from interchange of the methyl side chain hydrogen atoms with the ring deuterium atoms were observed. This evidence suggests that the scrambling processes include chiefly those atoms associated with the ring structure. The origin of neutral fragments containing 2 or more carbon atoms is more difficult to establish. For example, $C_2H_2$ from ring-$d_5$-toluene could arise from loss of an initial hydrogen atom followed by loss of $C_2H_2$. However, loss of $C_2HD$ (m/e = 27) can arise from several pathways. The simplest of which involves a rearrangement of a ring deuterium atom to $C_1$ followed by loss of $C_2HD$ and $H_2$. Clearly, formation of acetylene involves more complex pathways including scrambling of the ring deuterium atoms and the side-chain hydrogen atoms, but no clear conclusions regarding relative contributions can be established. Also, the relatively large abundances of $C_2H_2$ and $C_2HD$

(compared to $C_2D_2$ (m/e = 28)) suggest that either the loss of $C_2H_2$ from toluene involves chiefly the loss of $C_1$ and the methyl carbon, or that the ring deuterium atoms scramble with the side-chain hydrogen atoms. In any case, it is extremely difficult to reach any firm conclusions based on the neutral fragment spectra of these compounds, as virtually every combination of isotopes is observed for each fragment. It is certain that scrambling processes precede dissociations in most cases, but the scrambling has yet to be characterized. The results on loss of methyl radicals from toluene were very illuminating, but the validity of extending these results to interpretation of processes producing other neutral fragments is subject to question, as those processes arise from different states of the molecular ion and may involve differing amounts of scrambling of the hydrogen or carbon atoms before dissociation occurs.

## C. Neutral Fragment Ionization Potentials

The neutral fragment ionization efficiency curves of $CH_3^{\cdot}$, $C_2H_2$, $C_3H_3^{\cdot}$, $C_4H_2$, $C_4H_3^{\cdot}$, and $C_4H_4$ from toluene as obtained by direct recording from the instrument are presented as typical examples in Figures 67, 68. Note the excellent signal/noise ratios obtained, even though these curves cover an energy range of less than two volts above onset potential.

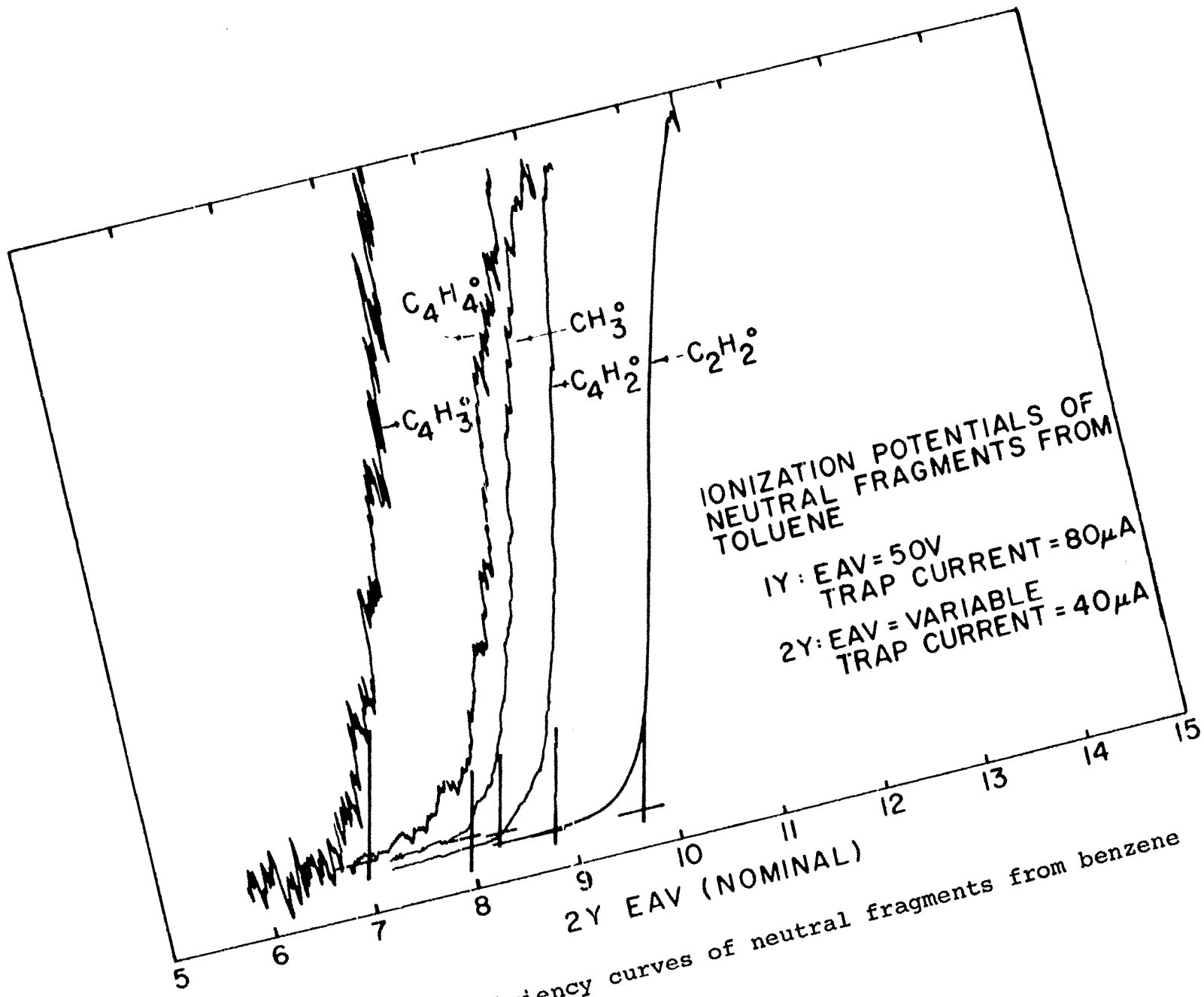


Figure 67. Ionization efficiency curves of neutral fragments from benzene

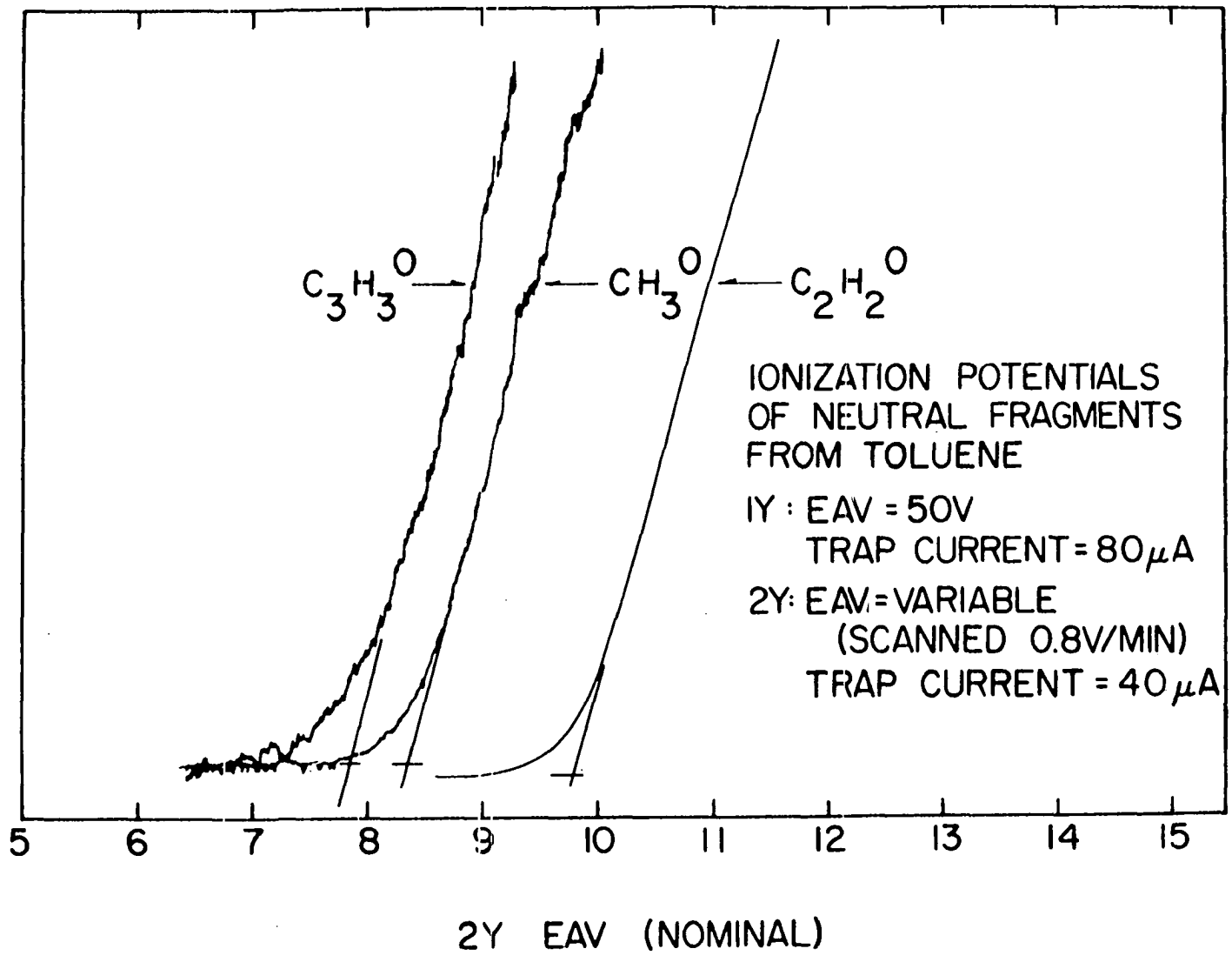


Figure 68. Ionization efficiency curves of neutral fragments from benzene

The experimental values of neutral fragment ionization potentials measured with this instrument are compared with literature ionization potentials in Table 2. All ionization efficiency data were treated using the extrapolated difference method. Where more than a single literature value was available, or more than one structure was possible, the one whose value was closest to the experimental value was chosen for placement in the table.

In general, the determination of neutral fragment ionization potentials are reproducible to $\pm$0.1 volt. The accuracy of the individual measurements is difficult to generalize, as so many instrumental variables are included. Also, the accuracy and precision vary with the abundances of the neutral fragments, being better for the high abundant neutral fragments, and errors of $\pm$0.25 volt cannot be ruled out for low abundant fragments. For some neutral fragments (notably $CH_3^{\cdot}$ and $C_2H_2$) the experimental ionization potentials obtained were precise to $\pm$0.05 volt or less. Thus, $C_2H_2$ and $CH_3^{\cdot}$ ionization efficiency curves were used in many cases as secondary standards for calibrating the energy of the secondary electron beam.

The neutral fragments for which no literature ionization potentials were available, and for which ionization potentials were obtained in this study are as follows: $CNH_3$ (12.21), $C_2NH$ (11.10), $C_3H_2$ (9.17), $C_2NH_4$ (13.2), CSH (7.97), $CSH_2$

Table 2. Values of experimentally measured neutral fragment ionization potentials and comparison with literature values

| Neutral fragment m/e | Parent compound | Molecular formula or structure | Measured I.P. | Literature I.P. | Reference |
|---|---|---|---|---|---|
| 15 | Toluene | $CH_3^{\cdot}$ | 9.94 | 9.91±0.13 | 40, p. 29 |
| | m-Xylene | $CH_3^{\cdot}$ | 9.90 | " | " |
| | Mesitylene | $CH_3^{\cdot}$ | 9.84 | " | " |
| | Pyridine | $CH_3^{\cdot}$ | 9.87 | " | " |
| | Pyrrole | $CH_3^{\cdot}$ | 9.95 | " | " |
| 18 | $d_8$-Toluene | $CD_3^{\cdot}$ | 9.5 | 9.91±0.13 | 40, p. 29 |
| 26 | Benzene | CH≡CH | 11.42 | 11.40±0.01 | 40, p. 34 |
| | Toluene | CH≡CH | 11.37 | " | " |
| | 0,0-$d_2$-Toluene | CH≡CH | 11.40 | " | " |
| | m-Xylene | CH≡CH | 11.41 | " | " |
| | Mesitylene | CH≡CH | 11.38 | " | " |
| | Thiophene | CH≡CH | 11.40 | " | " |
| | Pyridine | CH≡CH | 11.36 | " | " |
| | Pyridine | $CN^{\cdot}$ | 14.3 | 14.2±0.3 | 40, p. 92 |
| | Pyrrole | CH≡CH | 11.40 | 11.40±0.01 | 40, p. 34 |
| | Pyrrole | $CN^{\cdot}$ | 14.50 | 14.2±0.3 | 40, p. 92 |

| | | | | | |
|---|---|---|---|---|---|
| 27 | 1,2-$^{13}$C-3,4,5,6-$d_4$-Benzene | $^{13}$CH≡CH, CH≡CD | 11.0 | 11.40±0.01 | 40, p. 34 |
| | ring-$d_5$-Toluene | CH≡CD | 11.25 | " | " |
| | 0,0-$d_2$-Toluene | CH≡CD | 11.47 | " | " |
| | α-$d_1$-Toluene | CH≡CD | 11.25 | " | " |
| | Pyridine | HC≡N | 13.72 | 13.73±0.09 | 40, p. 93 |
| | Pyrrole | HC≡N | 13.59 | " | " |
| | Pyrrole | $C_2H_3$ | 9.6 | 9.4 ±0.2 | 22, p. 695 |
| 28 | 1,2-$^{13}$C-3,4,5,6-$d_4$-Benzene | CD≡CD | 11.1 | 11.42±0.006 | 40, p. 35 |
| | 0,0-$d_2$-Toluene | CD≡CD | 11.42 | " | " |
| | $d_5$-Toluene | CD≡CD | 11.20 | " | " |
| | $d_8$-Toluene | CD≡CD | 11.42 | " | " |
| 29 | Pyrrole | $C_2H_5^{\cdot}$ | 8.67 | 8.76 | 40, p. 38 |
| | Pyrrole | $CH_2$=NH | 12.21 | | |
| 34 | Thiophene | $H_2S$ | 10.42 | 10.46 | 40, p. 173 |
| 38 | Thiophene | $C_3H_2$ | 9.17 | | |
| 39 | Benzene | $C_3H_3$ | 8.86 | 8.65±0.3 | 21, p. 333 |
| | Toluene | $C_3H_3$ | 8.95 | " | " |
| | α-$d_1$-Toluene | $C_3H_3$ | 8.90 | " | " |
| | ring-$d_5$-Toluene | $C_3H_3$ | 8.90 | " | " |
| | m-Xylene | $C_3H_3$ | 8.90 | " | " |
| | 0,0-$d_2$-Toluene | $C_3H_3$ | 8.6 | " | " |
| | Pyridine | $C_3H_3$ | 8.89 | " | " |
| | Thiophene | $C_3H_3$ | 8.73 | " | " |
| | Pyrrole | $C_3H_3$ | 8.94 | " | " |
| | Pyrrole | $C_2NH$ | 11.10 | | |

Table 2 (Continued)

| Neutral fragment m/e | Parent compound | Molecular formula or structure | Measured I.P. | Literature I.P. | Reference |
|---|---|---|---|---|---|
| 40 | α-$d_1$-Toluene | $C_3H_2D$ | 8.93 | 8.65±0.3 | 21, p. 333 |
| | ring-$d_5$-Toluene | $C_3H_2D$ | 8.63 | " | " |
| | 0,0-$d_2$-Toluene | $C_3DH_2, C_3D_2$ | 9.22 | | |
| | Thiophene | $CH_2=C=CH_2$ | 9.96 | 10.16±0.02 | 40, p. 43 |
| | |  | | 9.95 | 40, p. 43 |
| | Pyrrole | $CH_2=C=CH_2$ | 10.00 | 10.16±0.02 | 40, p. 43 |
| | Pyrrole | $CH_2CN$ | 11.94 | 10.9 ±0.2 | 40, p. 94 |
| 41 | 1,2-$^{13}$C-3,4,5,6-$d_4$-Benzene | $C_3D_2H, C_2{}^{13}CDH_2$ | 9.26 | 8.65±0.3 | 21, p. 333 |
| | α-$d_1$-Toluene | $C_3H_3D$ | 10.0 | 10.0 ±0.15 | 21, p. 333 |
| | 0,0-$d_2$-Toluene | $C_3H_3D$ | 9.91 | 10.0 ±0.15 | 21, p. 333 |
| | ring-$d_5$-Toluene | $C_3D_2H$ | 9.22 | 8.65±0.3 | 21, p. 333 |
| | Pyrrole | $C_3H_5$ | 9.43 | 8.2 ±0.1 | 40, p. 43 |
| | Pyrrole | $C_2NH_3$ | 12.4 | 12.205±0.004 | 40, p. 94 |
| 42 | ring-$d_5$-Toluene | $C_3D_3$ | 9.12 | 8.65±0.3 | 21, p. 333 |
| | $d_8$-Toluene | $C_3D_3$ | 8.90 | 8.65±0.3 | " |
| | Pyrrole | $C_2NH_4$ | 13.2 | | |
| 44 | $d_8$-Toluene | $C_3D_4$ | 9.69 | 10.0 ±0.15 | 21, p. 333 |
| | Thiophene | CS | 11.60 | 11.8 ±0.2 | 40, p. 173 |
| 45 | Thiophene | HCS | 7.97 | | |
| 46 | Thiophene | $CH_2S$ | 9.77 | | |

| | | | | | |
|---|---|---|---|---|---|
| 50 | Benzene | $CH{\equiv}C{-}C{\equiv}CH$ | 10.27 | 10.2 ±0.1 | 40, p. 47 |
| | Toluene | $CH{\equiv}C{-}C{\equiv}CH$ | 10.32 | " | " |
| | m-Xylene | $CH{\equiv}C{-}C{\equiv}CH$ | 10.10 | " | " |
| | Mesitylene | $CH{\equiv}C{-}C{\equiv}CH$ | 10.16 | " | " |
| | Pyridine | $CH{\equiv}C{-}C{\equiv}CH$ | 10.18 | " | " |
| | Thiophene | $CH{\equiv}C{-}C{\equiv}CH$ | 10.10 | " | " |
| | ring-$d_5$-Toluene | $CH{\equiv}C{-}C{\equiv}CH$ | 10.08 | " | " |
| | $\alpha$-$d_1$-Toluene | $CH{\equiv}C{-}C{\equiv}CH$ | 10.20 | " | " |
| | 0,0-$d_2$-Toluene | $CH{\equiv}C{-}C{\equiv}CH$ | 10.40 | " | " |
| | Pyrrole | $CH{\equiv}C{-}C{\equiv}CH$ | 10.18 | " | " |
| | Pyridine | $C_3N$ | 14.5 | 14.4 | 40, p. 93 |
| 51 | m-Xylene | $C_4H_3$ | 8.31 | | |
| | ring-$d_5$-Toluene | $CH{\equiv}C{-}C{\equiv}CD$ | 9.90 | 10.2 ±0.1 | 40, p. 47 |
| | Pyridine | $CH{\equiv}C{-}C{\equiv}N$ | 11.50 | 11.6 ±0.2 | 40, p. 96 |
| | Pyrrole | $CH{\equiv}C{-}C{\equiv}N$ | 11.81 | 11.6 ±0.2 | 40, p. 96 |
| 52 | Benzene | $C_4H_4$ | 9.60 | 10.10±0.15 | 21, p. 332 |
| | Toluene | $C_4H_4$ | 9.63 | " | " |
| | 0,0-$d_2$-Toluene | $C_4H_4$ | 9.60 | " | " |
| | Thiophene | $C_4H_4$ | 9.64 | " | " |
| | m-Xylene | $CH_2{=}C{=}C{=}CH_2$ | 9.33 | 9.28 | 40, p. 48 |
| | $d_8$-Toluene | $CD{\equiv}C{-}C{\equiv}CD$ | 10.20 | 10.2 ±0.1 | 40, p. 47 |
| | ring-$d_5$-Toluene | $CD{\equiv}C{-}C{\equiv}CD$ | 10.00 | 10.2 ±0.1 | 40, p. 47 |
| | $\alpha$-$d_1$-Toluene | $C_4H_4$ | 9.09 | 9.00±0.15 | 21, p. 333 |
| | Pyridine | $C_4H_4$ | 9.00 | 9.00±0.15 | 21, p. 333 |

Table 2 (Continued)

| Neutral fragment m/e | Parent compound | Molecular formula or structure | Measured I.P. | Literature I.P. | Reference |
|---|---|---|---|---|---|
| 52 | Pyridine | $C_3H_2N$ | 13.78 | | |
| | Pyrrole | $CH_2=C=C=CH_2$ | 9.50 | 9.28 | 40, p. 48 |
| | Pyrrole | $C_3NH_2$ | 13.90 | | |
| 53 | 0,0-$d_2$-Toluene | $C_4H_3D$ | 8.92 | 9.00±0.15 | 21, p. 333 |
| 54 | ring-$d_5$-Toluene | $C_4D_2H_2$ | 9.00 | 9.00±0.15 | 21, p. 333 |
| | $d_8$-Toluene | $C_4D_3$ | 8.90 | | |
| | Pyrrole | $C_3H_3N$ | 11.05 | 11.10±0.05 | 40, p. 96 |
| 58 | Thiophene | $C_2H_2S$ | 8.92 | | |
| 63 | m-Xylene | $C_5H_3$ | 8.40 | | |
| 65 | m-Xylene | $C_5H_5$ (cyclopentadienyl) | 8.69 | 8.69±0.1 | 40, p. 53 |
| 66 | $d_8$-Toluene | $C_5D_3$ | 8.00 | | |
| 68 | ring-$d_5$-Toluene | $C_5D_3H_2$ | 8.91 | 8.69±0.1 | 40, p. 53 |
| 69 | ring-$d_5$-Toluene | $C_5D_4H$ | 8.93 | 8.69±0.1 | 40, p. 53 |
| 70 | $d_8$-Toluene | $C_5D_5$ | 8.57 | 8.69±0.1 | 40, p. 53 |
| 74 | m-Xylene | $C_6H_2$ | 9.34 | 9.83±0.1 | 21, p. 332 |
| 76 | m-Xylene | $C_6H_4$ | 9.12 | 9.5 ±0.1 | 21, p. 332 |
| 78 | m-Xylene | $C_6H_6$ (Benzene) | 9.03 | 9.25 | 40, p. 60 |
| | | $CH_3C\equiv C-C\equiv CCH_3$ | | 9.20 | 40, p. 60 |
| 84 | Thiophene | $C_4H_4S$ (excited) | 8.62 | 9.2 ±0.2 | 40, p. 179 |
| 91 | α-$d_1$-Toluene | $C_7H_7^{\cdot}$ (Benzyl) | 7.66 | 7.76±0.08 | 40, p. 66 |
| | m-Xylene | $C_7H_7^{\cdot}$ (Benzyl) | 7.70 | 7.76±0.08 | 40, p. 66 |

| | | | | | |
|---|---|---|---|---|---|
| 98 | $d_8$-Toluene | $C_7D_7$ (Benzyl) | 7.50 | 7.76±0.08 | 40, p. 66 |
| 102 | m-Xylene | $C_8H_6$ (phenylacetylene) | 8.95 | 8.815±0.005 | 40, p. 71 |
| 104 | m-Xylene | $C_8H_8$ (styrene) | 8.23 | 8.47±0.02 | 40, p. 72 |
| | | $C_8H_8$ (cyclooctatetraene) | | 7.99±0.02 | 40, p. 72 |

(9.77), $C_4H_3$ (8.31), $C_3NH_2$ (13.78, 13.90), $C_4D_3$ (8.90), $C_2SH_2$ (8.92), $C_5H_3$ (8.40), and $C_5D_3$ (8.00).

The agreement between the experimentally measured ionization potentials and the literature ionization potentials is excellent in most cases. In those cases where there is a large discrepancy, the difference between the two values can be explained on the basis that the literature ionization potential was not obtained from measurements on neutral fragments, or that the methods of measuring the ionization potential were different.

Thus, the instrument has already proved to be an invaluable tool for the measurement of neutral fragment ionization potentials.

## D. Neutral Fragment Appearance Potentials

The neutral fragment appearance potential curves of $C_2H_2$, $C_2H_3^{\cdot}$, $C_4H_2$, and $C_4H_4$ from benzene are presented in Figures 69-71. As these curves illustrate, the poor signal/noise ratio obtained precludes the determination of an accurate onset potential. As Figures 69, 70 illustrate, longer time constants for the lock-in amplifier can be utilized to improve the observed signal/noise ratio, but the length of the scan time required to prevent distortion of the curve is prohibitively long.

Figure 69. Neutral fragment appearance potential curves for $C_2H_2$ and $C_3H_3^{\cdot}$ from benzene. These curves were obtained utilizing a 10 second time constant on the lock-in amplifier

NEUTRAL FRAGMENT APPEARANCE POTENTIAL CURVES

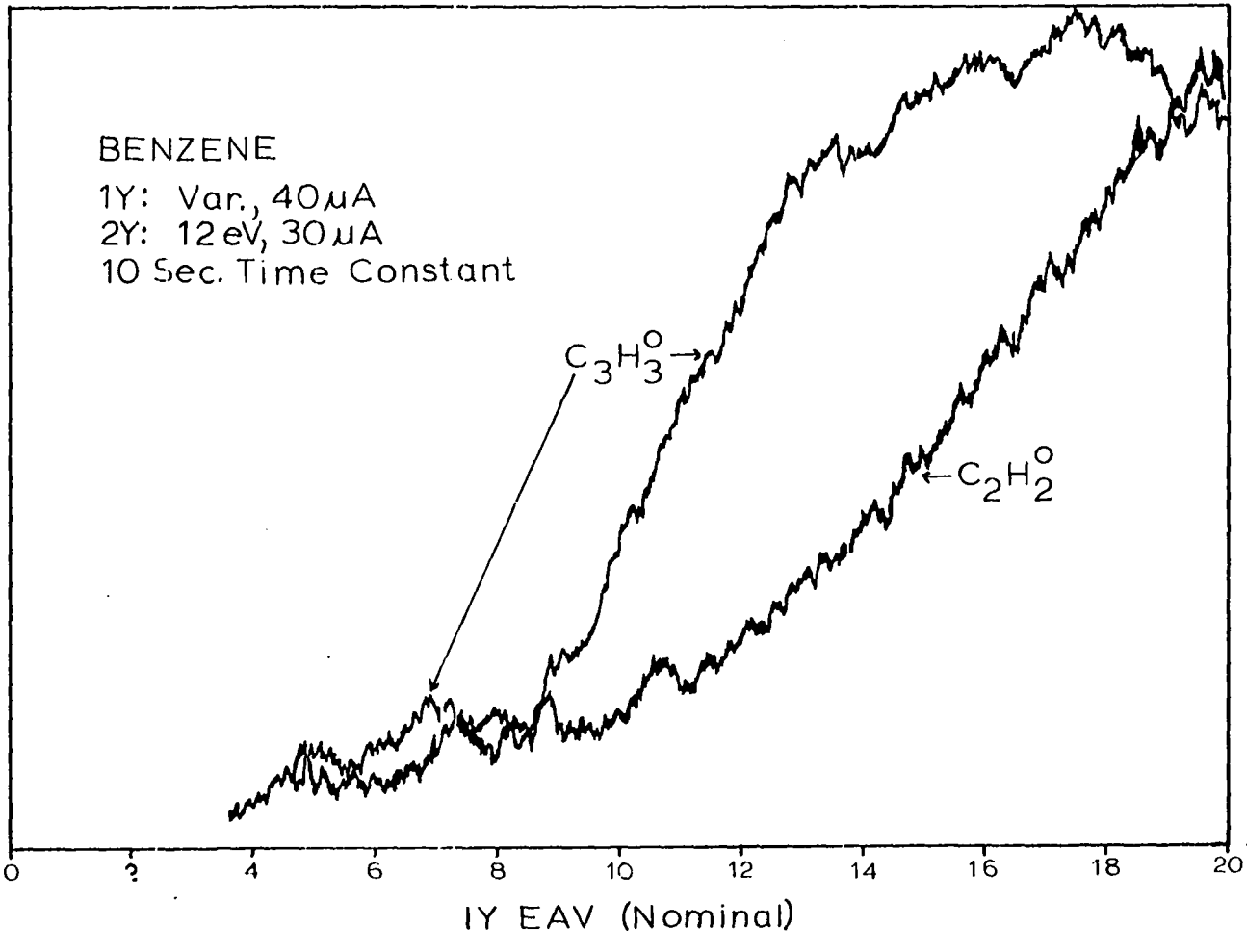

Figure 70. Neutral fragment appearance potential curves for $C_2H_2$ and $C_3H_3^{\bullet}$ from benzene utilizing a 30 second time constant in the lock-in amplifier

NEUTRAL FRAGMENT APPEARANCE POTENTIAL CURVES

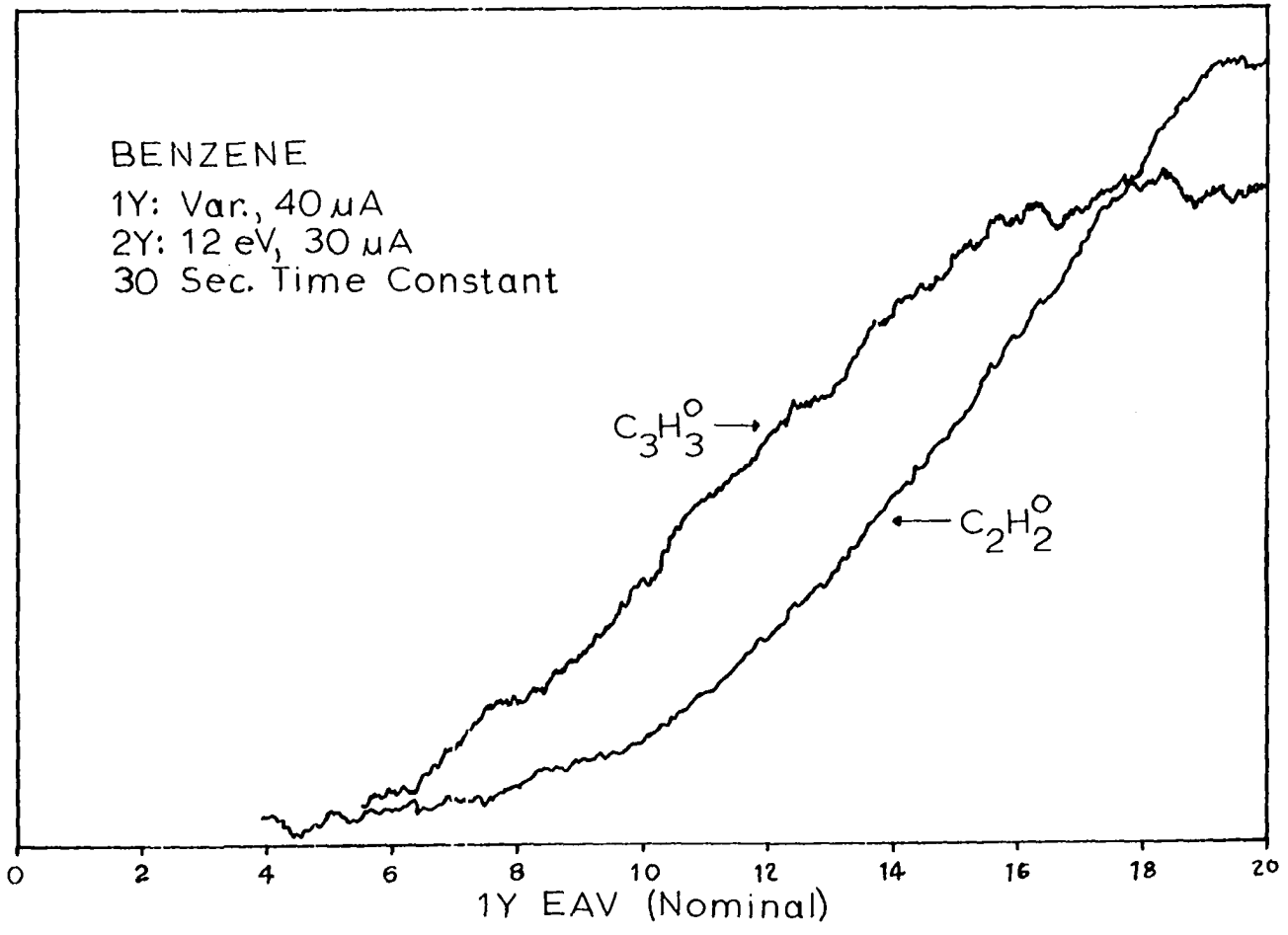

Figure 71. Neutral fragment appearance potential curves for $C_4H_2$ and $C_4H_4$ from benzene utilizing a 10 second time constant on the lock-in amplifier

NEUTRAL FRAGMENT APPEARANCE POTENTIAL CURVES

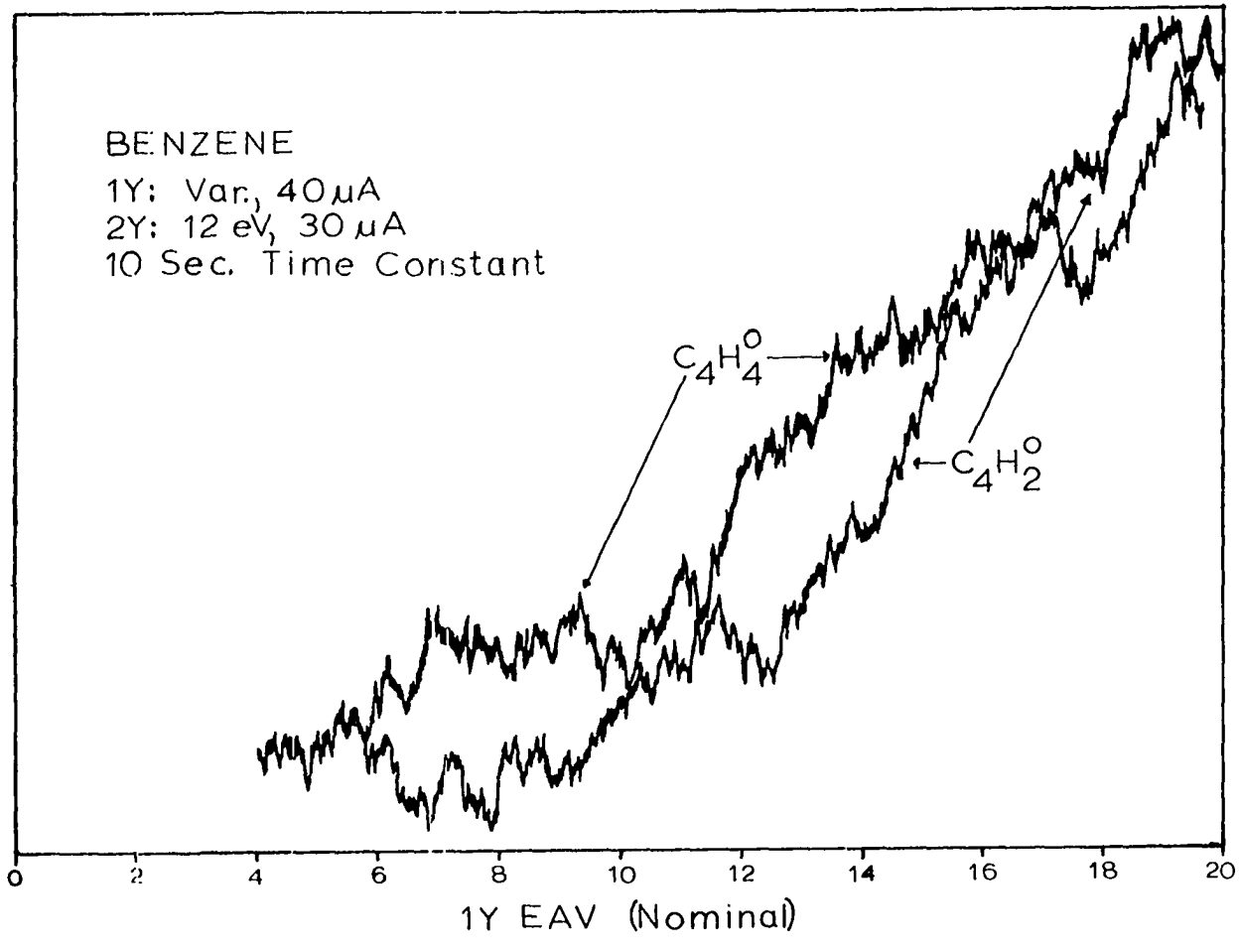

It was hoped that better measurements of neutral fragment appearance potentials would be possible with this instrument, but as these data illustrate, improvements to the 1Y Grid II pulse circuitry and the 1Y electron gun are necessary to improve the signal/noise ratio so that more accurate and meaningful measurements can be made. In any event, for reasons discussed previously, the measurement of neutral fragment appearance potentials will always be somewhat limited by a lower signal/noise ratio than that obtained for measurements of neutral fragment ionization potentials.

# VII. PROPOSED INSTRUMENT MODIFICATIONS

## A. Improved Grid Pulsing Circuitry

The grid pulsing circuit could be greatly improved by replacing the two 1000 μF capacitors (Figure 28) which transmit the pulse signal from the square wave generator to 1Y Grid II with a solid state circuit consisting of a light-emitting diode and a photosensitive transistor. The light-emitting diode would be powered by the square wave generator and a transistor could be chosen which would provide a 0 to -50 V pulse signal directly to 1Y Grid II. The solid state circuit would have three main advantages over the present circuit.

1. The pulse shape would be improved, resulting in improved S/N for detecting neutral fragments.
2. The time constant of the circuit would be much shorter, allowing faster scanning of the primary electron energy.
3. The 50 V pulse amplitude at 1Y Grid II (versus the 35 V amplitude with the present circuit) would allow the 1Y Grid II to be adjusted more positive with respect to the filament. Thus, higher trap currents could be maintained at low primary electron energies, resulting in a better S/N for obtaining neutral fragment appearance potentials.

## B. Addition of a Second Mass Filter

A second mass filter could be attached to the ion source to mass analyze the ion currents generated in the primary reaction chamber. The ion source is designed to

accommodate a second mass filter, the addition of a 1Y Focus electrode being the only modification required. The addition of a second mass filter would make possible the simultaneous detection of a neutral fragment and its complementary ion, leading to a better characterization of the processes occurring in the primary reaction chamber.

# VIII. SUMMARY AND CONCLUSIONS

## A. Instrument Capabilities and Limitations

The capability of the quadrupole mass spectrometer described herein to detect neutral fragments formed by the interaction of a variety of aromatic chemical compounds with energetic electrons has been demonstrated. In fact, all of the neutral fragment mass spectra presented herein (Figures 38-66) were obtained by direct recording from the instrument as the mass range was scanned automatically. The capability of the instrument for providing a convenient means for measuring neutral fragment ionization potentials, including those of low abundance neutral fragments, has also been clearly demonstrated.

The instrument has also shown potential for measuring neutral fragment appearance potentials, although it must be admitted that the neutral fragment appearance potential data obtained in this study were somewhat disappointing. It is hoped that an improved grid-pulsing circuit will improve the instruments capability for acquiring neutral fragment appearance potentials so that more meaningful neutral fragment-positive ion correlations might be easily made.

The main limitation of the instrument at present is the electronic artifact which causes a negative ac signal when a large dc signal is present. Hopefully, future work will yield

some clues as to the source of this problem and its eventual elimination.

## B. Results

The neutral fragment mass spectra of benzene, toluene, o-xylene, m-xylene, p-xylene, mesitylene, pyridine, thiophene, pyrrole, $d_8$-toluene, ring-$d_5$-toluene, $d_1$-toluene, 0,0-$d_2$-toluene, and 1,2-$^{13}$C-3,4,5,6-$d_4$-benzene have been measured and compared with their corresponding positive ion spectra. In general, reasonable correlations between the two types of spectra were obtained, the differences between the two types of spectra being explained by differing ionization potentials of the neutral fragments, and by the fact that H$^{\cdot}$ and $H_2$ were by choice not observed, and thus could not be included in the overall mass balance.

Numerous neutral fragment ionization potentials were measured and found to be in excellent agreement with available literature values. In addition, the following neutral fragment ionization potentials, for which no literature values were available, were measured and reported: $CNH_3$ (12.21), $C_2NH$ (11.10), $C_3H_2$ (9.17), $C_2NH_4$ (13.2), CSH (7.97), $CSH_2$ (9.77), $C_4H_3$ (8.31), $C_3NH_2$ (13.78, 13.90), $C_4D_3$ (8.90), $C_2SH_2$ (8.92), $C_5H_3$ (8.40), and $C_5D_3$ (8.00).

# IX. BIBLIOGRAPHY


1. H. J. Svec and G. D. Flesch, Int. J. Mass Spectrom. Ion Phys. 1, 41 (1968).

2. C. G. McDonald and J. Shannon, Aust. J. Chem. 15, 771 (1962).

3. H. M. Grubb and S. Meyerson, in Mass Spectrometry of Organic Ions, edited by F. W. McLafferty (Academic Press, New York, 1963), Chap. 10.

4. K. R. Jennings, Z. Naturforsch. A22, 454 (1967).

5. S. Meyerson, H. Hart, and L. C. Leitch, J. Am. Chem. Soc. 90, 3419 (1968).

6. M. A. Baldwin, D. P. Craig, and A. Maccoll, in Seventeenth Annual Conference on Mass Spectrometry and Allied Topics, ASTM Committee E-14, Dallas, Texas, 1969) Paper No. 142.

7. I. Horman, A. N. H. Yeo, and D. H. Williams, J. Am. Chem. Soc. 92, 2131 (1970).

8. R. J. Dickinson and D. H. Williams, J. Chem. Soc. B, 249 (1971).

9. J. H. Beynon, R. M. Caprioli, W. O. Perry, and W. E. Baitinger, J. Am. Chem. Soc. 94, 6828 (1972).

10. D. H. Williams, R. G. Cooks, J. Ronayne, and S. W. Tam, Tetrahedron Lett., 1777 (1968).

11. D. H. Williams, S. W. Tam, and R. G. Cooks, J. Am. Chem. Soc. 90, 2150 (1968).

12. M. T. Robert-Lopes, in Recent Topics in Mass Spectrometry, edited by R. I. Reed (Gordon and Breach, New York, 1971), p. 27.

13. G. R. Lester, in Recent Topics in Mass Spectrometry, edited by R. I. Reed (Gordon and Breach, New York, 1971), p. 48 .

14. G. D. Flesch and H. J. Svec, J. Chem. Phys. 54, 2681 (1971).

15. G. D. Flesch and H. J. Svec, J. Chem. Phys. 55, 4310 (1971).

16. G. D. Flesch and H. J. Svec, Fragmentation Reactions in the Mass Spectrometer for $C_2$-$C_5$ Alkanes, submitted for publication in J. Chem. Soc.

17. M. A. A. Ferreira, in Recent Topics in Mass Spectrometry, edited by R. I. Reed (Gordon and Breach, New York, 1971), p. 11.

18. D. Beck and O. Osberghaus, Z. Physik 160, 406 (1960).

19. D. Beck, Discussions Faraday Soc. 36, 56 (1964).

20. D. Beck and A. Niehaus, J. Chem. Phys. 37, 2705 (1962).

21. H. Genzel and O. Osberghaus, Z. Naturforsch. A22, 331 (1967).

22. A. Niehaus, Z. Naturforsch. A22, 690 (1967).

23. F. W. Lampe and A. Niehaus, J. Chem. Phys. 49, 2949 (1968).

24. C. E. Melton, J. Sci. Instr. 43, 927 (1966).

25. C. E. Melton, Int. J. Mass Spectrom. Ion Phys. 1, 353 (1968).

26. C. E. Melton, J. Chem. Phys. 45, 4414 (1966).

27. C. E. Melton and P. S. Rudolph, J. Chem. Phys. 47, 1771 (1967).

28. C. E. Melton, in Seventeenth Annual Conference on Mass Spectrometry and Allied Topics, (ASTM Committee E-14, Dallas, Texas, 1969), Paper No. 63.

29. C. E. Melton, J. Chem. Phys. 74, 582 (1970).

30. R. A. Saunders, J. T. Larkins, and F. E. Saalfeld, Int. J. Mass Spectrom. Ion Phys. 3, 203 (1969).

31. F. J. Preston, M. Tsuchiya, and H. J. Svec, Int. J. Mass Spectrom. Ion Phys. 3, 323 (1969).

32. H. M. Rosenstock, M. B. Wallenstein, A. L. Wahraftig, and H. Eyring, Proc. Natl. Acad. Sci. U.S. 38, 667 (1952).

33. H. M. Rosenstock and M. Krauss, in Advances in Mass Spectrometry, edited by R. M. Elliott (Pergamon Press, New York, 1963), Vol. 2, p. 251.

34. D. P. Stevenson, J. Chem. Phys. 10, 291 (1942).

35. R. M. Fristrom and A. A. Westenberg, Flame Structure, (McGraw-Hill, New York, 1968), p. 178.

36. G. R. Sparrow, Ph.D. thesis, Iowa State University, 1966 (unpublished).

37. W. M. Brubaker, in Fifteenth Annual Conference on Mass Spectrometry and Allied Topics, (ASTM Committee E-14, Denver, Colorado, 1967).

38. J. W. Otvos and D. P. Stevenson, J. Am. Chem. Soc. 78, 546 (1956).

39. J. W. Warren, Nature 165, 810 (1950).

40. J. L. Franklin, J. G. Dillard, H. M. Rosenstock, J. T. Herron, K. Draxl, and F. H. Field, Ionization Potentials, Appearance Potentials, and Heats of Formation of Gaseous Positive Ions, Nat. Stand. Ref. Data Ser., Nat. Bur. Stand. (U.S.), 26 (1969).

# X. ACKNOWLEDGEMENTS

The author wishes to express his deepest appreciation to Dr. H. J. Svec for his patient guidance and encouragement and for his many helpful suggestions, both professional and personal, throughout the author's graduate experience, and to Linda, the author's wife, whose patience, support, and personal sacrifices made this work possible.

The author also extends his sincere appreciation to all the members of Physical and Inorganic Chemistry Group VII and Analytical Chemistry Group III for their technical assistance and invaluable discussions throughout the development of the instrument, especially Dr. F. J. Preston, Mr. G. D. Flesch, Mr. R. J. Conzemius, and Mr. G. A. Junk (who suggested the use of a quadrupole mass filter); to the personnel of the Metals Development and Research shops and the glass shop for technical advice and construction and repair of various instrument components; to the personnel of the Electronics and Instrumentation Group for constructing and repairing electronic components, especially Mr. George Holland who designed the preamplifier and provided invaluable assistance in debugging the instrument; to the Ames Laboratory drafting service for reproducing the numerous illustrations; to Dr. R. G. Cooks (Department of Chemistry, Purdue University) for his generosity in supplying the isotopically-labelled aromatic compounds, and to numerous

other friends who helped to make this work in particular, and the graduate experience in general, both interesting and pleasant.